Twin-Image Problems in Optical Scanning Holography

by

Kyu-Bong Doh

Dissertation submitted to the Faculty of the

Virginia Polytechnic Institute and State University

in partial fulfillment of the requirements for the degree of

Doctor of Philosophy

in

Electrical Engineering

APPROVED:

Dr. Ting-Chung Poon, Chairman

Dr. Guy J. Indebetouw

Dr. Ioannis M. Besieris

Dr. Ahmad Safaai-jazi

Dr. A. Lynn Abbott

December 12, 1996

Blacksburg, Virginia

Keywords: Optical scanning holography, Twin-image, Fresnel zone pattern, Gaussian beam, Electronic holography, Microscopy

Twin-Image Problems in Optical Scanning Holography

by

Kyu-Bong Doh

Ting-Chung Poon, Chairman

Electrical Engineering

(ABSTRACT)

Real-time optical scanning holography, which was first suggested by Poon and Korpel, was originally analyzed by Poon using an optical transfer function approach. The recording of holographic information using the optical heterodyne scanning technique has several advantages over conventional nonscanning optical holographic recording methods. We first review a new 3-D imaging technique called optical scanning holography (OSH) by acousto-optic two-pupil synthesis. We then derive 3-D holographic magnification, using three points configured as a 3-D object. We demonstrate three-dimensional imaging capability of OSH by holographically recording two planar objects at different depths and reconstructing the hologram digitally and optically using an electron-beam-addressed spatial light modulator (EBSLM). The second part of this dissertation investigates twin-image noise in optical scanning holography. In optical scanning holography, holographic information of an object is generated by 2-D active optical scanning. The optical scanning beam can be a time-dependent Gaussian apodized Fresnel zone pattern. We derive the resolution achievable with such a scanning beam. We then discuss the use of a larger and a smaller Fresnel zone pattern for holographic recording to investigate twin-image noise which results in the unwanted image in the reconstructed field. Finally, we discuss a novel multiplexing technique to solve the twin

image problem in optical scanning holography without the use of a spatial carrier as commonly used in conventional off-axis holography. The technique involves simultaneously acquiring a sine and cosine Fresnel zone-lens pattern coded images by optical scanning. A complex addition of the two coded images then will be performed and decoded to give a twin-image rejection reconstruction.

Acknowledgments

I would like to express my sincere appreciation to my advisor, Professor Ting-Chung Poon, for his invaluable guidance and support to foster a happy research environment in Optical Image Processing Laboratory, dedicated to the state-of-the-art, but a place where one can enjoy the students and work that are involved. I would also like to thank, Professor Guy J. Indebetouw, for his helpful suggestions and comments to enhance this research. In addition, my appreciation is extended to Professor Ioannis M. Besieris, Professor Ahmad Safaai-Jazi, and Professor A. Lynn Abbott.

Many thanks to Dr. Ming Wu (Hamamatsu Corporation, NJ), Mr. K. Shinoda and Dr. Y. Suzuki (Hamamatsu Photonics K.K., Japan) for their comments and the valuable equipment supply. Thanks also to my fellows, Bradley Schilling, Derrek Dunn, Jiangang Xia, and other members of the Optical Image Processing Lab for their advice, consultation, but more importantly for their friendship.

Finally, I would like to thank my family, who grew tired of hearing "leave me alone, I need to go school, I am busy for my works." for so many nights, and who never give up their support throughout the year as I pursued my dreams. In particular, I want to

thank my wife and sons, Lambert and Nicholas, for their love, support, and understanding during this dissertation work.

This research is supported in part by the National Science Foundation (Grant No. ECS-9319211) and in part by the National Institutes of Health (Grant No. 1-R03-RR08698-01). Material support was also provided by Hamamatsu Corporation and Hamamatsu Photonics K.K., Japan.

Table of Contents

List of Illustrations

CHAPTER 1: INTRODUCTION

Optical scanning holography (OSH) is a technique in which 3-D information of an object can be recorded by 2-D scanning [1-4]. In a conventional incoherent scanning or imaging system, limitations exist on image processing that are due to the resulting nonnegative intensity spread function, which imposes severe constraints on both the amplitude and the phase of the optical transfer function (OSH) [5]. Such limitations can be circumvented by introducing a two-pupil system [6,7] that is characterized by a great flexibility in pupil-function specification for a desired synthesized point-spread function (PSF). Accordingly, a new scanning technique to generate optical holograms has been proposed and analyzed.

A new holographic recording technique using optical transfer function of an acousto-optic heterodyning processor was first proposed by Poon [8] in 1985. The technique involves a direct application of a defocused incoherent image processing employing acousto-optic heterodyning and two-pupil optical transfer function synthesis. Since then, aggressive further researches have been conducted and demonstrated [2,3,9-11]. In this dissertation, the principle of optical scanning holography is extended to derive 3-D holographic magnification, using three points configured as a 3-D object and

to show how hologram scaling and wavelength scaling can be accomplished with the OSH system. we also demonstrate three-dimensional imaging capability of OSH by holographically recording two planar objects at different depths and reconstructing the hologram digitally and optically in conjunction with an electron-beam-addressed spatial light modulator (EBSLM) for real-time coherent image reconstruction. We also investigate the effects of the size of the scanning beam in relation to twin-image noise upon image reconstruction. It has been shown that by scanning an object with a temporally modulated Gaussian apodized Fresnel zone pattern to acquire holographic information, the resolution achievable is directly proportional to the size of the beam and the number of zones within the beam. If the object is in the near field and as the object becomes more and more complicated, it is advantageous to use a smaller beam rather than a larger beam even though the two beams may lead to the same nominal resolution upon image reconstruction. Physically, one may argue that scanning with a larger beam causes twin-image noise to interact with a broader part of the image. This effect may prove to be more important if the object is contaminated with noise. Another reason may be that when the size of the scanning zone plate is larger than that of the object so that the scanning beam always illuminates the entire object, we have a situation reminiscent of coherent holographic recording since the hologram is the simultaneous superposition of the individual holograms of each within the object. On the contrary, if the zone pattern size is much smaller than that of the object, the zone plate overlaps only a small part of the object at any instant of the scanning process, a situation reminiscent of a partially coherent recording [12]. We propose a novel multiplexing technique to solve the twin-image problem in optical scanning holography without the use of a spatial carrier as commonly used in conventional off-axis holography. The technique involves simultaneously acquiring a sine and cosine Fresnel zone-lens pattern coded images by

optical scanning. A complex addition of the two coded images then will be performed and decoded to give a twin-image rejection reconstruction. Computer simulations and experimental results will be presented to demonstrate the validity of the idea.

This dissertation provides a comprehensive and detailed treatment of twin-image analysis and optical scanning holography. This dissertation consists of six chapters which are outlined as below.

Chapter 2 provides the main concepts and the basic terminology used in optical scanning holography. It first introduces an acousto-optic heterodyne image processor which is a new scanning technique to generate optical holograms by employing acousto-optic heterodyning and two-pupil optical transfer function synthesis. Then it discusses Gaussian beam analysis of optical scanning holography. Chapter 3 addresses the 3-D imaging techniques in microscopy and scanning holographic microscopy. Then it looks at in detail recording stage, reconstruction stage, and holographic magnification (hologram scaling and wavelength scaling).

Chapter 4 presents twin-image noise analysis based on Gaussian beam propagation. It first derive the resolution achievable with an optical scanning beam. It then shows the use of a smaller and larger Fresnel zone plate for holographic recording to examine the effects of the twin-image in the near and far field. Chapter 5 is dedicated to elimination techniques of twin-image in optical scanning holography. The technique involves simultaneously acquiring a sine and cosine Fresnel zone-lens pattern coded images. Chapter 6 presents a summary of relevant results and concluding remarks as well as a discussion of present and future research directions.

CHAPTER 2: SCANNING IMAGE PROCESSOR AND OPTICAL SCANNING HOLOGRAPHY

In this chapter we shall pay special attention to optical transfer function (OTF) of an acousto-optic heterodyning image processor. In a conventional incoherent scanning or imaging system, limitations exist on image processing because of the constraints on magnitude and phase of the optical transfer function (OTF) [5]. It has been pointed out that such limitation may be overcome by using a two-pupil image-forming system [6,7]. We will proceed from the point form of optical transfer function of an acousto-optic two-pupil synthesis [1,8]. We will also introduce Gaussian beam analysis of optical scanning holography [2].

2.1 Optical Transfer Function Synthesis

2.1.1 One-Pupil Synthesis

Refer to the geometry of Fig. 2.1, where the system is under coherent illumination. Lens L1 forms the Fourier transform U_1' of the optical field U_0 in its focal plane 1, where a beam-shaping transparency Γ_1 multiples U_1' to create U_1. Lens L_2 forms the Fourier transform U_2 of U_1 in its back focal plane. The field U_2 in plane 2 is used to scan out a transparency $\Gamma_2(x, y)$. By scanning is meant that successive points (x, y in transparency coordinates) of Γ_2 are brought into coincidence with the center (x_2, y_2=0, 0) of the field in the $x_2\, y_2$ plane. This is most easily accomplished by keeping the beam fixed while moving the transparency across it. The photo-diode PD, which responds to the incident intensity of the optical wave field, accepts the entire field $\Gamma_2 U_2$ and generates a direct current that is given by

$$I(x,y) = \int\int |\Gamma_2(x_2, y_2)|^2 \times |U_2(x_2 - x, y_2 - \mathrm{y})|^2 dx_2 dy_2 \tag{2.1}$$

with an inessential constant left out.

Eq. (2.1) may be readily recognized as the correlation of two functions $|\Gamma_2|^2$ and $|U_2|^2$:

$$\begin{aligned} I(x,y) &= \int\int |\Gamma_2(x_2, y_2)|^2 \times |U_2(x_2 - x, y_2 - y)|^2 dx_2 dy_2 \\ &= |\Gamma_2(x,y)|^2 \otimes |U_2(x,y)|^2, \end{aligned} \tag{2.2}$$

where $\otimes$ denotes the correlation operation, i.e.,

$$g(x,y) \otimes s(x,y) = \int\int g(x', y') s^*(x' - x, y' - y) dx' dy' \tag{2.3}$$

By taking the Fourier-transform of Eq. (2.2), we have

$$\mathfrak{F}\{I\} = \mathfrak{F}\{|\Gamma_2|^2\}\mathfrak{F}^*\{|U_2|^2\}, \tag{2.4}$$

where $\mathfrak{F}$ denotes the Fourier-transform operation, i.e.,

$$\mathfrak{F}\{I\}(f_x, f_y) = \int\int I(x,y)exp(-j2\pi f_x x - j2\pi f_y y)dxdy, \tag{2.5}$$

with f_x and f_y denoting the spatial frequencies. Since the field U_1 and U_2 are in the front and back focal plane of lens 2, respectively, an exact Fourier-transform relation holds between these two fields [13]. We have, with an inessential constant and a phase factor left out,

$$\begin{aligned} U_2(x_2, y_2) &= \mathfrak{F}\{U_1\}\left(\tfrac{x_2}{\lambda f_2}, \tfrac{y_2}{\lambda f_2}\right) \\ &= \int\int U_1(x_1, y_1)exp\Big(-j\tfrac{2\pi}{\lambda f_2}(x_1x_2 + y_1y_2)\Big)dx_1dy_1, \end{aligned} \tag{2.6}$$

where λ is the optical wavelength.

The OTF of the scanning system can be defined as

$$\begin{aligned} \text{OTF}(f_x, f_y) &= \mathfrak{F}\{I\}/\mathfrak{F}\{|\Gamma_2|^2\} \\ &= \mathfrak{F}^*\{U_2^*U_2\}. \end{aligned} \tag{2.7}$$

In terms of the pupil field U_1 and using Eq. (2.6), Eq. (2.7) becomes

$$\begin{aligned} \text{OTF} &= \mathfrak{F}^*\{U_2^*U_2\} \\ &= [\int\int U_2^*(x_2, y_2)U_2(x_2, y_2) \times exp(-j2\pi f_x x_2 - j2\pi f_y y_2)dx_2dy_2]^* \end{aligned}$$

$$
\begin{aligned}
&= [\int\int\int\int\int\int U_1^*(x_1, y_1) \times exp[j\tfrac{2\pi}{\lambda f_2}(x_1 x_2 + y_1 y_2)] U_1(x_1', y_1') \\
&\quad \times exp[-j\tfrac{2\pi}{\lambda f_2}(x_1' x_2 + y_1' y_2)] \\
&\quad \times exp(-j2\pi f_x x_2 - j2\pi f_y y_2) \\
&\quad \times dx_1 dy_1 dx_1' dy_1' dx_2 dy_2]^* \\
&= [\int\int\int\int\int\int U_1^*(x_1, y_1) U_1(x_1', y_1') \times \delta[\tfrac{2\pi}{\lambda f_2} x_1 - 2\pi f_x - \tfrac{2\pi}{\lambda f_2} x_1'] \\
&\quad \times \delta[\tfrac{2\pi}{\lambda f_2} y_1 - 2\pi f_y - \tfrac{2\pi}{\lambda f_2} y_1'] dx_1 dy_1 dx_1' dy_1']^* \\
&= [\int\int U_1^*(x_1, y_1) U_1(x_1 - \lambda f_2 f_x, y_1 - \lambda f_2 f_y) dx_1 dy_1]^* \\
&= \int\int U_1(x_1, y_1) U_1^*(x_1 - \lambda f_2 f_x, y_1 - \lambda f_2 f_y) dx_1 dy_1 \\
&= U_1 \otimes U_1, \qquad (2.8)
\end{aligned}
$$

where in this derivation we have left out inessential factors.

We see that the OTF of the system is simply the autocorrelation of the pupil function of the scanning field. The right-hand side of Eq. (2.7) is the Fourier transform of the scanning beam $U_2 U_2^*$, and the left-hand side is the filter function. As we are Fourier transforming the beam profile to obtain the filter function, a coarse (i.e., broad) beam will result in a narrow band in the spatial-frequency domain. This is the reason why we cannot resolve high spatial frequencies with a coarse beam.

For coherent systems shown in Fig. 2.2, we may find the complex field in the image plane $U_i(x_i, y_i)$ by convolving the field in the object plane $U_0(x_0, y_0)$ with the system impulse response $h(x_i, y_i; x_0, y_0)$, the coherent spread function. For a spatially invariant system, we have

$$
U_i(x_i, y_i) = \int\int U_0(x_0, y_0) h(x_i - x_0, y_i - y_0) dx_0 dy_0 = U_0 * h, \qquad (2.9)
$$

where h is the amplitude at image coordinates (x_i, y_i) in response to a point-source object at (x_0, y_0) and $*$ denotes the convolution operation. The image intensity distribution is then obtained by

$$I_i(x_i, y_i) = U_i(x_i, y_i)U_i^*(x_i, y_i), \tag{2.10}$$

Fourier transforming Eq. (2.9), we have

$$\mathfrak{F}\{U_i\} = \mathfrak{F}\{U_0\}\mathfrak{F}\{h\} \tag{2.11}$$

The coherent transfer function of the imaging system is defined on the basis of amplitudes:

$$H(f_x, f_y) = \frac{\mathfrak{F}\{U_i\}}{\mathfrak{F}\{U_0\}} = \mathfrak{F}\{h\} \tag{2.12}$$

However,

$$h = \mathfrak{F}\{P\} \tag{2.13}$$

under the ideal condition (i.e., when the system is properly focused), so that combining Eq. (2.12) with the definition of H gives

$$H(f_x, f_y) = \mathfrak{F}\{h\} = \mathfrak{F}\{\mathfrak{F}\{P\}\} = P(f_x, f_y) \tag{2.14}$$

Strictly speaking, the coherent transfer function is the pupil function of the system in a reflected frame of reference that is due to the double Fourier-transform operation in Eq. (2.14). The coherent transfer function $H(f_x, f_y)$ characterizes the performance of the coherent imaging system as it specifies the passband of the spatial frequency.

In the case of an incoherent imaging system, the image intensity distribution is

$$I_i(x_i, y_i) = \int\int I_0(x_0, y_0)|h(x_i - x_0, y_i - y_0)|^2 dx_0 dy_0, \tag{2.15}$$

where $|h|^2$ is the intensity spread function (PSF). Expressing the relationship in the frequency domain, we have

$$\mathfrak{F}\{I_i\} = \mathfrak{F}\{I_0\}\mathfrak{F}\{|h|^2\}. \tag{2.16}$$

The OTF of the incoherent imaging system is defined on the basis of intensities:

$$OTF = \frac{\mathfrak{F}\{I_i\}}{\mathfrak{F}\{I_0\}} = \mathfrak{F}\{|h|^2\}. \tag{2.17}$$

In terms of the pupil function P, we have, using Eqs. (2.13) and (2.14) in Eq. (2.17),

$$OTF = P \otimes P. \tag{2.18}$$

Hence, for incoherent imaging systems, the OTF is simply the autocorrelation of the pupil function of the system. By comparing Eqs. (2.8) and (2.18), the equivalence between the scanning system and the incoherent system is established. We claim no novelty in

deriving this equivalence. Its derivation does, however, help understand the material to follow.

2.1.2 Two-Pupil Synthesis

As we have seen from Eq. (2.15), the impulse response (PSF) of an incoherent optical system is a real and nonnegative function that imposes restrictions on both the magnitude and the phase of the OTF. Consequently, it limits the range of processing. For instance, suppose that we want to process picture to obtain contrast enhancement in order that fine detail may be seen better. In that case, we could never create a filter to block off the dc background by autocorrelation the pupil function, because the autocorrelation of any function exhibits a central maximum. Another example is the decoding of information recorded on a spatial carrier on the transparency. For this, we have to use a bandpass filter to separate the carrier and its sidebands from the rest of the spectrum. One-pupil synthesis clearly cannot perform this task. In fact, many processing operations require a PSF's that are bipolar. In order to overcome the limitation of a positive PSF, the so-called two-pupil synthesis method has been introduced. There are basically two kinds of syntheses possible: nonpupil interaction synthesis and pupil interaction synthesis.

In the nonpupil interaction synthesis, we may obtain a bipolar PSF or eliminate the central maximum by subtracting the PSF's of two different filter functions OTF_1 and OTF_2:

$$\begin{aligned} OTF_{tot} &= \mathfrak{F}\{|h_1|^2 - |h_2|^2\} = OTF_1 - OTF_2 \\ &= U_1 \otimes U_1 - V_1 \otimes V_1, \end{aligned} \tag{2.19}$$

where U_1 and V_1 are the different pupil functions. Because we cannot subtract intensities directly, this method requires special techniques.

In the pupil interaction synthesis, we add U_1 to V_1 in order to produce an effective pupil function, which is given by

$$U_{eff} = U_1 + V_1. \tag{2.20}$$

The PSF is given by

$$\begin{aligned} PSF &= |\mathfrak{F}\{U_{eff}\}|^2 = |U_2 + V_2|^2 \\ &= |U_2|^2 + |V_2|^2 + U_2V_2^* + U_2^*V_2, \end{aligned} \tag{2.21}$$

where $U_2 = \mathfrak{F}\{U_1\}$ and $V_2 = \mathfrak{F}\{V_1\}$.

The corresponding OTF of the system is given by [see Eq. (2.17)]

$$\begin{aligned} OTF &= \mathfrak{F}\{PSF\} \\ &= \mathfrak{F}\{|U_2|^2\} + \mathfrak{F}\{|V_2|^2\} + \mathfrak{F}\{U_2V_2^*\} + \mathfrak{F}\{U_2^*V_2\} \\ &= U_1 \otimes U_1 + V_1 \otimes V_1 + U_1 \otimes V_1 + V_1 \otimes U_1. \end{aligned} \tag{2.22}$$

The last two terms of Eq. (2.22), which contain the bipolar information, are the cross correlations of U_1 and V_1, V_1 and U_1, respectively. Interaction of the pupils actually occurs in this sense. The autocorrelation terms are considered as bias. To retrieve the bipolar information, it is necessary to separate the signal from the bias by a subtraction operation, unless carrier methods are used.

A simple pupil interaction processing technique exists in which both spatial and temporal frequency offsets are brought about by acousto-optic Bragg diffraction without complicated geometrical configurations or moving mirrors. An idealized version of the system is shown in Fig. 2.3.

A He-Ne laser L directs a collimated beam of light onto a Bragg diffraction sound cell S, which is basically a device that create two identical light beams, differing in frequency by $\triangle\nu$ and in direction of propagation by $\alpha \simeq (\lambda/V_s)\triangle\nu$, V_s being the velocity of sound. Lens L_1 forms, in its back focal plane, the Fourier transforms $U_1^{'}$, $V_1^{'}$ of the field U_0, V_0 describing the two beams in S. A beam-shaping transparency Γ_1 acts on $U_1^{'}$, $V_1^{'}$ to create U_1, V_1, after which a second lens L_2 forms Fourier transforms U_2, V_2 in its back focal plane. The total field $U_2 + V_2$ is used to scan out a transparency $\Gamma_2(x, y)$. In contrast to the case of a one-pupil optical scanner, in which a direct current is delivered at the photodiode output, photodiode (PD) now delivers a rf heterodyne current at the beat frequency $\triangle\nu$ of the two fields U_2 and V_2. The current is given by

$$i(x,y,t) = \int\int \Big| [U_2(x_2,y_2)exp(-j\tfrac{2\pi\triangle\nu t}{2}) + V_2(x_2,y_2)exp(j\tfrac{2\pi\triangle\nu t}{2})] \times \Gamma_2(x+x_2, y+y_2)\Big|^2 dx_2 dy_2, \tag{2.23}$$

where the two scanning fields in the x_2y_2 plane are given by

$$U_2(x_2,y_2)exp(-j\tfrac{2\pi\triangle\nu t}{2}),\ V_2(x_2,y_2)exp(+j\tfrac{2\pi\triangle\nu t}{2}),$$

and where the optical convention for the phasor , $\tilde{A} = |\tilde{A}|exp(-j\phi)$, is adopted.

The time-varying part of Eq. (2.23) is

$$\begin{aligned}\tilde{i}(x,y,t) &= \int\int [U_2(x_2,y_2)V_2^*(x_2,y_2)exp(-j2\pi\triangle\nu t) \\ &\quad + V_2(x_2,y_2)U_2^*(x_2,y_2)exp(j2\pi\triangle\nu t)] \\ &\quad \times |\Gamma_2(x+x_2,y+y_2)|^2 dx_2 dy_2 \\ &= Re[\int\int U_2(x_2,y_2)V_2^*(x_2,y_2) \\ &\quad \times |\Gamma_2(x+x_2,y+y_2)|^2 dx_2 dy_2 \\ &\quad \times exp(-j2\pi\triangle\nu t)] \end{aligned} \tag{2.24}$$

with an inessential constant left out.

In terms of a phasor $\tilde{I}(x,y)$, such that

$$\tilde{i}(x,y,t) = Re[\tilde{I}(x,y)exp(-j2\pi\triangle\nu t)],$$

we find, from Eq. (2.24), that

$$\begin{aligned}\tilde{I}(x,y) &= \int\int U_2(x_2,y_2)V_2^*(x_2,y_2) \\ &\quad \times |\Gamma_2(x+x_2,y+y_2)|^2 dx_2 dy_2. \end{aligned} \tag{2.25}$$

The phase and the amplitude of the photodiode current, as a function of x and y, constitute the scanned and processed version of the transparency $\Gamma_2(x,y)$. From the analysis of one-pupil synthesis, we can immediately write down the OTF of the two-pupil systems:

$$OTF = \mathfrak{F}\{\tilde{I}(x,y)\}/\mathfrak{F}\{|\Gamma_2|^2\}, \tag{2.26}$$

or, equivalently,

$$OTF = \mathfrak{F}^*\{U_2^* V_2\} = U_1 \otimes V_1, \tag{2.27}$$

by which is meant

$$OTF(f_x, f_y) = \int\int U_1(x_1, y_1) \times V_1^*(x_1 - \lambda f_2 f_x, y_1 - \lambda f_2 f_y) dx_1 dy_1. \tag{2.28}$$

At this point, it is clear that the system is incoherent in the sense that its operation is described by the same formalism as that used for incoherent pupil interaction methods, even though the system uses coherent light and its output (a heterodyne current) is characterized by amplitude and phase, which is generally characteristic of coherent systems.

It has been demonstrated [8] that the acousto-optical technique is relatively easy to implement and leads to the desired result of more general OTF synthesis. Specifically, a bandpass response centered at $f_y = 0$ has been generated through the practical implementation of the idealized version (Fig. 2.3). However, the resulting OTF is essentially one dimensional.

2.1.3 Optical Transfer Function Synthesis in Defocused Case

In this section, we show that more interesting OTF's can be obtained by drastically modifying U_1 relative to V_1. In this context, a chirp-type response in an out-of-focus

plane near plane 2 is derived. Refer to Fig. 2.3, Γ_2 is now placed in an out-of-focus plane, plane 2', near plane 2. Following the procedures leading to Eq. 2.27 we have

$$\begin{aligned} OTF(f_x, f_y) &= \mathfrak{F}\{\tilde{I}(x,y)\}/\mathfrak{F}\{|\Gamma_2|^2\} \\ &= \mathfrak{F}^*\{U_2^{'*}(x_2^{'}, y_2^{'})V_2^{'}(x_2^{'}, y_2^{'})\}, \end{aligned} \tag{2.29}$$

where $U_2^{'}$ and $V_2^{'}$ are obtained through the Fresnel diffraction of U_2 and V_2, respectively, and U_2 and V_2 are related to U_1 and V_1, respectively, through the action of the lens L_2. The explicit relations are given as follows:

$$\begin{aligned} U_2(x_2, y_2) &= \frac{exp(jkf_2)}{j\lambda f_2}\int\int U_1(x_1, y_1) \\ &\quad \times exp\Big[\frac{-j2\pi}{\lambda f_2}(x_1x_2 + y_1y_2)\Big]dx_1dy_1, \end{aligned} \tag{2.30}$$

$$\begin{aligned} U_2^{'}(x_2^{'}, y_2^{'}) &= \frac{exp(jkz)}{j\lambda z}exp\Big[j\frac{k}{2z}(x_2^{'2} + y_2^{'2})\Big] \\ &\quad \times \int\int U_2(x_2, y_2)exp\Big[j\frac{k}{2z}(x_2^2 + y_2^2)\Big] \\ &\quad \times exp\Big[-j\frac{k}{z}(x_2x_2^{'} + y_2y_2^{'})\Big]dx_2dy_2, \end{aligned} \tag{2.31}$$

where $k = 2\pi/\lambda$. Substituting Eq. (2.30) into Eq. (2.31), we have

$$\begin{aligned} U_2^{'}(x_2^{'}, y_2^{'}) &= \Big\{-exp(jkf_2)exp(jkz) \\ &\quad \times exp\Big[j\frac{k}{2z}(x_2^{'2} + y_2^{'2})\Big]/\lambda^2 f_2 z\Big\}\int\int\int\int U_1(x_1, y_1) \\ &\quad \times exp\Big[-\frac{2\pi}{\lambda f_2}(x_1x_2 + y_1y_2)\Big]exp\Big[j\frac{k}{2z}(x_2^2 + y_2^2)\Big] \\ &\quad \times exp\Big[-j\frac{k}{z}(x_2x_2^{'} + y_2y_2^{'})\Big]dx_1dy_1dx_2dy_2 \end{aligned} \tag{2.32}$$

The expression for $V_2^{'}(x_2^{'}, y_2^{'})$ can be found identically, with $U_2^{'}$ and U_1 replaced by $V_2^{'}$ and V_1, respectively, in the above expression.

Using the expressions of U_2' and V_2', it may be shown that

$$OTF(f_x, f_y) = exp[j\pi\lambda z({f_x}^2 + {f_y}^2)]$$
$$\times \int\int U_1(x_1, y_1)V_1^*(x_1 - \lambda f_2 f_x, y_1 - \lambda f_2 f_y)$$
$$\times exp[-j\tfrac{2\pi z}{f_2}(x_1 f_x + y_1 f_y)]dx_1 dy_1 \qquad (2.33)$$

Equation (2.33) is the OTF for the defocused system, where Γ_2 is placed in plane 2'.

The situation is further illustrated and explained in Fig. 2.4 by making V_1 a delta function and U_1 a plane-wave function. U_1 and V_1 are first made to be plane waves by narrowing the incoming beam in the front focal plane of lens L_1 (Fig. 2.3). Intercepting V_1 in plane 1 by a narrow slit will result in a delta function. The overlapping of two beams creates a chirp-type fringe pattern along plane 2'. The fringe wavelength is increasing from point A to point B because the two wave fronts intercept at a larger angle at point A than at point B.

If we let $U_1(x_1, y_1) = \delta(x_1, y_1)$ and $V_1(x_1, y_1) = 1$, where we assume the delta function to be located at the center of the $x_1 y_1$ plane, we obtain, using Eq. (2.33),

$$OTF(f_x, f_y) = exp[j\pi\lambda z(f_x^2 + f_y^2)]. \qquad (2.34)$$

By using the above expression for the OTF, the impulse response function $\tilde{I}\,(x, y; z)$ may be expressed as

$$\tilde{I}\,(x, y; z) = \mathfrak{F}^{-1}\{OTF\} = \tfrac{exp(j\pi/2)}{\lambda z} exp[-j\tfrac{\pi}{\lambda z}(x^2 + y^2)], \qquad (2.35)$$

which is obviously a chirp-type impulse response. In fact, by moving a slit along plane 2' and measuring $\tilde{I}(x, y; z)$, we should be able to observe this. By investigating the chirp rate, we can deduce how far plane 2' is out of focus from plane 2. This scanning system is thus able to encode position (x, y coordinate) and depth of focus (z coordinate), and thus it carries obvious implication to holographic recording. In the next section we will see in detail how the two-pupil scanning image processor can be used in holographic application.

2.2 Optical Scanning Holography

2.2.1 Heterodyne Scanning Processing

The principle of optical heterodyne scanning image processing is schematically illustrated in Fig. 2.5. U_1 and V_1 denote the pupil functions in the pupil plane, located in the front focal plane of lens L_2. The two pupil fields are offset in temporal frequency by f_c. The Fourier transforms of the pupil functions, U_2 and V_2, are superposed upon the mirror of an $x - y$ scanning device. After propagating a distance z, the Fresnel diffraction pattern of this composite field $(U_2 + V_2)$ is used to scan the object amplitude transparency Γ_2. After scanning, all light passing through Γ_2 is collected by a photodetector and converted into a corresponding scanned electrical signal $v(x, y; z, t)$. Mathematically, this electrical signal can be written as

$$v(x, y; z, t) = \int\int \left| \left[V_2'(x_2' - x, y_2' - y; z) + U_2'(x_2' - x, y_2' - y; z) \right.\right. \\ \left.\left. \times exp(-j2\pi f_c t) \right] \Gamma_2(x_2', y_2') \right|^2 dx_2' dy_2' \qquad (2.36)$$

where $U_2^{'}$ and $V_2^{'}$ are the Fresnel diffraction patterns of U_2 and V_2, respectively, and the variables x and y are, in general, functions of time determined by the scanner's motion. After optical heterodyning, the electrical signal at the heterodyne frequency f_c is

$$\tilde{v}(x,y;z,t) = Re\Big[\int\int U_2^{'}(x_2^{'}-x, y_2^{'}-y; z) V_2^{'*}(x_2^{'}-x, y_2^{'}-y; z) \times \left|\Gamma_2(x_2^{'}, y_2^{'})\right|^2 dx_2^{'} dy_2^{'} exp(-j2\pi f_c t)\Big] \tag{2.37}$$

where the superscript * denotes the complex conjugate.

The signal can then be extracted by electrical bandpass filtering centered at f_c, with the phase and amplitude of this heterodyne signal constituting the scanned and processed version of the object $\left|\Gamma_2\right|^2$. This processed information can then be sent to a real-time monitor for display.

In terms of a phasor $\tilde{V}(x,y;z)$, such that

$$\tilde{v}(x,y;z,t) = Re\Big[\tilde{V}(x,y;z) exp(-j2\pi f_c t)\Big] \tag{2.38}$$

we find that

$$\begin{aligned}\tilde{V}(x,y;z) &= \int\int U_2^{'}(x_2^{'}-x, y_2^{'}-y; z) V_2^{'*}(x_2^{'}-x, y_2^{'}-y; z) \\ &\quad \times \left|\Gamma_2(x_2^{'}, y_2^{'})\right|^2 dx_2^{'} dy_2^{'} \\ &= (U_2^{'} V_2^{'*}) \otimes \left|\Gamma_2\right|^2 \end{aligned} \tag{2.39}$$

where $\otimes$ denotes two-dimensional correlation. If $\left|\Gamma_2(x,y)\right|^2 = \delta(x,y)$, Eq. (2.39) represents the impulse response of the defocused system and is given by

$$\tilde{V}_\delta(x,y;z) = U_2'(-x,-y;z)V_2'^*(-x,-y;z) \tag{2.40}$$

Note that $\tilde{V}_\delta$ is complex in general and that bipolar incoherent spatial filtering [6, 14, 15] based on this approach has been demonstrated. A similar system was also been used recently for applications in textural edge extraction [16] as well as in real-time tunable incoherent spatial filtering [17].

To illustrate that the optical heterodyne scanning system can indeed be used to record holographic information, we consider an idealized situation in which $U_1 = \delta(x-d,y)$ and $V_1 = 1$. This situation is shown in Fig 2.5. With this choice of U_1 and V_1 and the use of Fourier optical analysis, Eq. (2.40) becomes

$$\tilde{V}_\delta(x,y;z) = \frac{exp(j\pi/2)}{\lambda z} exp\Big\{-j\frac{\pi}{\lambda z}\Big[\Big(x - d\frac{z}{f_2}\Big)^2 + y^2\Big]\Big\}, \tag{2.41}$$

where $\tilde{V}_\delta(x,y;z)$ can be recognized as a quadratic phase factor, or complex chirp-type impulse response. The scanned, heterodyne signal from the photodetector is the given by Eq.(2.38) with $\tilde{V}(x,y;z)$ replaced by Eq. (2.41). Since the signal represented by Eq. (2.38) is bipolar, to preserve the phase of the signal a dc bias voltage V_{DC} must be added before recording. Hence the total signal to be recorded can be represented as

$$v(x,y;z,t) = V_{DC} + Re[\tilde{V}_\delta(x,y;z)exp(-j2\pi f_c t)]. \tag{2.42}$$

If recording is done by feeding $v(x,y;z,t)$ into an intensity-modulation input of a 2-D display device whose electron gun (in the case of EBSLM) is synchronized with the x and

y scans of the $x-y$ scanning device, Eq. (2.42) can be written in the form of a 2-D displayed signal as

$$v(x,y;z) = V_{DC} + Re[\tilde{V}_{\delta}(x,y;z)exp(-j2\pi\frac{f_c}{v_x}x)], \tag{2.43}$$

where the temporal carrier frequency f_c in Eq. (2.42) has been translated into a spatial carrier frequency f_c/v_x, with v_x denoting the electron gun velocity of the displayed device in the x direction.

2.2.2 Gaussian beam analysis

Generally speaking it is impossible to choose U_1 and V_1 such that at the scanner we have the superposition of a true plane wave and a true point source. Since the spatial distribution of the scanning laser beam is in general taken to be Gaussian, we consider the superposition of a broadened and a focused Gaussian beam. The effective values for U_1 and V_1 have to be determined. The functional form of the effective pupil function V_1 is given by

$$V_1(x,y) = \frac{1}{\pi\omega_v^2}exp[-\frac{(x^2+y^2)}{\omega_v^2}], \tag{2.44}$$

where $\omega_v = M_{cv}\omega_0$, M_{cv} is the magnification of the collimator in the path of V_1, and ω_0 is the Gaussian waist of the laser source beam.

As for the specification of pupil function U_1, since lens L_2 has been removed we find the effective pupil function U_1 by specifying the broadened Gaussian distribution at

the scanning mirror and equating this distribution to the Fourier transform of U_1. Mathematically, this is written as

$$exp[-\frac{(x^2+y^2)}{(M_{cv}\omega_0)^2}] = \mathfrak{F}\{U_1\}$$
$$= \int\int U_1(x,y)exp(-j2\pi f_x x - j2\pi f_y y)dxdy, \qquad (2.45)$$

where $f_x = x/\lambda f_2$, $f_y = y/\lambda f_2$ are the spatial frequencies employed in the Fourier transformation of Eq. , λ is the wavelength of the optical beams, and M_{cv} denotes the magnification of the collimator in the path of U_1. Solving for U_1 gives

$$U_1(x,y) = \frac{1}{\pi\omega_u^2}exp\{-\frac{[(x-d)^2+y^2]}{\omega_u^2}\}, \qquad (2.46)$$

where $\omega_u = \lambda f_2/\pi\omega_0 M_{cu}$ and we have introduced an offset d.

Note that, because of the phase-flattening properties of the collimators, Eqs. (2.44) and (2.46) represent real Gaussian functions. Also note that U_1 and V_1 have been chosen to be normalized Gaussians;

$$\int_{-\infty}^{\infty}\int_{-\infty}^{\infty}\Psi_1 dxdy = 1, \qquad (2.47)$$

where Ψ_1 represents either U_1 or V_1.

For U_1 and V_1 given as in Eqs. (2.44) and (2.46), respectively, the impulse response is found to be, with an inessential constant left out,

$$\tilde{V}_\delta(x,y;z) = \frac{1}{G}exp(-K)exp\Big\{-\frac{\pi^2}{G}\Big[\Big(x+j\frac{H}{\pi}\Big)^2 + y^2\Big]\Big\}, \qquad (2.48)$$

where

$$G = \left[\eta\left(\frac{\lambda f_2}{\omega_v}\right)^2 + \eta\left(\frac{\pi\omega_u z}{f_2}\right)^2 + j\pi\lambda(1-2\eta)z\right],$$
$$H = \eta d\left(\frac{\lambda f_2}{\omega_v^2} + j\frac{\pi z}{f_2}\right),$$
$$K = \frac{d^2\eta}{\omega_v^2},\ \eta = \frac{\omega_v^2}{\omega_u^2+\omega_v^2}\ .$$

As a check, letting $\omega_v \to \infty$ and $\omega_u \to 0$, we readily see, for the ideal case (i.e., $U_1 = \delta(x-d,\ y)$ and $V_1 = 1$), that $\eta \to 1$, $G \to\ -j\pi\lambda z$, $H \to jd\pi z/f_2$, $K \to 0$, and Eq. (2.48) reduces to the same functional form as that of Eq. (2.41)

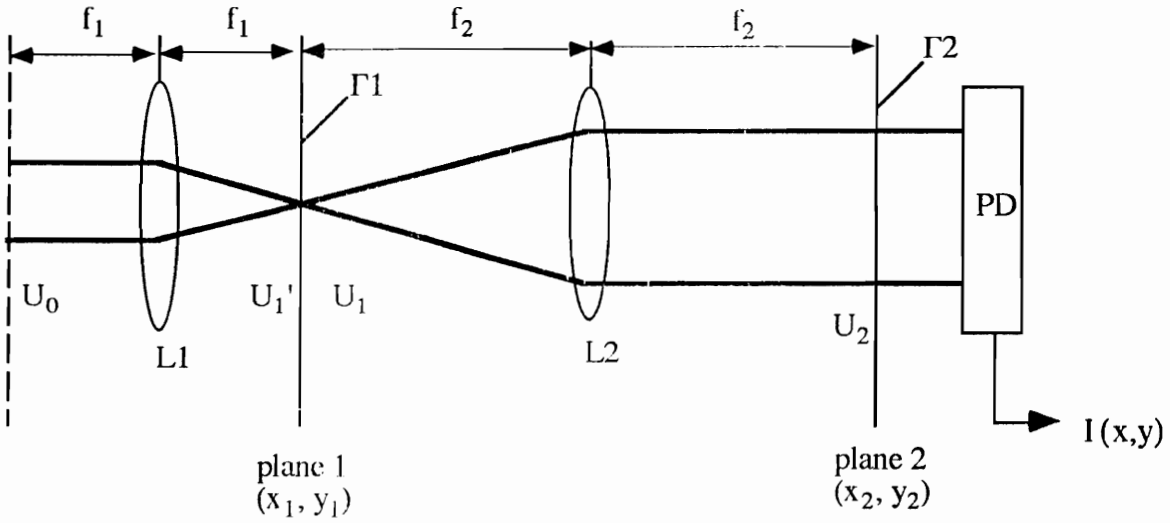

Fig. 2.1 One-pupil optical scanner [1].

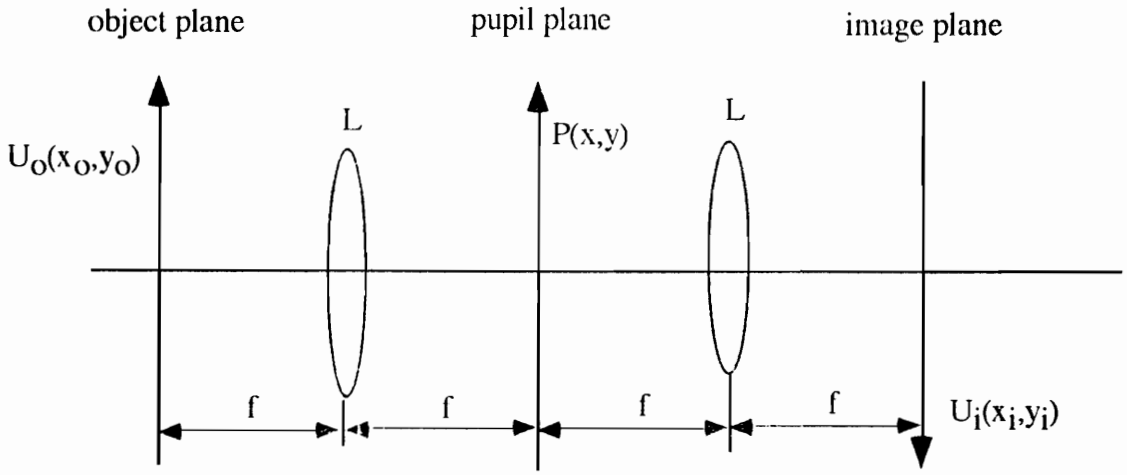

Fig. 2.2 Coherent image processing system

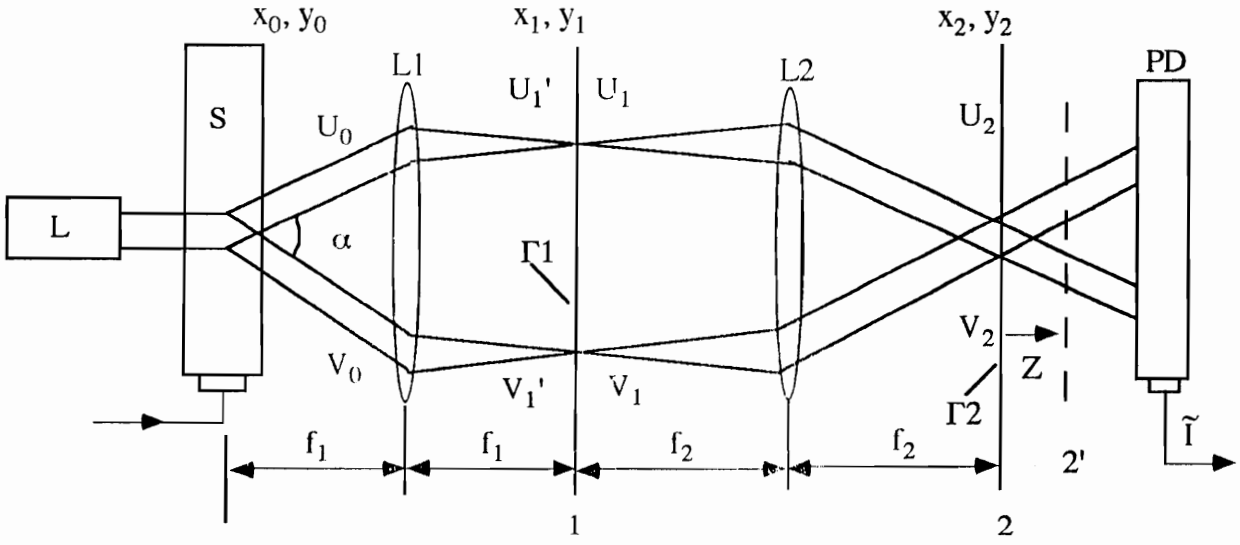

Fig. 2.3 Acousto-optic heterodyning image processor [1].

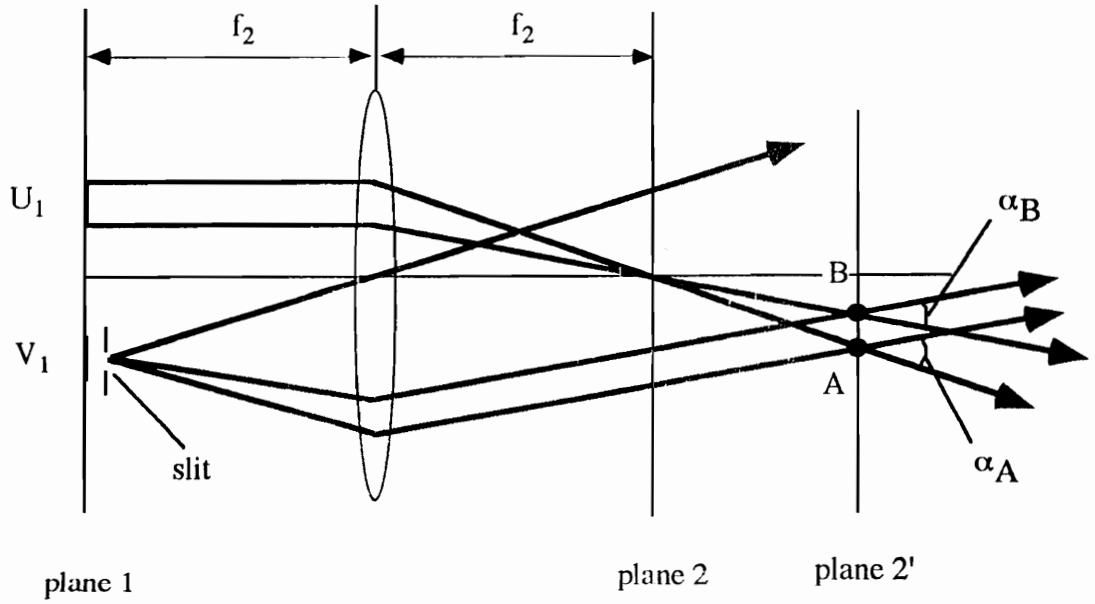

Fig. 2.4 Interference pattern in out-of-focus plane 2', created by line source and plane wave [1].

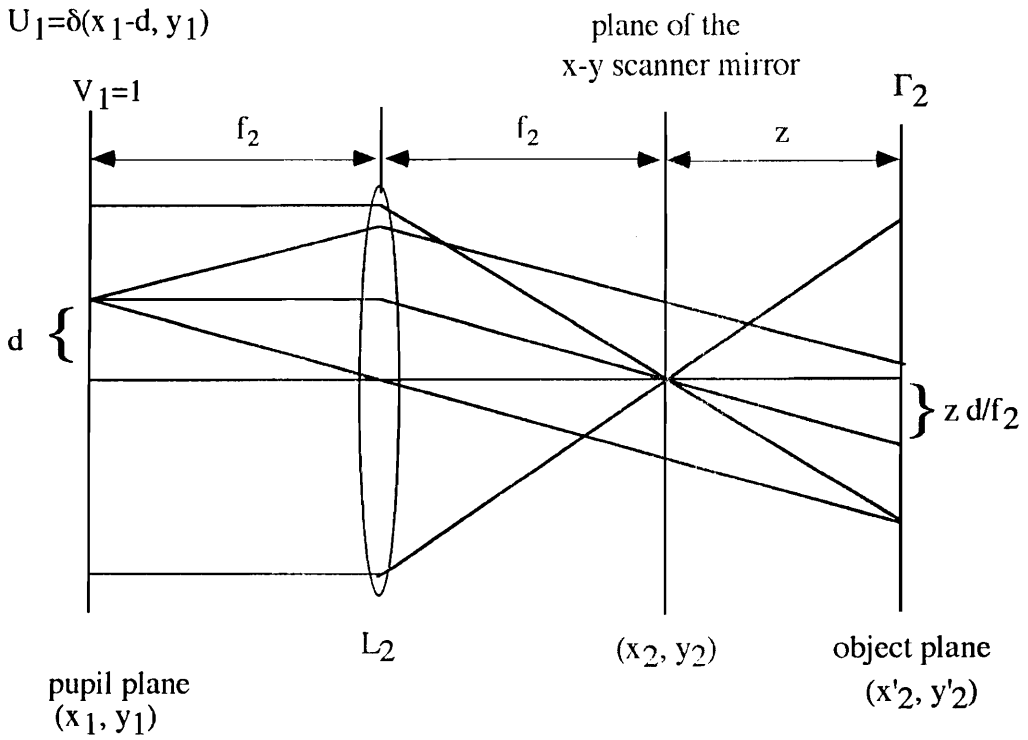

Fig. 2.5 Optical heterodyne system [2].

CHAPTER 3: IMAGING CAPABILITY IN OPTICAL SCANNING HOLOGRAPHIC MICROSCOPY

3.1 Perspective

Three-dimensional (3D) imaging is a formidable task in optical microscopy as it is well-known that the greater the lateral magnification, the smaller the depth of field. The past decade has witnessed an impressive emergence of three-dimensional (3-D) imaging techniques in microscopy. Optical sectioning microscopy (OSM) and a radically new microscope design, scanning confocal microscopy (SCM), are the two common techniques available in practice. In optical sectioning microscopy (OSM), 3-D information is collected by recording a series of 2-D images at various focal planes throughout the 3-D specimen [18], as shown in Fig. 3.1. The distance between the objective lens and the image plane is fixed in a microscope and the object plane may be moved through the specimen by moving the objective lens and image plane up and down as a unit. More conveniently, however, the object is moved up and down on a stage. Typically, 20 - 100 different image slides throughout the specimen are required,

depending on the thickness of the specimen. Since each 2-D image contains the in-focus as well as the out-of-focus information, reconstruction of the 3-D information, i.e., extraction of the in-focus information from these 2-D images, is required. Many reconstruction algorithms have been developed for this purpose [18]. The difficulty of optical sectioning lies in the fact that during the recording stage it is important that exact longitudinal spacing between adjacent 2-D images be accurately controlled. Also during the reconstruction, precise registration of the 2-D images are critical even before processing can be performed. Recognizing these problems, a radically new microscope design, the scanning confocal microscope (SCM), has emerged [19]. In SCM, a doubly focused objective lens system and a pin-hole aperture in front of a photomultiplier are used to image only a single point within the 3-D specimen. The situation is shown in Fig. 3.2. Light emitted by points outside the plane of focus (dashed line) is rejected by the pin-hole aperture in front of the photodetector. Three-dimensional information is gathered by scanning the specimen in three dimensions while collecting the light transmitted through the specimen with the photodetector. The main problem of SCM is that the scanning instrumental tolerances required to achieve high resolution imaging are very difficult to obtain and 3-D scanning is time-consuming.

Holography is another way to achieve 3-D imaging [20,21]. It can record a large volume of object space without loss of resolution and it has been used successfully for many applications, such as particle sizing and microscopy [22-25]. Holographic magnification can be achieved by scaling the size of the holograms, scaling the reconstructing wavelength, or using spherical waves in one or both steps of the holographic process [25]. Another popular technique to achieve holographic magnification is called microscopically augmented holography [26]. In the technique the object either can be magnified first before it is holographically recorded

(premagnification) or the object is holographically recorded and then inspected through a microscope (postmagnification). In this paper, we shall review a newly developed 3-D imaging technique called optical scanning holography (OSH) [1]. It is a hybrid (optical/electronic) holographic technique based on optical scanning. Its principle along with the use of the technique in the context of 3-D microscopy are discussed in next Sections. We describe the system components and hardware used in the system and present 3-D imaging results in the following sections .

3.2 Optical Scanning Holography

Optical scanning holography (OSH) is a novel technique in which 3-D information of an object can be recorded using heterodyne optical scanning. The system consists of two stages: the recording or coding stage, and the reconstruction or decoding stage. In the recording stage, the 3-D specimen is two-dimensionally scanned by a time-dependent Fresnel zone-lens plate (TDFZP). The TDFZP is created by the superposition of a plane wave and a spherical wave of different temporal frequencies. The situation is shown in Fig. 3.3. While the specimen is scanned, a photodetector collects the light transmitted through the specimen and delivers a heterodyne current as an output. The current, which contains the Fresnel zone-lens plate (FZP) coded information of the specimen, is then mixed down to become a demodulated signal and stored on a computer. The stored image is an on-axis FZP-coded image or essentially a hologram which contains the 3-D information of the specimen. In the reconstructing or decoding stage, the stored hologram in the computer could be sent to a display and photographed as a transparency. A laser then illuminates the transparency to reconstruct a 3-D image. The coded image can also be reconstructed both digitally and optically. To reconstruct the

image at some depth, the coded image is simply treated with a filter matched to the depth required. We shall now describe the two stages in more detail.

3.3 Recording Stage

We need to create a time-dependent Fresnel zone-lens plate (TDFZP). Fig. 3.4) shows a version of the practical implementation. The two beamsplitters and the two mirrors form a standard interferometer configuration. Lens L1 is inserted in the lower arm of the interferometer to produce a spherical wave on the thick specimen, whereas an acousto-optic frequency shifter in the lower arm provides a frequency shift Ω of the incident plane wave [27]. Thus, a time-dependent zone-lens-plate created by the interference of mutually coherent spherical and plane wavefronts is formed on the specimen. The intensity pattern of the TDFZP is thus given by the following expression:

$$\left|A\exp(j\omega_0 t) + B\left(\tfrac{jk_0}{2\pi z}\right)\exp[-jk_0(x^2+y^2)/2z]\exp[j(\omega_0+\Omega)t]\right|^2 \qquad (3.1)$$

where A and B are some constants, representing the amplitude of the plane wave and the diverging spherical wave, respectively. k_0=2π/λ is the light wave number and ω_0 and ω_0+Ω are the temporal frequencies of the plane wave and the spherical wave, respectively. z is a depth parameter measured away from the focal plane of lens L1, as indicated in Fig. 3.4). Equation (3.1) can be expanded and written as

$$I(x,y,\Omega) = A^2 + C^2 + 2\,A\,C\sin\left[\tfrac{k_0}{2z}(x^2+y^2) - \Omega t\right], \qquad (3.2)$$

Where $C = B\,k_0/2\pi z$. In writing (3.2), we have assumed that $\omega_0 \gg \Omega$; hence the wave numbers of the spherical wave and the plane wave are treated to be the same and equal to k_0. Note that the expression of (3.2) is a familiar zone-lens plate (FZP) expression [25] but has a time-dependent variable. We shall call it a time-dependent FZP (TDFZP). This TDFZP is now used to scan the thick specimen in two dimensions. Lens L2 simply serves as a collector that focuses the transmitted light on the photodetector. For the sake of explaining the concept, let us assume that a single off-axis point object $\delta(x - x_0, y - y_0)$ is located z_0 away from the focal plane of lens L1. The scanning of the TDFZP on the point object will cause the photodetector to deliver a heterodyne current i(x,y) [28] :

$$i(x,y) \sim \sin\{\tfrac{k_0}{2z_0}[(x - x_0)^2 + (y - y_0)^2] - \Omega t\} \tag{3.3}$$

After electronic multiplying with cos(Ωt) and bandpass filtering at Ω, the scanned demodulated electrical signal i_d , as indicated in Fig. 3.4), is given by

$$i_d(x,y) \sim \sin\{\tfrac{k_0}{2z_0}[(x - x_0)^2 + (y - y_0)^2]\}, \tag{3.4}$$

where x and y in the above equation are determined by the motion of the scanning mechanism. Note that the electrical signal i_d contains the location (x_0, y_0) as well as the depth (z_0) information of the off-axis point object. If this scanned demodulated signal is stored in synchronizm with the xy scan signals of the scanning mechanism, what is stored is then a 3-D information of the specimen. The stored information is effectively a FZP-coded information or a hologram with transmission function t(x,y) given by

$$t(x,y) \sim \text{constant bias} + i_d$$
$$\sim 1 + \sin\left\{ \frac{k_0}{2 z_0} [(x - x_0)^2 + (y - y_0)^2] \right\} \qquad (3.5)$$

Note that in the above expression, a constant bias has been added to i_d to preserve phase information so that the hologram can be stored in a square-law device such as films or displayed in a monitor. We shall describe the hardware used for recording in the following section in detail. The pattern shown in (3.5) is immediately identified as a hologram of a point source, i.e., a zone-lens-plate. The center of the zone plate specifies the location x_0 and y_0 of the point object, and the chirp rate of the zone plate allows us to deduce the depth information z_0 . The principle of this novel coding technique has been demonstrated by Duncan and Poon for 1-D objects [2]. Recently, 2-D experiment has also been demonstrated [3]. We shall demonstrate 3-D imaging capability of the system.

3.4 Reconstruction Stage

Reconstruction of the coded image can be achieved optically by producing a transparency of the coded image, illuminating it with coherent light and observing the diffraction pattern at some distance, z, away. Mathematically, this can de described as multiplying the point-source hologram, t(x,y), with a plane wave of wavelength λ_0 and propagating the resulting field using diffraction theory. As propagation of light wave through free space is equivalent to a linear operation with the filter response [commonly known as a free-space impulse response, 11] given by

$$h(x,y; z; k_0) = \frac{j k_0}{2\pi z} \exp (- j k_0 (x^2 + y^2)/ 2 z) . \qquad (3.6)$$

The complex field distribution f(x,y) at a distance z away from the hologram is given by the convolution of the wave emerging from the the hologram and h(x,y; z; k_0) as

$$f(x,y) = t(x,y) * h(x,y;z,k_0)\,, \tag{3.7}$$

where $*$ denotes the convolution operation. One of the advantages of optical scanning holography is the introduction of the constant bias during recording, as opposed to the spatially variant bias present in standard holographic recording. Specifically, in standard holographic recording, $|O+R|^2$ is recorded, where O and R represent the wavefronts of the object and the reference waves, respectively, on the surface of the recording material. We see that $|O+R|^2 = |O|^2 + |R|^2 + O R^* + O^* R$, where the first two terms are the spatially variant bias recorded in the hologram which produces annoying effects in on-axis holography when the image is reconstructed. These terms also cause unnecessary information to be recorded and stored in the hologram, which is undesirable in off-axis holography. Since the bias term in optical scanning holography is constant, less spatial resolution is required of the recording medium to achieve a higher quality reconstructed image. Indeed, the idea of eliminating the conventional holographic bias term is commonly used in computer generated holography (CGH). This is an issue of major concern in TV transmission of holographic information as well as in SLM-based holography.

If reconstruction is to be performed numerically, the digitally stored hologram can be convolved by the filter response, h(x,y; z; k_0), at the desired plane of interest, z. By selecting different planes of interest, we bring different depths of the thick specimen into focus, effectively viewing plane slices of the specimen. We have successfully achieved numerical reconstruction of holograms recorded in this manner, and will report our

results in the next section. Up to this point, we have discussed the recording and reconstruction of a point object using the principle of optical scanning holography(OSH). The OSH principles we have discussed are valid not only for point objects, but also for three dimensional objects as well in general, since any objects can be decomposed into a collection of points. The mathematical derivation is readily expandable to higher dimensions [2].

3.5 Holographic Magnification

If the hologram is recorded by optical scanning holography using the scanning beam given by (3.1), and if the reconstruction is performed by standard optical illumination with a reconstruction beam, the aspects of image reconstruction, magnification are well-documented [21, 29-31]. In addition, magnification and third-order aberration have also been studied [32]. However, in actuality, since optical scanning holography employs optical scanning to acquire holographic information of the object, the shape of the optical scanning beam plays an important role in the recording process. Analysis of optical scanning holography based on the interaction of Gaussian beams has been studied [2].

In this section, we shall derive 3-D holographic magnification in the context of OSH. We consider three point objects given by

$$\delta(x,y;\, z-z_0) + \delta(x-x_0,y;\, z-z_0) + \delta(x,y;\, z-(z_0+\Delta z_0)) , \tag{3.8}$$

where the first two points are located z_0 away from the focal plane of lens L1 with lateral separation x_0, and the third point is located $z_0+ \Delta z_0$ away from the first two points.

When this three-point object is scanned, the scanned demodulated electrical signal i_d is given by

$$i_d \sim \sin\left[\frac{k_0}{2z_0}(x^2+y^2)\right] + \sin\left\{\frac{k_0}{2z_0}[(x-x_0)^2+y^2]\right\} + \sin\left[\frac{k_0}{2(z_0+\Delta z_0)}(x^2+y^2)\right]. \quad (3.9)$$

Hence the transmission function of the hologram of the three-point object becomes

$$t_{3D}(x,y) = C + \sin\left[\frac{k_0}{2z_0}(x^2+y^2)\right] + \sin\left\{\frac{k_0}{2z_0}[(x-x_0)^2+y^2]\right\} + \sin\left[\frac{k_0}{2(z_0+\Delta z_0)}(x^2+y^2)\right], \quad (3.10)$$

where C is again a constant necessary to properly bias the hologram. If this hologram is illuminated by a plane weave at λ_0 , the three points will be reconstructed at their perspective locations. We now consider holographic magnification.

3.5.1 Hologram Scaling

As mentioned in the previous sections, magnification can be achieved by enlarging holograms, but it is a difficult task especially dealing with off-axis holograms in which fringes density is of the order of 1,000 lines/mm and most photographic enlargers do not have sufficient resolution to handle these details. Hence the method is not practical. In our scanning technique, however, on-axis holograms are generated and scaling is straightforward. The hologram can be scaled by a factor M, simply by displaying the hologram in an area that is different from the optical scan area. In this case, (3.10) becomes

$$t_{3D}(Mx, My) = C + \sin\left[\frac{k_0}{2z_0}(Mx)^2 + (My)^2)\right] + \sin\left\{\frac{k_0}{2z_0}\left[(Mx - x_0)^2 + (My)^2\right]\right\}$$
$$+ \sin\left\{\frac{k_0}{2(z_0+\Delta z_0)}\left[(Mx)^2 + (My)^2\right]\right\}. \quad (3.11)$$

For M<1, we have magnification and M>1 corresponds to demagnification. Rewriting (3.11), we have

$$t_{3D}(Mx, My) = C + \sin\left[\frac{k_0}{2z_0/M^2}(x^2 + y^2)\right] + \sin\left\{\frac{k_0}{2z_0/M^2}\left[(x - x_0/M)^2 + y^2\right]\right\}$$
$$+ \sin\left\{\frac{k_0}{2(z_0+\Delta z_0)/M^2}(x^2 + y^2)\right\}. \quad (3.12)$$

For optical reconstruction with wavelength λ_0, we see that by inspection of the second and third term in (3.11), the two real image points are now formed at a distance z_0/M^2 away from the hologram, and with reconstructed lateral distance x_0/M away from each other. Defining the lateral magnification M_{lat} as the ratio of the reconstructed lateral distance to the original lateral distance x_0 , we have $M_{lat}=1/M$. To determine the magnification along the longitudinal direction, we inspect the second and the fourth terms and see that the two points are reconstructed at z_0/M^2 and $(z_0+\Delta z_0)/M^2$, respectively. Defining the longitudinal magnification M_{long} as the ratio of the reconstructed longitudinal distance $\Delta z_0/M^2$ to the original longitudinal distance Δz_0 , we have $M_{long}=1/M^2$.

3.5.2 Wavelength Scaling

We could reconstruct the hologram with different wavelength, say $m\lambda_0$ (or k_0/m), where m is a constant. Hence the field distribution at z away from the hologram is now given by

$$
\begin{aligned}
& t_{3D}(x,y) * h(x,y; z, k_0/m) \\
& \quad = \{C + \sin\left[\frac{k_0}{2z_0}(x^2+y^2)\right] + \sin\left\{\frac{k_0}{2z_0}\left[(x-x_0)^2+y^2\right]\right\} \\
& \quad + \sin\left[\frac{k_0}{2(z_0+\Delta z_0)}(x^2+y^2)\right]\} * \frac{jk_0/m}{2\pi z}\exp\left[-j\frac{k_0/m}{2z}(x^2+y^2)\right] \qquad (3.13)
\end{aligned}
$$

This suggests that there will be no magnification in the lateral direction. For longitudinal direction, considering real image reconstruction again, the second and the third term will form the image at $z=z_0/m$. The third term gives rise to a real image at $z = (z_0+\Delta z_0)/m$. Hence, in this case $M_{lat}=1$, and $M_{long}=1/m$. The reconstructed volume is compressed or expanded by a factor of 1/m with the same lateral magnification [32]. For m>1, we have compression. With visible light for recording and reconstruction, m is in the range of 0.5 to 1.8. However, using digital reconstruction, m can be picked arbitrarily large.

3.5.3 Reconstruction Combining Hologram Scaling and Wavelength Scaling

If both the scaled change of the hologram and the use of different wavelength for reconstruction, the combined magnification along the lateral and longitudinal direction will be $M_{lat}=1/M$ and $M_{long}=1/mM^2$. We thus see that the reconstructed volume $x_0\ \Delta z_0/mM^3$ is different from the original volume $x_0\ \Delta z_0$. These are well-known results for conventional holography. For reconstruction having a true 3-D perspective, if the scale change of the hologram is given by M, we should let m=1/M which gives $M_{lat}=m$, and $M_{long}= m$ and therefore $M_{lat}= M_{long}= m$. In other words, to achieve no distortion in 3-D

imaging, when we scale the hologram by a factor M, the reconstructing wavelength should be $m\lambda_0$, where λ_0 is the recording wavelength and m should be equal to 1/M. This is the original idea of Gabor who first conceptualized it in the pre-laser era to improve the electron microscope [20] . Indeed electron microscopy was the motivation for the development of holography.

3.6 System and Three-dimensional Imaging Results

We shall first describe the components and the hardware used in the holographic system and then present optical holographic recording and digital reconstruction results of a 3-D object. With reference to Fig. 3.4, the HeNe laser beam has a beam waist $w \sim 1$ mm. The two collimators have 10-X magnification. With the focal length f=17.5 cm in lens L1, the focused spot on the 2-D scanning mirror is $\lambda f/\pi w \sim 3.5$ μm as λ =0.63 μm for HeNe laser. This focused spot will serve as a point source and the output of the other collimator will serve as a plane wave of the size of about 10 mm. The frequency difference between the plane wave and the spherical wave is provided by the acousto-optic frequency shifter operating at 40 MHz. The scanning frequencies of the x- and y-scan of the 2-D galvanometers scanner are about 10 Hz and 10/512 Hz, respectively. Hence the hologram consists of 512 scan lines. For the 3-D object, it consists of two transparencies of letter "V" and "T", located side by side but separated by a depth distance of about 15 cm with "V" located closer to the 2-D scanner at a distance of about 23 cm, i.e., z = 23 cm. Both letters are approximately 0.4 mm by 0.4 mm, has line width of about 100 μm, and are transmissive on an opaque background. After 2-D scanning of the object, the demodulated current i_d carrying the holographic information is sent to the Image Processing and Measuring System (IPMS) [33]. The IPMS is a digital

storage/interface device which accepts a slow-scan electrical signal, such as i_d in our case, store the holographic information in its digital memory and then converts this information into a NTSC video signal. This standardized video can now be delivered to a TV monitor for displaying the hologram or could be delivered to a remote site through a cable. Fig. (3.5) displays a typical hologram of a pinhole object achievable with the optical scanning system. The display is a well-known zone-lens-plate, the hologram of a point object. In fact this approximates an impulse response of our scanning system. The pinhole is about 50 μm in diameter and at a distance about 10 cm away from the 2-D scanning mirror. Another way to deliver the holographic information to a remote site may employ wireless transmission. This could be easily done as the holographic information right at the output of the tuned amplifier i(x,y) is riding on a 40 MHz temporal carrier [see eq.(3.3)]. This information could be directly radiated by an antenna, indeed a viable scheme for TV transmission of holographic information. The output of the IPMS could be switched to a personal computer (PC) for digital reconstruction. For reconstruction, since the system is hybrid in nature, it is flexible and either optical method or digital method could be employed easily with the system. Optical reconstruction has been demonstrated for 2-D reconstruction using a spatial light modulator [3]. We shall demonstrate digital reconstruction of a 3-D object. Fig. 3.6 displays the hologram of our 3-D object on the TV monitor, the letter "V" and "T". To extract the "V", we convolve the hologram digitally with $h(x,y; z; k_0)$ matched with the depth of the letter, as explained in the last section. This is done similarly to the letter "T". Figures 3.7(a) to 3.7(c) show the reconstruction of the hologram for three different depths.

3.7 Real-time 3-D Holographic Imaging by Using Electron-Beam-addressed Spatial Light Modulator

Real-time holographic recording by using an active optical heterodyne scanning technique has recently been studied and demonstrated [1]. Real-time application include spatial light modulator (SLM)-based holography and the transmission of holographic data for television systems. In this section, we shall demonstrate three-dimensional holographic imaging using an electron-beam-addressed spatial light modulator. The technique is based on optical scanning holography. To reconstruct the obtainable holographic information, digital techniques have been used and demonstrated [4]. For real-time reconstruction of scanned optical hologram, spatial-light-modulator-based systems need to be investigated. We present experimental results of three-dimensional image reconstruction using an electron-beam-addressed spatial light modulator (EBSLM). Results will be compared to digital methods.

3.7.1 The Electron Beam-addressed Spatial Light Modulator

Prior to discussing three-dimensional holographic reconstruction we first provide a general description of the EBSLM [34], which have been used as a real-time holographic display device. A schematic diagram of the EBSLM as it is used in a coherent light conversion system is shown in figure 3.8. Here we see that a serial video signal is the required input to the EBSLM controller (Hamamatsu model C3637). The controller in turn provides the signal which intensity modulates the emission from the electron gun within the EBSLM head (Hamamatsu model X3636). This electron beam is then two-dimensionally scanned onto the surface of a 55-degree cut $LiNbO_3$ crystal with a deflection coil. As a result, electric charges accumulate on the surface of the crystal. Through the Pockets effect then, the field associated with the charges changes the refractive index of the crystal on a point-by-point basis. To read out these results, a

linearly polarized laser is used to illuminate the crystal from an external source. In the coherent light conversion technique, a pointwise varying elliptical polarization due to the corresponding pointwise change in refractive index change of the crystal is manifest within the reflected light. By passing this reflected light through an analyzer, a converted coherent image is obtained [34]. We mention that after being written onto the EBSLM, the hologram in essence appears as a coherently back illuminated transmittance function in the plane of the analyzer of figure. The reconstructed real object image then can be found a distance zM_{long} in front of the analyzer, where z is the distance, shown in figure, at which the object is initially scanned and M_{long} is the longitudinal magnification of the holographic imaging system arising due to various scaling factors which discussed in section 3.5.

3.7.2 Real-time Reconstruction of Scanned Optical Holograms

Note that the demodulated signal expressed as Eq. 3.4 contains the location (x_0, y_0) as well as the depth (z) of the off-axis point object. To preserve the phase of i_d, a dc bias signal is added before feeding i_d to the Image Processing and Measuring System (IPMS) [33]. The real-time Optical Scanning Holography Imaging System is shown in Fig. 3.9. The IPMS is a digital storage device and then converts this information into a NTSC video signal. This video signal now be delivered to a TV monitor for displaying the hologram as shown in figure 3.5. The hologram of the object is thus presented on the 2-D display. For reconstruction, the IPMS subsequently delivers a video signal to the electron-beam-addressed spatial-light modulator (EBSLM) for immediate coherent reconstruction. The EBSLM is used as a coherent-light conversion system.

The EBSLM accepts a serial video signal that intensity modulates the emission from the electron gun within the modulator. This electron beam is then scanned onto the surface of a $LiNbO_3$ crystal. Consequently, electric charges accumulate on the surface of the crystal, and the hologram is stored as a charge pattern on the crystal. A linearly polarized light then illuminates the crystal for image reconstruction of the hologram. By passing the reflected light through an analyzer, a reconstructed image of the hologram is observed through the movable CCD camera which in turn display the image on the TV monitor. Fig. 3.6 displays the hologram of 3-D object on the TV monitor, the letter "V" and "T". Figures 3.10 to 3.12 show the real-time reconstruction of the hologram using an electron beam addressed spatial light modulator. Note the similarity between the image of digital reconstruction and that of optical reconstruction.

3.8 Concluding Remarks

We have discussed optical scanning holography (OSH) and its application to 3-D microscopy. Specifically, we have elucidated the concept by analyzing the recording and reconstruction of point objects. The principle of OSH is based on optical heterodyning scanning and therefore is an electro-optical hybrid system which is real-time in nature. We have also derived holographic magnification in the context of OSH and shown how hologram scaling and wavelength scaling can be accomplished easily with this hybrid system. To demonstrate that depth information is stored in a hologram recorded using the OSH system, a single hologram was recorded of two transparencies at different depths. The 3-D image was numerically reconstructed at different depths in order to demonstrate how a single plane can be brought into focus, effectively reconstructing one slice of the

object or a thick specimen at a time. We reiterate that with the OSH system, only a single 2-D raster scan is required to store the 3-D information. The usefulness of the OSH is not limited to the microscopy field. In fact, OSH is especially suited for generating holograms of large-scale objects owing to the inherent qualities of scanning, efficient light utilization and ambient light rejection. This can lead to applications in 3-D optical remote sensing and 3-D robotic vision. Finally, the information reduction and the hybrid property inherent in the OSH technique may make it a viable scheme for the transmission of holographic information for television systems.

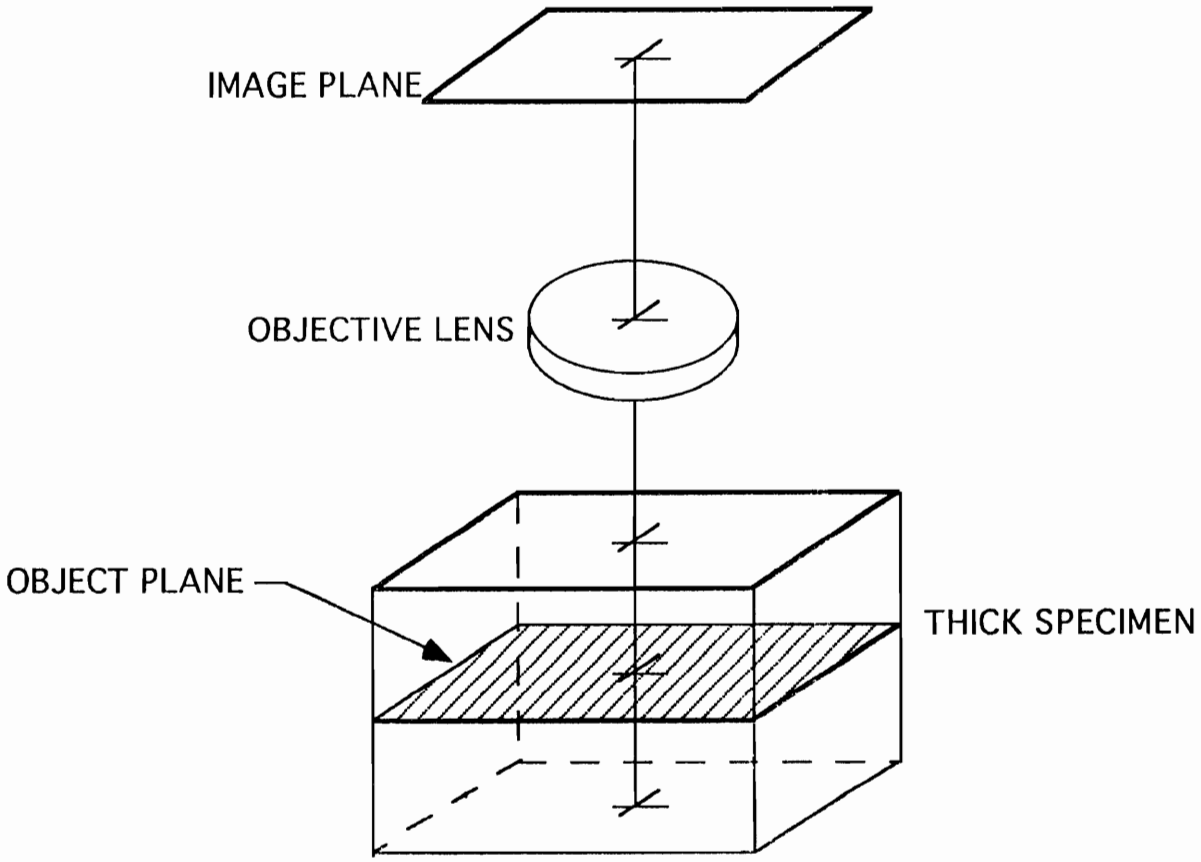

Fig. 3.1 Principle of optical sectioning

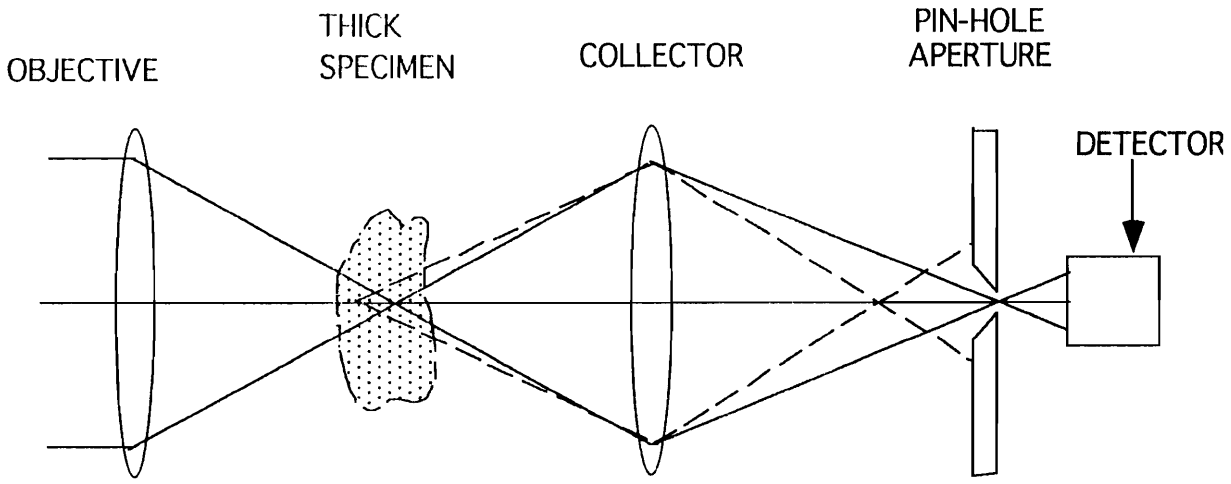

Fig. 3.2 Principle of scanning confocal holography

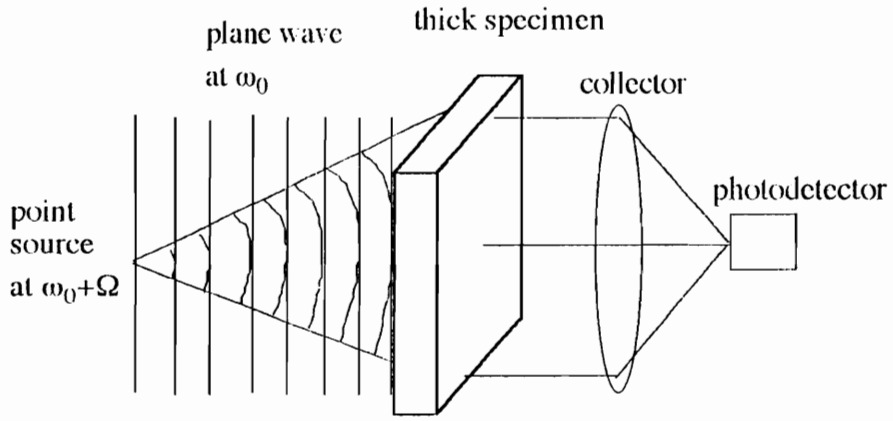

Fig. 3.3 Principle of optical scanning holography (The specimen is 2-D scanned)

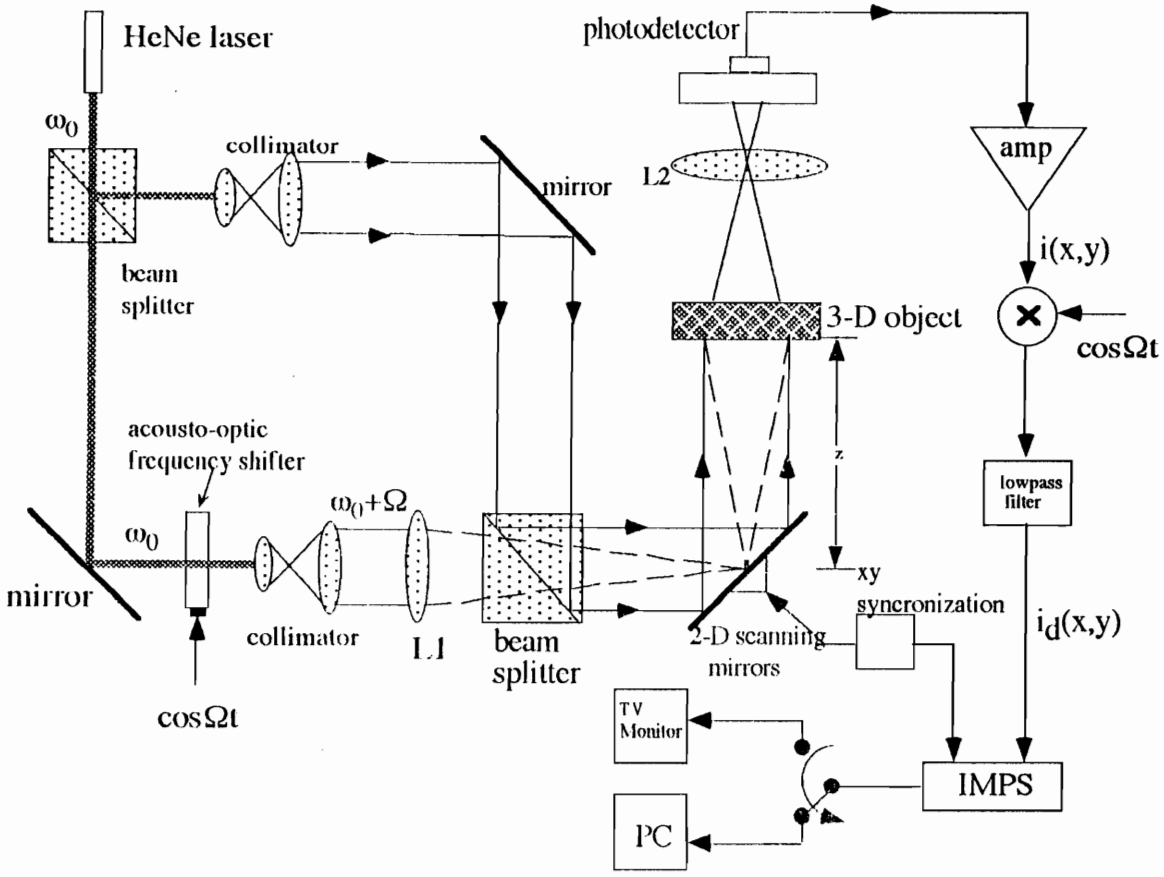

Fig. 3.4 Practical implementation of optical scanning holography

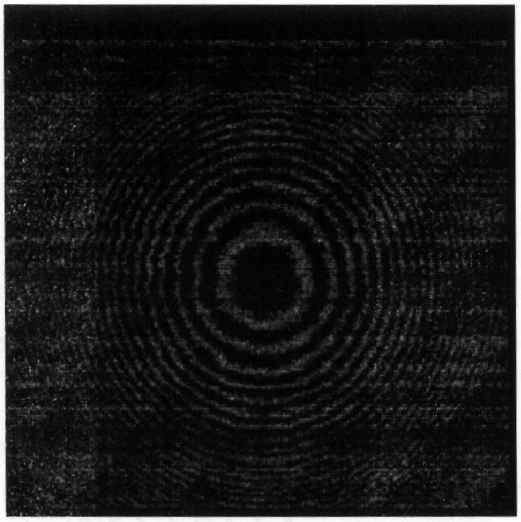

Fig. 3.5 Typical hologram of a point source object achievable with the system shown in Fig. 3.4

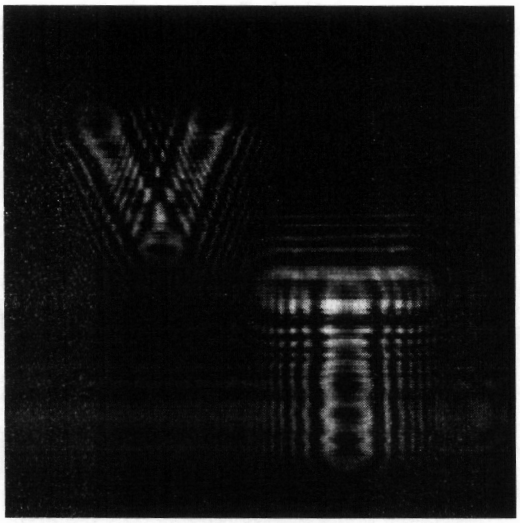

Fig. 3.6 Hologram of two letters "V" and "T", located at different depths.

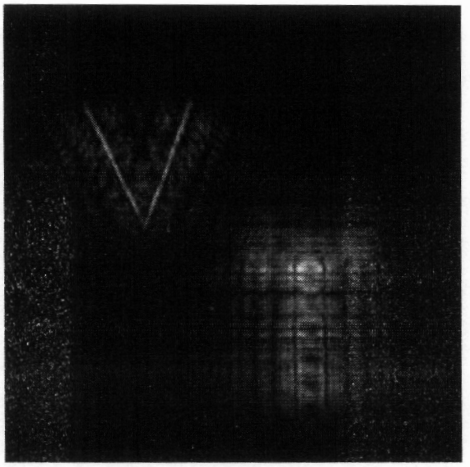

(a)

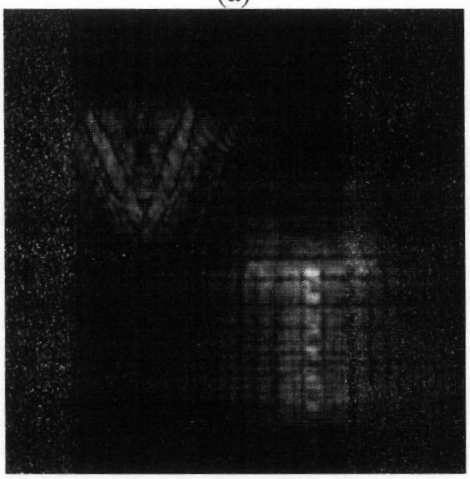

(b)

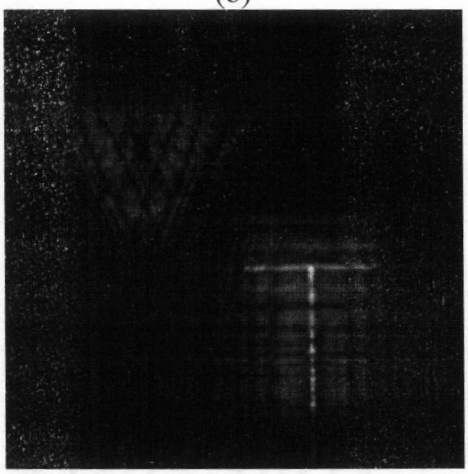

(c)

Fig. 3.7 Digital reconstruction of Fig. 3.6 through different depths. Fig. 3.7a) shows that "V" is in focus, while Fig. 3.7c) shows that "T" is in focus.

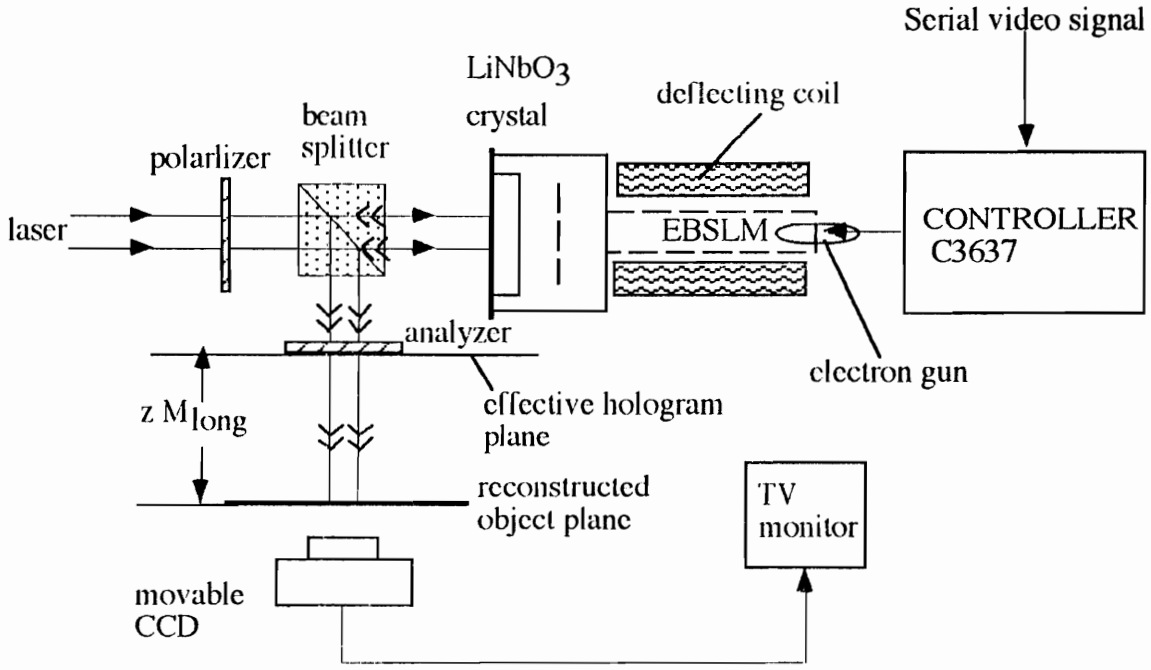

Fig. 3.8 Diagram of the electron beam-addressed spatial light modulator (EBSLM) [4]

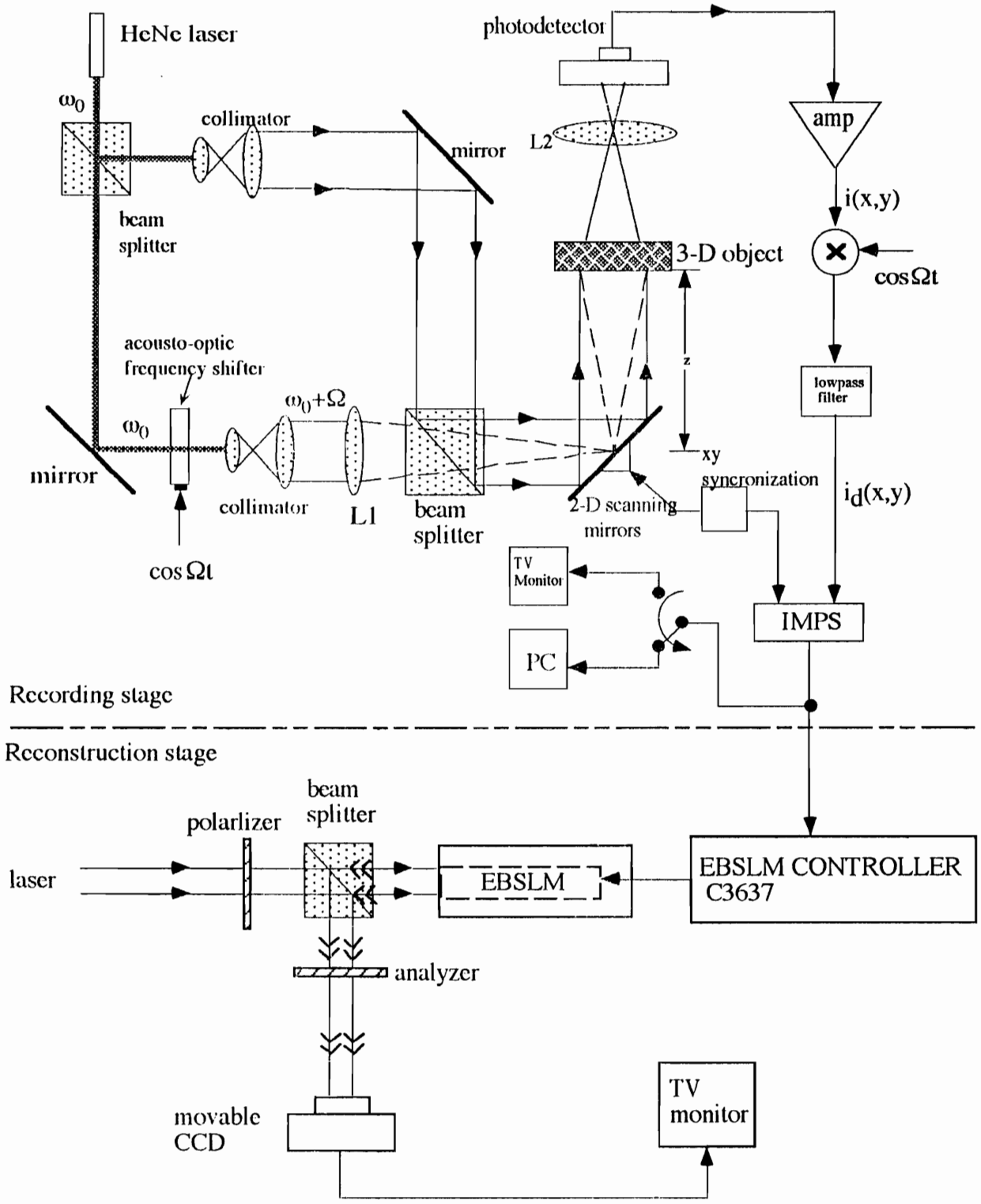

Fig. 3.9 Optical scanning holographic system with EBSLM

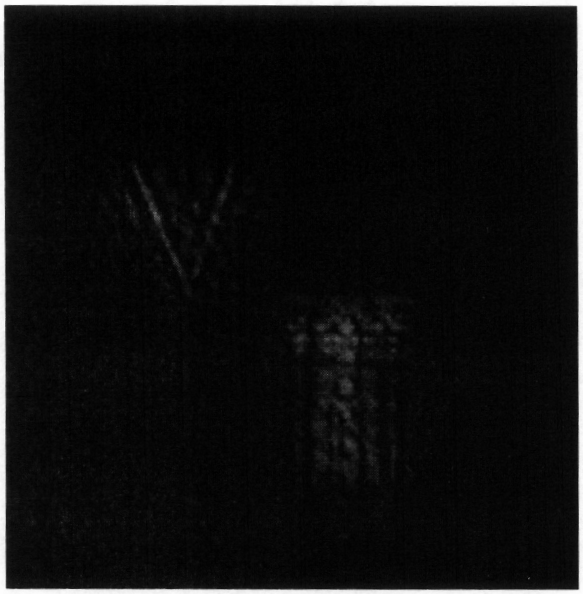

Fig. 3.10 Optical reconstruction of Fig. 3.6 in conjuction with the EBSLM. It shows that "V" is in focus

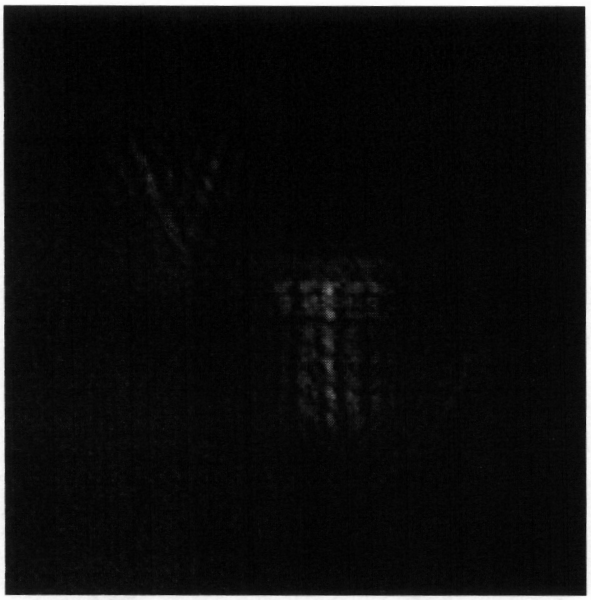

Fig. 3.11 Optical reconstruction of Fig. 3.6 in conjuction with the EBSLM. It shows that the focus is between "VT" is in focus

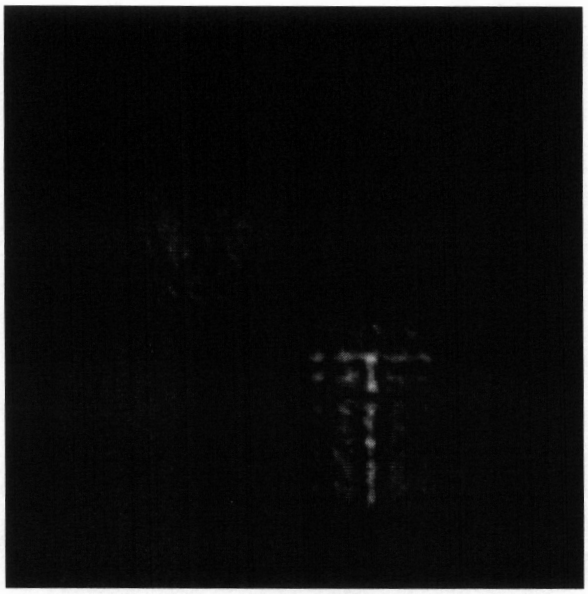

Fig. 3.11 Optical reconstruction of Fig. 3.6 in conjuction with the EBSLM. It shows that "T" is in focus

CHAPTER 4: TWIN-IMAGE NOISE IN OPTICAL SCANNING HOLOGRAPHY

In optical scanning holography, holographic information of an object is generated by 2-D active optical scanning. The optical scanning beam can be a time-dependent Gaussian apodized Fresnel zone pattern. We first discuss in detail the origin of twin-image. Then we derive the resolution achievable with a scanning beam. We show through computer simulations that the use of a larger Fresnel zone pattern for holographic recording leads to a noisier twin image reconstruction in the near field, thereby degrading the resolution. This is particularly noticeable with objects of complicated structures.

4.1 Introduction

Electronic holography is a technique in which electronic processing is used in the context of holography, allowing holographic recording to be performed in real time,

bypassing the use of films for recording [35-41]. Thus electronic holography lends itself to real-time applications. In this chapter, we concentrate on one type of electronic holography in which an active optical heterodyne scanning technique is used to achieve holographic recording. Two main features of this technique known as optical scanning holography (OSH) are that the recording is incoherent (phase insensitive) and that a large area detector can be used. [2,42]. Specifically, in this chapter we investigate the effects of the size of the scanning beam in relation to twin-image noise upon image reconstruction.

4.2 Origin of Twin-Image

It is well known in optics that if we describe the amplitude and phase of a light field in a plane, say $z = 0$, by a complex function $\psi(x, y)$, we can obtain for the light field a distance away, $z = z_0$, according to Fresnel diffraction

$$\psi(x, y; z_0) = \psi(x, y) * h(x, y; z = z_0) \tag{4.1}$$

where the symbol $*$ denotes convolution and $h(x, y; z)$ is called the free space impulse response given by

$$h(x, y; z) = \frac{jk_0}{2\pi z} exp(-jk_0(x^2 + y^2)/2z). \tag{4.2}$$

In (4.2), $k_0 = 2\pi/\lambda$, λ being the wavelength of the light field. Now, let's model the point object at a distance z_0 from the recording film by an offset delta function, i.e.,

$\psi(x,y) = \delta(x - x_0,\ y - y_0)$. According to (4.1), the object wave arises from the point object on the film is given by

$$\psi_o = \psi(x,y;z_0) = \frac{jk_0}{2\pi z_0} exp\{ - jk_0[(x - x_0)^2 + (y - y_0)^2]/2z_0\} \tag{4.3}$$

This object wave is spherical wave.

For the reference plane wave, the field distribution is constant on the film, say, $\psi_r = a$ (a constant) for simplicity. Hence the intensity distribution being recorded on the film is

$$\begin{aligned} t(x,y) &= \left|\psi_r + \psi_o\right|^2 \\ &= \left|a + \frac{jk_0}{2\pi z_0} exp\{ - jk_0[(x - x_0)^2 + (y - y_0)^2]/2z_0\}\right|^2 \\ &= A + Bsin\{\frac{k_0}{2z_0}[(x - x_0)^2 + (y - y_0)^2]\} \end{aligned} \tag{4.4}$$

where $A = a^2 + (\frac{k_0}{2\pi z_0})^2$ and $B = \frac{ak_0}{\pi z_0}$. This expression is called a Fresnel zone plate (FZP), which is the hologram of a point object and we shall call it a point-object hologram. Note that the center of the zone plate specifies the location x_0, and y_0 of the point object and the spatial variation of the zone plate is governed by a sine function with a quadratic spatial dependence. Hence, the spatial rate of change of the phase of the zone plate, the fringe frequency, increases linearly with the spatial coordinates, x and y. The fringe frequency then depends on the depth parameter, z_0. In communications and radar, a 1-D version of this signal is known as a chirp signal. If the reference wave were not there as in conventional photography, what is recorded on the film is $t(x,y) = \left|\psi_o\right|^2 = (\frac{k_0}{2\pi z_0})^2$ which is a uniform intensity pattern. The 3-D information, i.e., x_0, y_0, and z_0, is mostly lost. For an arbitrary 3-D object, we can think of the object as a

collection of points and therefore we can envision that we have a collection of zones on the hologram, with each zone carrying the transverse location as well as the depth information of each individual point.

We have discussed the transformation of a point object to a zone plate on the hologram and this corresponds to a coding process. In order to decode it, we need to obtain the point object back from the hologram. This can be done by simply illuminating the hologram with a reconstruction wave as shown in Fig. 4.1. Fig. 4.1 corresponds to the reconstruction of a hologram of the point object located on-axis, for the simple case where $x_0 = y_0 = 0$.

Note that in practice, the reconstruction wave usually is identical to the reference wave, therefore we assume the reconstruction wave to have a field distribution on the plane of the hologram given by $\psi_{rc}(x, y) = a$. Hence, the field distribution of the transmitted wave immediately after the hologram is $\psi_{rc}(x, y)t(x, y) = at(x, y)$ and the field at arbitrary distance of z away is according to (4.1), given by the evaluation of $at(x, y) * h(x, y; z)$. For the point-object hologram given by (4.4), we have, after expanding the sine term of the hologram $t(x, y)$.

$$t(x,y) = A + \frac{B}{2j}\Big\{exp\Big\{j\frac{k_0}{2z_0}[(x-x_0)^2 + (y-y_0)^2]\Big\} - exp\Big\{-j\frac{k_0}{2z_0}[(x-x_0)^2 + (y-y_0)^2]\Big\}\Big\}. \tag{4.5}$$

Therefore, we have three terms resulting from the illumination of the hologram by the reconstruction wave. These contributions at $z = z_0$, according to the convolution operation, $at(x, y) * h(x, y; z_0)$, are as follows.

First term:

$$aA * h(x, y; z = z_0) = aA \tag{4.6a}$$

Second term:

$$\begin{aligned} & exp\left\{\mathrm{j}\tfrac{k_0}{2z_0}[(x - x_0)^2 + (y - y_0)^2]\right\} * h(x, y; z = z_0) \\ & = exp\left\{\mathrm{j}\tfrac{k_0}{2z_0}[(x - x_0)^2 + (y - y_0)^2]\right\} * \tfrac{jk_0}{2\pi z_0} exp\{ - jk_0(x^2 + y^2)/2z_0\} \\ & \sim \delta(x - x_0,\ y - y_0)\text{(real image)} \end{aligned} \tag{4.6b}$$

Third term:

$$\begin{aligned} & exp\left\{\mathrm{j}\tfrac{k_0}{2z_0}[(x - x_0)^2 + (y - y_0)^2]\right\} * h(x, y; z = \text{-}z_0) \\ & = exp\left\{\text{-}\mathrm{j}\tfrac{k_0}{2z_0}[(x - x_0)^2 + (y - y_0)^2]\right\} * \tfrac{jk_0}{2\pi(\text{-}z_0)} exp\{jk_0(x^2 + y^2)/2z_0\} \end{aligned} \tag{4.6c}$$

Returning to (4.6b), this term is the reconstructed real image. In order to reconstruct the point image, the filter response $h(x, y; z; k_0)$ should match to the depth distance z_0 in front of the hologram. To see this, we evaluate the third term at $z = -z_0$ and that gives

$$\begin{aligned} & \sim exp\left\{ - j\tfrac{k_0}{2z_0}\left[(x - x_0)^2 + (y - y_0)^2\right]\right\} * h(x, y; z = -z_0, k_0) \\ & = exp\left\{ - j\tfrac{k_0}{2z_0}\left[(x - x_0)^2 + (y - y_0)^2\right]\right\} * j\tfrac{k_0}{2\pi(-z_0)} exp\left[+ j\tfrac{k_0}{2z_0}(x^2 + y^2)\right] \\ & \sim \delta(x - x_0, y - y_0)\text{,(virtual image)} \end{aligned} \tag{4.6d}$$

In the terminology of holography, the first term is the zero-order beam due to the bias in the hologram. The result of the second term is called the real image and the third term is

the virtual image. Note that the real image and the virtual image are located at a distance z_0 in front and back of the hologram, respectively. The virtual image and the real image are formed along the same axis, illustrating the problem of twin image. This situation is shown in Fig. 4.1.

4.3 Fresnel Zone Plate and Resolution

Consider a spherical wave of wavelength λ, traveling from left to right as shown in Fig. 4.2. The spherical wave is produced by a point source and is assumed to be incident on the plate. The wavefront at a given instant of time may be divided into a number of concentric zones in such a way that each zone is one-half of a wavelength farther away from point O. If the distance from the wavefront to O is S, the distances from successive boundaries between zones to O are given by

$$S+\tfrac{\lambda}{2},\ S+\tfrac{2\lambda}{2},\ S+\tfrac{3\lambda}{2},\ \ldots\ S+\tfrac{m\lambda}{2} \tag{4.7}$$

Let R_m be the radius of the m-th boundary. Then R_m is given by

$$R_m = \sqrt{(S + m\tfrac{\lambda}{2})^2 - S^2} \tag{4.8}$$

Usually, these are either opaque or transparent, that is, Fresnel zone plates. This result was obtained by integration over all waves passing through the circular opening. The boundaries between zones have radii that are proportional to the square root of the integer number,

$$R_m = R_1\sqrt{m} \quad m = 1, 2, 3, \ldots \tag{4.9}$$

where R_1 is the radius of the innermost boundary. From Eq. 4.8

$$S^2 = (S + m\tfrac{\lambda}{2})^2 - R_m^2 \qquad R_m^2 \approx mS\lambda \tag{4.10}$$

Since λ is small compared with S, the term λ/S may be neglected. However S is also the focal length of the zone plate because of its focusing properties. Thus

$$f = \frac{R_m^2}{m\lambda} \tag{4.11}$$

A zone lens does act both as a positive and a negative lens. Its focal length is $\pm f$. That is because light diffracted at the boundaries will be diffracted not only toward the optic axis, but away from it as well. Now consider Fig. 4.3 in which Fresnel zone plates have R_m and R_n as radii of the boundary and f_l and f_s are their focal lengths respectively. According to Eq. 4.11 we can have

$$f_l = \frac{R_m^2}{M\lambda} \qquad f_s = \frac{R_n^2}{N\lambda} \tag{4.12}$$

where M, N are the integer. Resolution limit is defined as $R \approx \frac{\lambda}{\theta}$. In order to make the two zone lens to give the same resolution on image reconstruction, we need to have

$$(R)_l = (R)_s \qquad \frac{f_l}{D_l}\lambda = \frac{f_s}{D_s}\lambda \qquad \frac{M}{N} = \frac{R_m}{R_n} \tag{4.13}$$

which shows that the ration of the number of zones is inversely proportional to that of the radius of the zone lens plate.

4.4 Theory of Optical Scanning Holography

To achieve holographic recording using active optical scanning, a temporally modulated Fresnel zone plate is used as a 2-D scanning beam on the object. A photodetector collects the scattered light and delivers a current which, after demodulation, is synchronized with the x and y scans of the x-y optical scanning system and then fed to a 2-D monitor for display. What is displayed is a hologram. The hologram can be reconstructed by a spatial light modulator in real time [3], or can be reconstructed by a computer [4]. To create a temporally modulated Fresnel zone plate, one may superpose a planar and a spherical wave of different temporal frequency. In practice, a broad and a narrow Gaussian beam are combined with a beamsplitter [2]. One of the Gaussian beams is frequency-shifted so that the two beams interfere to form a temporally modulated Gaussian apodized Fresnel zone plate $S(x, y; z; t)$ at the location of the object $I(x, y; z)$:

$$S(x, y; z; t) = b(x, y; z) + exp(-(\frac{x^2+y^2}{w^2}))\, sin\big(\frac{k_o}{2z}(x^2 + y^2) + \Omega t\big), \qquad (4.14)$$

where k_o is the wave number of the light and z is the distance measured away from the waist of the narrow beam to the location of the object $I(x, y; z)$, as shown in Fig. (4.4). $b(x, y; z)$ is the DC term and the AC term, modulated at temporal frequency Ω , is the temporally modulated Gaussian apodized Fresnel zone plate. Ω denotes the temporal frequency shift between the narrow Gaussian beam and the board Gaussian beam. The

photodetector PD integrates the scattered or transmitted light after the modulated zone-lens plate interacts with the object, $I(x, y; z)$, to give a current

$$i(x, y; z; t) \sim \int\int_A I(x', y'; z) S(x(t) - x', y(t) - y'; z; t)\, dx' dy'$$

$$\begin{aligned} &= S(x, y; z; t) * I(x, y; z) \\ &= b(x, y; z) * I(x, y; z) + I(x, y; z) \\ &\quad * exp(-(\tfrac{x^2+y^2}{w^2})) sin\big(\tfrac{k_o}{2z}(x^2 + y^2) + \Omega t\big). \end{aligned} \tag{4.15}$$

Note that the integration is over the photodetector area A; $x(t)$ and $y(t)$ are determined by the xy-scanner's motion. Therefore, the convolution operation $*$ is effected by the physical scanning. The AC term can be separated by a bandpass filter (BPF) tuned at frequency Ω to give the signal $i_\Omega(x, y; z; t)$ which can be demodulated by mixing it with $\cos(\Omega t)$ and lowpass filtered to give a demodulated current $i_d(x, y; z)$:

$$i_d(x, y; z) \sim I(x, y; z) * exp(-(\tfrac{x^2+y^2}{w^2}))\, sin\,(\tfrac{k_o}{2z}(x^2 + y^2). \tag{4.16}$$

$i_d(x, y; z)$ contains the holographic information of the object being scanned. In fact it is a zone plate coded information of the object. $i_d(x, y; z)$ can be stored on a computer for digital reconstruction. If this holographic information needs to be displayed or stored on films, a constant bias b can be added to it to give a hologram of an amplitude transmittance $t(x, y; z)$:

$$\begin{aligned} t(x, y; z) &= b + i_d \\ &= b + I(x, y; z) * exp(-(\tfrac{x^2+y^2}{w^2}))\, sin(\tfrac{k_o}{2z}(x^2 + y^2). \end{aligned} \tag{4.17}$$

Note that the space-variant term $b(x, y; z)$ in $i(x, y; z; t)$ has been filtered out by the bandpass filter. Therefore, in computer simulations to be performed later, we will plot the scanning beam profile as

$$f_s(x, y; z) = S(x, y; z; t = 0) - b(x, y; z)$$

$$= exp(-(\frac{x^2+y^2}{w^2}))\, sin(\frac{k_o}{2z}(x^2 + y^2). \tag{4.18}$$

To reconstruct the hologram $t(x, y; z)$ optically, we can illuminate it with a plane wave.

Let us now concentrate on a point object reconstruction. We, therefore, let $I(x,y; z) = \delta(x, y)$ located at $z = z_0$ away from the waist of the narrow beam, the point-object hologram, according to (4.17) , is

$$t_\delta(x, y;z_o) = b + exp(-(\frac{x^2+y^2}{w^2}))\, sin(\frac{k_o}{2z_0}(x^2 + y^2)) \tag{4.19}$$

Upon plane wave illumination, the complex field distribution at a distance z away from the point-object hologram is given by

$$\psi(x, y;z) = t_\delta(x, y;z_o) * h(x, y;z)\,, \tag{4.20}$$

where $h(x, y; z)$ = exp($-jk_0(x^2 + y^2)/2z$) is the free space impulse response [13,29], neglecting some constants. By expanding (4.20), we have

$$\psi(x,y;z) \sim b * exp(-j\tfrac{k_o}{2z}(x^2+y^2))$$

$$+ \tfrac{1}{2j}exp(-(\tfrac{x^2+y^2}{w^2}))\,exp(j\tfrac{k_o}{2z_o}(x^2+y^2)) * exp(-j\tfrac{k_o}{2z}(x^2+y^2))$$

$$- \tfrac{1}{2j}exp(-(\tfrac{x^2+y^2}{w^2}))\,exp(-j\tfrac{k_o}{2z_o}(x^2+y^2)) * exp(-j\tfrac{k_o}{2z}(x^2+y^2)). \qquad (4.21)$$

At a distance $z = z_0$, the second term can be evaluated and gives rise to a real image reconstruction:

$$\psi_r = \tfrac{\pi w^2}{4}exp(-a^2w^2(x^2+y^2))\,exp(-ja(x^2+y^2)), \qquad (4.22)$$

where $a = k_0/2z_0$. Hence, a point-object gives rise to a Gaussian distribution with its waist given by $1/aw$, i.e., the resolution of the reconstructed point depends on the size of the scanning Gaussian beam, w, as well as the number of zones within the beam on the scanned object, i.e., $\sim a$. The third term in (4.21) gives a twin-image ψ_t in the $z = z_0$ plane:

$$\psi_t = \tfrac{\pi w^2}{4(1+4a^2w^4)^{1/2}}exp(-\tfrac{a^2w^2(x^2+y^2)}{1+4a^2w^4})exp[-ja(x^2+y^2)\left(\tfrac{1+2a^2w^4}{1+4a^2w^4}\right)]. \qquad (4.23)$$

The first term in (4.21) gives a constant background π/a. To find the intensity distribution on the real-image reconstruction plane, we calculate

$$I(x,y;z) = \psi(x,y;z)\psi^*(x,y;z) = |\,\pi/a + \psi_r + \psi_t\,|^2\,. \qquad (4.24)$$

We now want to investigate the effect of the parameters a and w on reconstruction based on the above equation. It is evident that the resolution limit is given by the waist of the reconstructed point and is equal to $1/aw$. The larger the scanning beam waist, w, the better is the resolution if a remains the same. Also, a larger number of zones within the Gaussian beam, i.e., the larger the a, will give a better resolution if the beam waist is the same. For a given $a \times w$, the resolution of the reconstructed image remains the same.

4.5 Computer Simulation Results

We first investigate the impulse response of the system under the condition that $a \times w =$ constant. We choose different sizes of the Gaussian waist w of the scanning beam and observe the difference in the reconstruction. In Fig. 4.5a), we plot the 1-D scanning beam profile $f_s(x;z)$, according to (4.18), with $w = 2.236$ mm and $a = 1.349$ mm^{-2}. Fig. 4.5b) shows the point-object reconstruction based on (4.24). Fig. 4.5c) plots a larger scanning beam with $3w$ and $a/3$. Note that the product of $3w$ and $a/3$ gives $a \times w$, and therefore, the two scanning beams will give the same resolution upon image reconstruction. Fig. 4.5d) shows the reconstruction when the larger beam is used to acquire holographic information. By comparing figs. 4.5b) and 4.5d), it is evident that both reconstruction show the same resolution. The oscillating noise in the two figures is due to the twin-image. It is clear that scanning with a smaller beam will lead to a less spread-out twin-image noise in the reconstruction plane. In light of this, we expect that the spread-out twin-image noise could degrade a more complicated object upon reconstruction, i.e., object consisting of a large collection of points, if a large scanning beam is employed in acquiring holographic information. Keeping this in mind, we further investigate holographic reconstruction in the context of optical scanning.

Fig. 4.6a) shows a scanning beam with $a = 0.27\,mm^{-2}$and $w = 9.99\,mm$ and fig.4.6b) shows a slit object of dimension D = 2mm. Fig. 4.6c) shows the reconstruction of the hologram, whereas fig. 4.6d) shows the reconstruction without the twin-image term. To simulate reconstruction without the twin-image term, we eliminate the exp(-jθ) term from the sin(θ) of eq.(4.17) [11] . In fig. 4.7, we keep the beam parameters, i.e., a and w, the same but reduce the size of the slit by a factor of two, i.e., D =1 mm. Fig. 4.7a) shows the slit object. Fig. 4.7c) and Fig. 4.7d) show the reconstruction with and without the twin-image term, respectively. As it turns out, the geometry of the situation in Figs. 4.6 and 4.7 satisfies the so-called far field condition in holography [24]. The far field condition, according to conventional Fraunhofer holography, is $z >> D^2/\lambda$, where z in the case of optical scanning holography is the distance from the scanning beam to the object, D is the size of the object and $\lambda = 2\pi/k_0$. Now, as $a = k_0/2z = \pi/\lambda z$, we can rewrite the far field condition in terms of a and the condition becomes $\pi/a >> D^2$. Clearly, the geometry of figs. 4.6 and 4.7 satisfies this condition. However, since the size of the object in Fig. 4.7a) is smaller, the object can be said to be even further in the far field as compared to that in Fig. 4.6b). This is borne out by comparing fig. 4.6c) and fig. 4.7b) as we can see that the twin-image noise in fig. 4.7b) has been spread out more with lower amplitude. Indeed this fact has been used successfully in in-line holography for particle sizing [24,43] as in the far field the twin-image noise would not interfere greatly with the real image reconstruction. These simulations demonstrate the principles of Fraunhofer holography in the context of optical scanning.

We now investigate the near field situation as we approach the case of image plane holography. Fig. 4.8a) shows a two-slit object of slit-width W ~ 2 cm. The separation of the slits d ~ 1cm, and the size of the object $D \sim 5$ cm. Fig. 4.8b) shows the scanning beam characterized by $a = 30\ mm^{-2}$and $w = 0.733\,mm$. This situation

corresponds to a near field case. Fig. 4.8c) and d) present the reconstruction with and without the twin-image term, respectively. Figs. 4.9 and 4.10 show the same type of simulations as those shown in fig. 4.8, but with the scanning beam characterized by $a/4$ and $4 \times w$; $a/8$ and $8 \times w$, respectively. Note that the scanning beam in fig. 4.8 is smallest in size in the three cases and this corresponds to the deepest near field situation. It is important to point out that all the simulations are performed with the same resolution even though the sizes of the scanning beam are different. We observe that the twin-image noise in fig. 4.8c) is less pronounced than that in fig. 4.9c) and 4.10c). In fact, the two-slit object in fig. 4.8c) are resolved better. Hence, the deeper the object is in the near field situation when the object is being scanned under the condition of $a \times w =$ constant, the better the reconstruction is. In other words, in the near field, it is better to use a smaller beam to scan an object in order to reduce the twin-image effect. We shall further demonstrate this effect by performing a 2-D simulation. Fig. 4.11a) shows a 2-D object (about 10 mm x 10 mm) with some fine structures, and figs. 4.11b) and 4.11c) show a small and a large 2-D Gaussian apodized Fresnel zone scanning beam used to acquire the holographic information. The parameters used put the object in the near field. Note that the $a \times w$ product is the same for the two beams, thereby giving the same resolution upon reconstruction. All the scales in fig.4.11) are the same. Figs. 4.12a) and 4.12b) show the reconstruction when the two beams, shown in 4.11b) and 4.11c), respectively, are used to scan the object. The effect of the twin image noise is seen to spoil the resolution in fig. 4.12b), which was acquired with a larger scanning beam, more than in fig. 4.12a), which corresponds to a nearer field.

4.6 Concluding remarks

It has been shown that by scanning an object with a temporally modulated Gaussian apodized Fresnel zone plate to acquire holographic information, the resolution limit achievable is directly proportional to the size of the beam and the number of zones within the beam. If the object is in the near field and as the object becomes more and more complicated, it is advantageous to use a smaller beam rather than a larger beam even though the two beams may lead to the same nominal resolution upon image reconstruction. Physically, one may argue that scanning with a larger beam causes twin-image noise to interact with a broader part of the image. This effect may prove to be more important if the object is contaminated with noise. Another reason may be that when the size of the scanning zone plate is larger than that of the object so that the scanning beam always illuminates the entire object, we have a situation reminiscent of coherent holographic recording since the hologram is the simultaneous superposition of the individual holograms of each point within the object. On the contrary, if the zone plate size is much smaller than that of the object, the zone plate overlaps only a small part of the object at any instant of the scanning process, a situation reminiscent of a partially coherent recording [12].

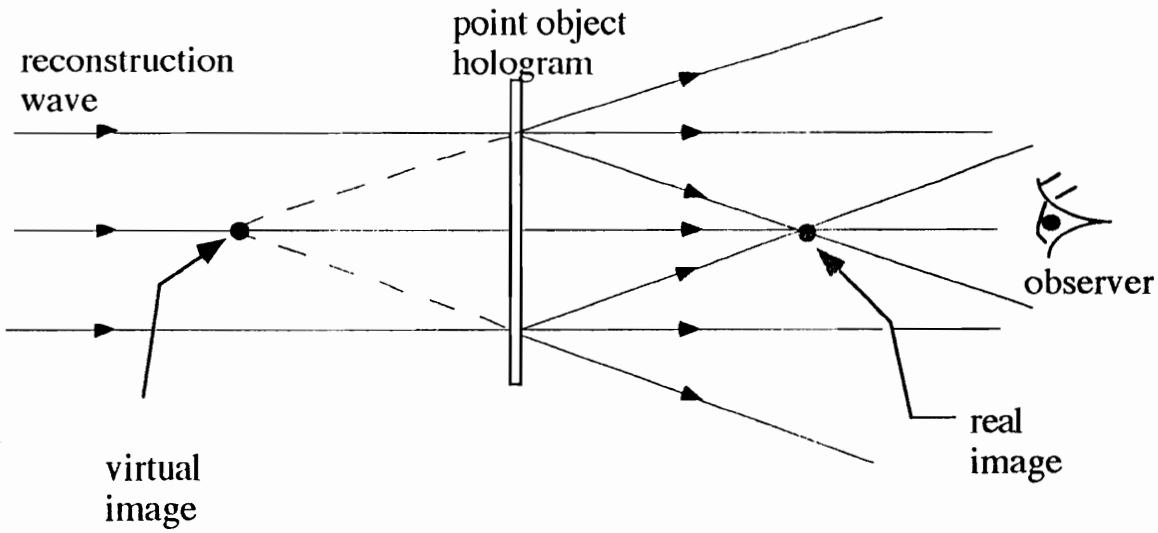

Fig. 4.1 Reconstruction of a point-object hologram which has been recorded with an on-axis reference wave. The virtual image and the real image are formed along the same axis, illustrating the problem of twin image.

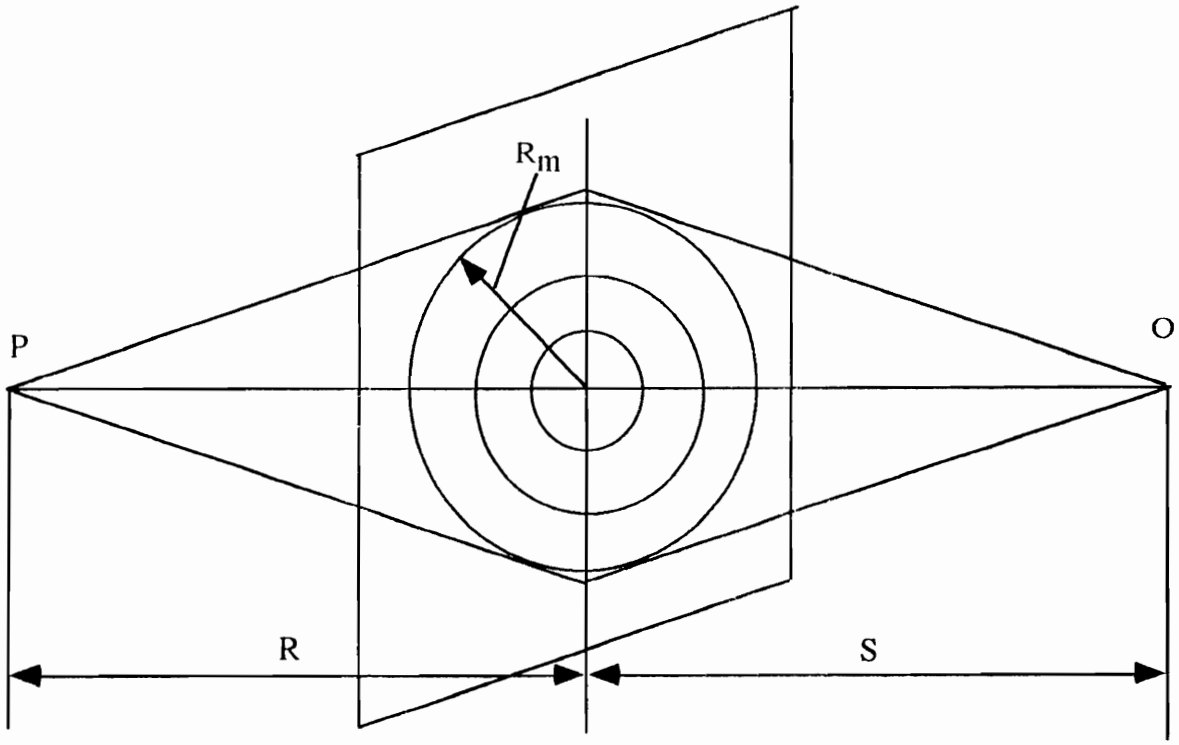

Fig. 4.2 Fresnel zone lens plate on a spherical wave front

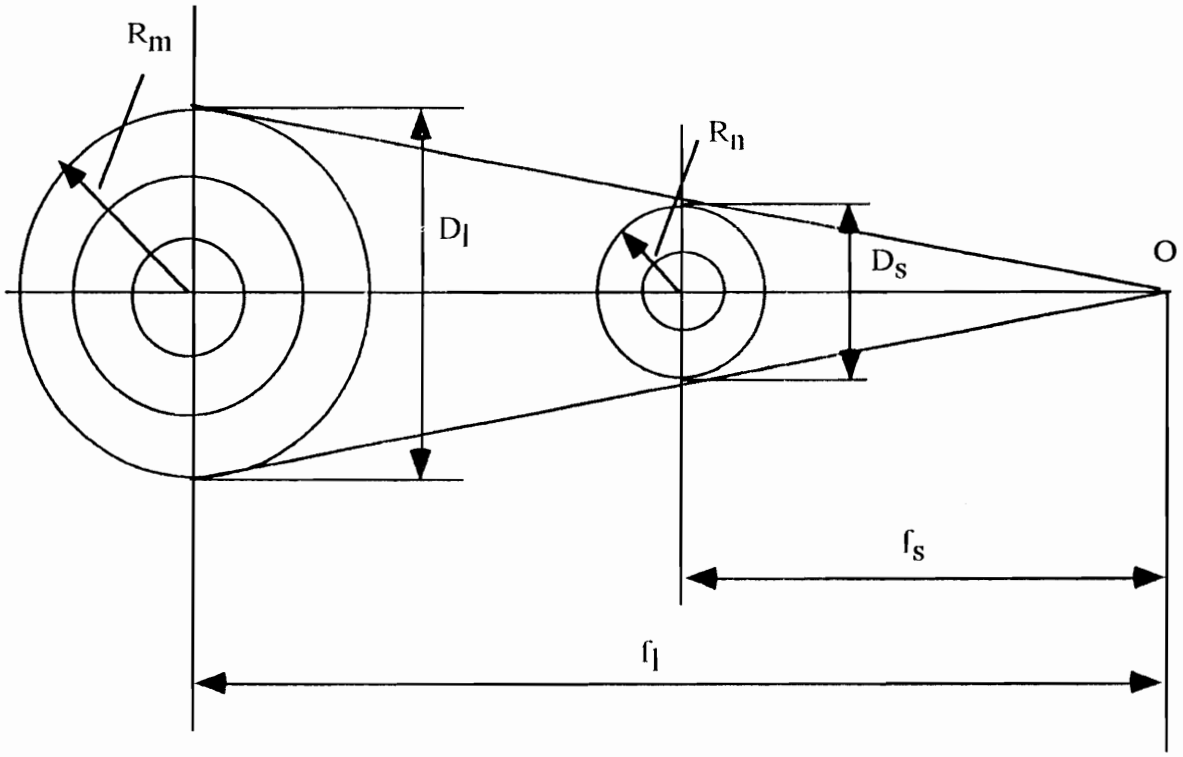

Fig. 4.3 Zone lens plate of two different sizes

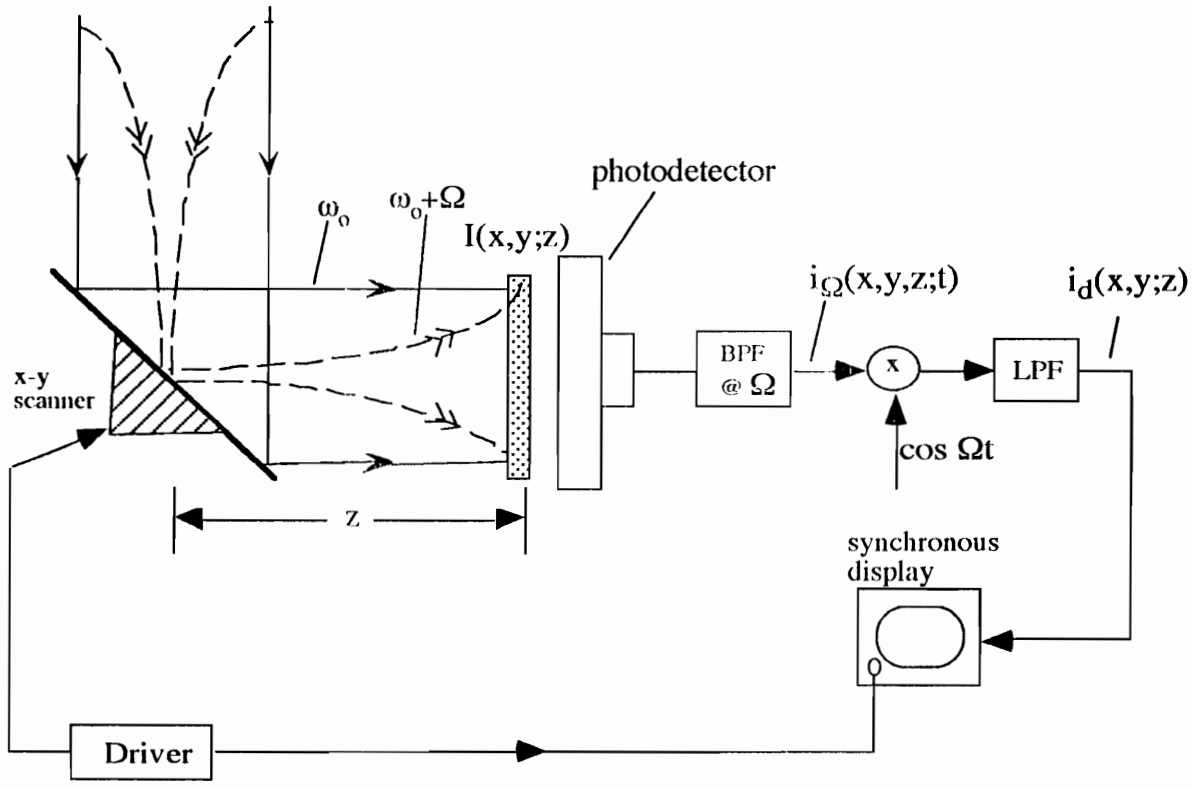

Fig. 4.4 Optical scanning holographic system illustrating a narrow and a broad Gaussian scanning beam at temporal frequency $\omega_o+\Omega$, and ω_o, respectively.

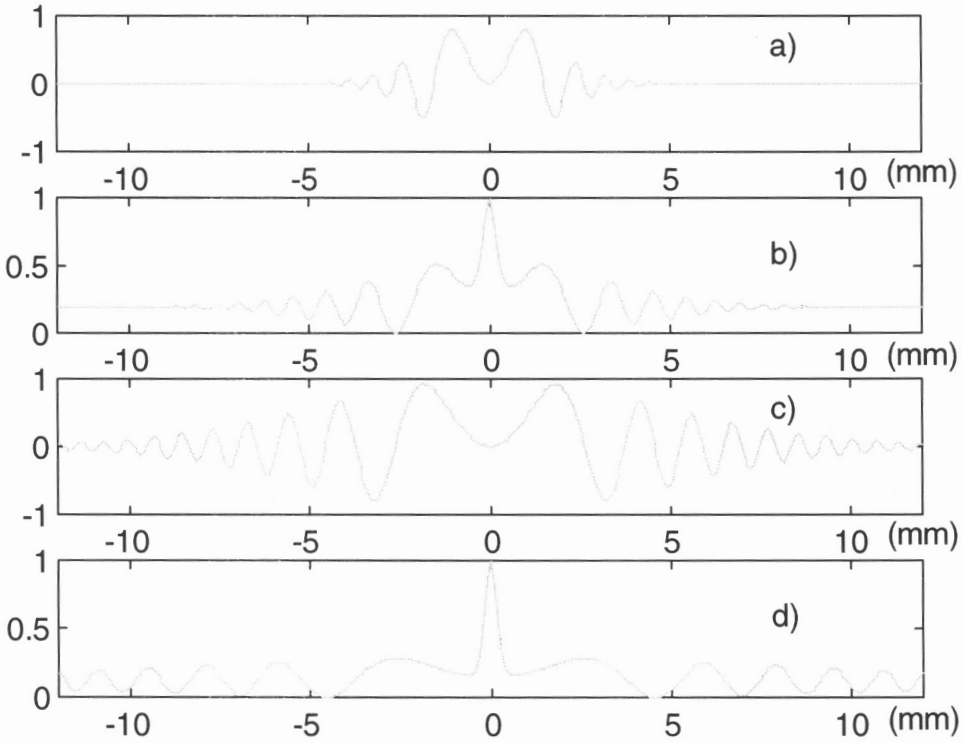

Fig. 4.5 (a) Scanning Gaussian apodized Fresnel zone plate $f_s(x;z) : a = 1.349\,mm^{-2}$, $w = 2.236\,mm$; (b) Point object reconstruction using the scanning beam of (a) to acquire holographic information; (c) Same as (a) but with $a/3\,and\,3w$; (d) Point object reconstruction using the scanning beam of (c) to acquire holographic information.

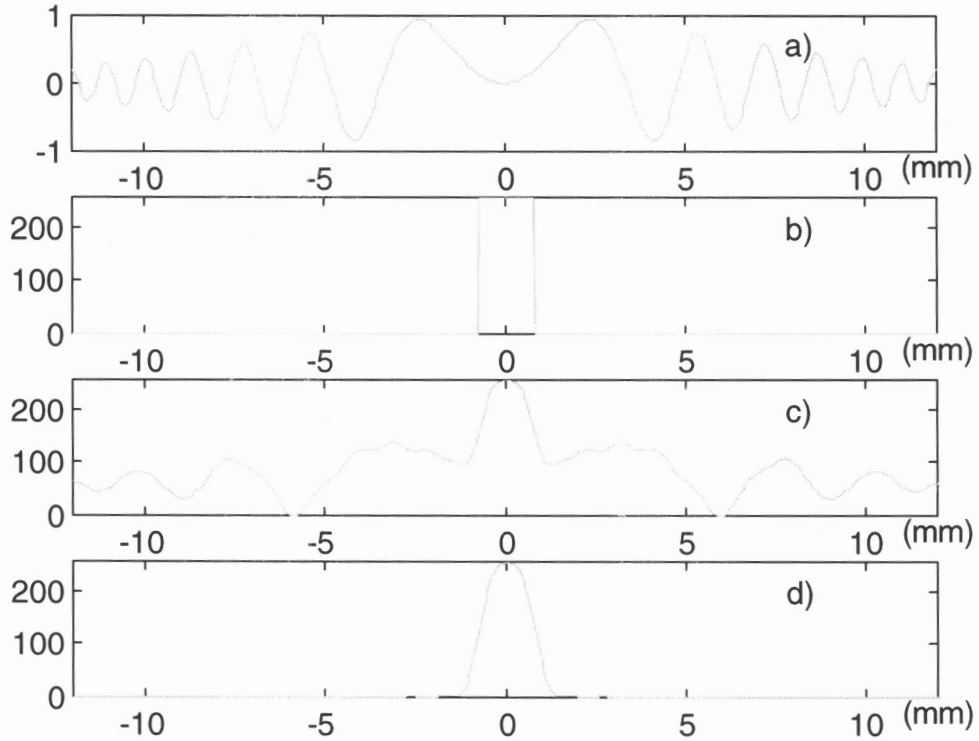

Fig. 4.6 (a) Scanning beam characterized by $a = 0.27\, mm^{-2}$ and $w = 9.99\, mm$, (b) slit object of $D = 2\, mm$, (c) far-field image reconstruction of (b) with the twin-image term, and (d) far-field image reconstruction of (b) without the twin-image term.

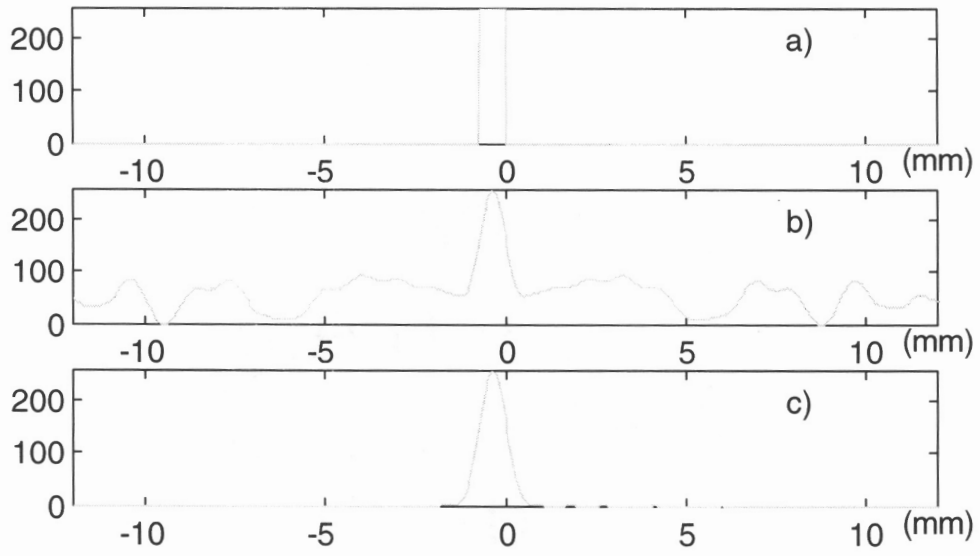

Fig. 4.7 (a) Slit object of $D = 1\,mm$, (b) far-field image reconstruction of (a) with the twin-image term, and (c) far-field image reconstruction of (a) without the twin-image term.

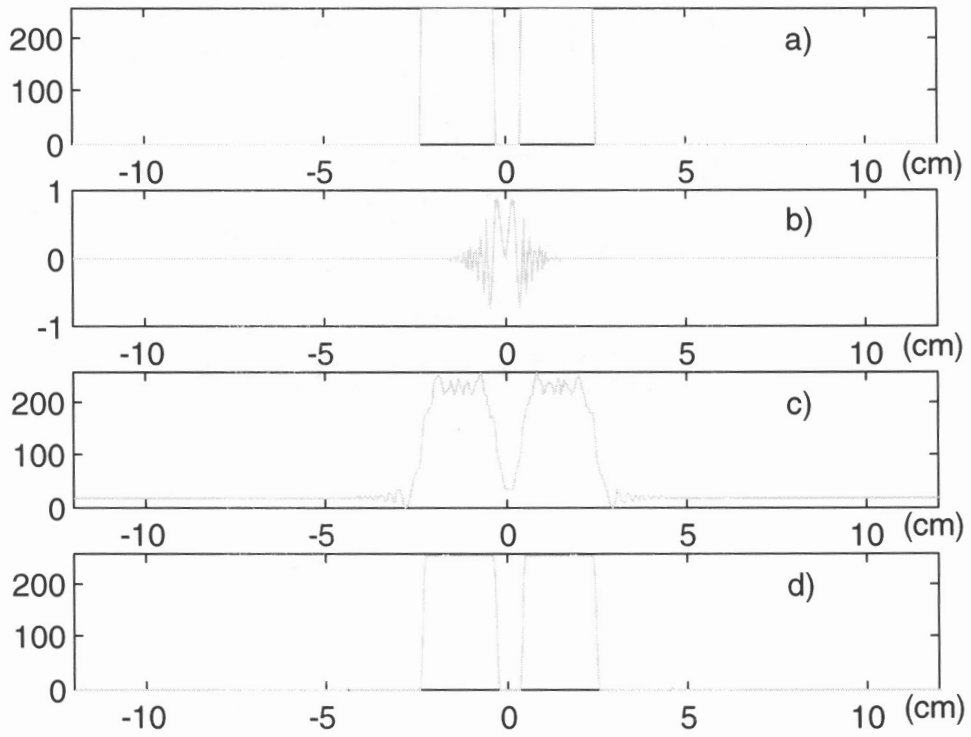

Fig. 4.8 (a)Two-slit object, (b) scanning beam characterized by $a = 30\,mm^{-2}$ and $w = 0.733\,mm$, (c) near-field image reconstruction of the two-slit object shown in (a) with the twin-image term, and (d) near-field image reconstruction of the slit object without the twin-image term.

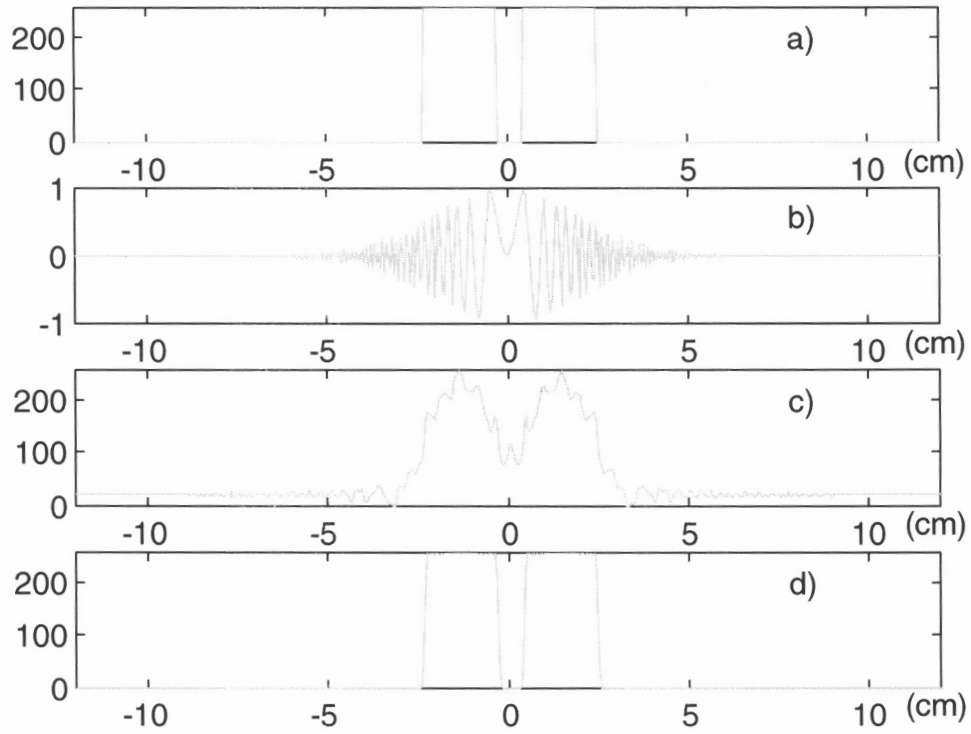

Fig. 4.9 (a)Two-slit object, (b) scanning beam characterized by $a/4$ and $4w$, (c) near-field image reconstruction of the two-slit object with the twin-image term, and (d) near-field image reconstruction of the slit object without the twin-image term.

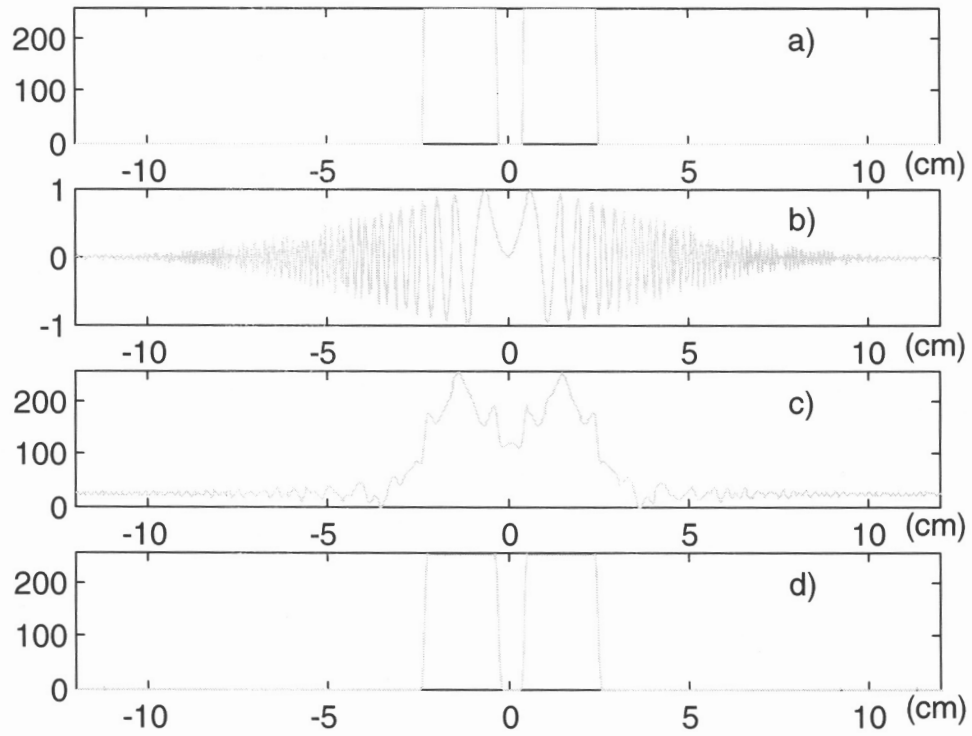

Fig. 4.10 (a)Two-slit object, (b) scanning beam characterized by $a/8$ and $8w$, (c) near-field image reconstruction of the two-slit object with the twin-image term, and (d) near-field image reconstruction of the slit object without the twin-image term.

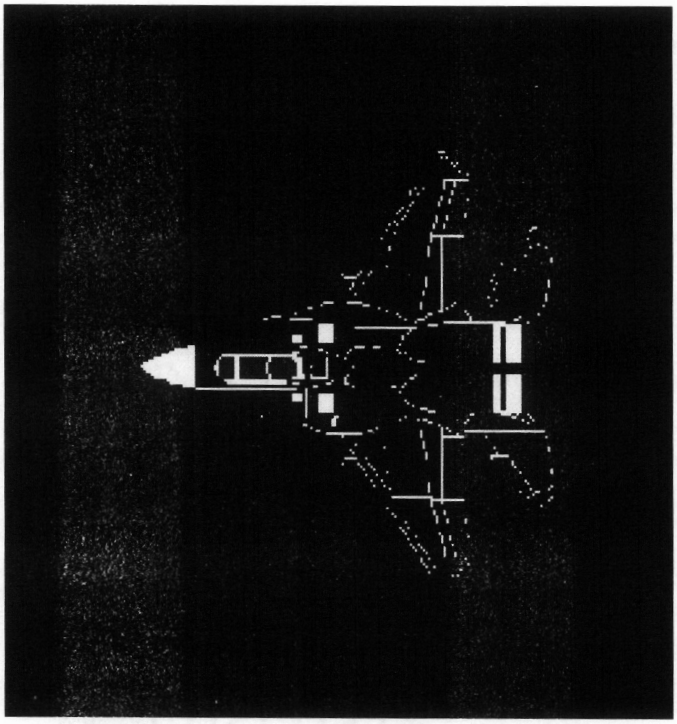

Fig. 4.11 (a) 2-D image of size about $10 \times 10\,mm$

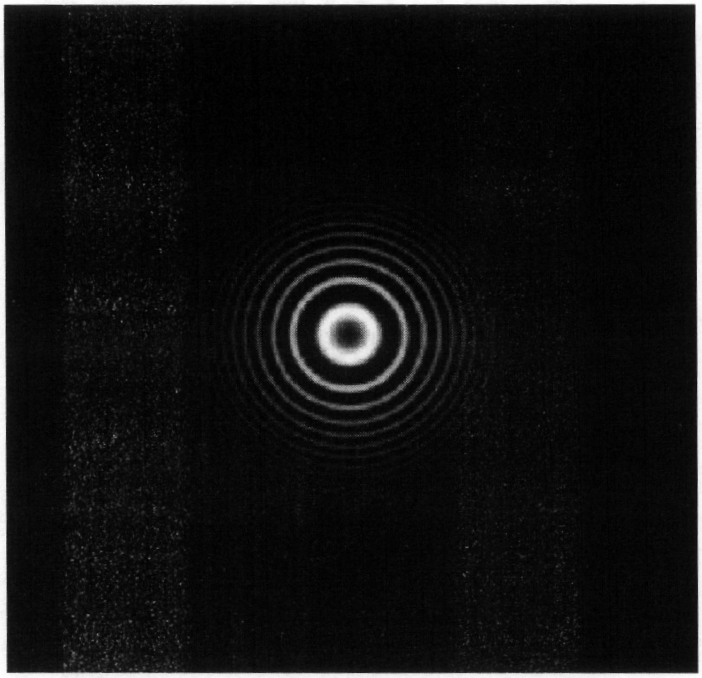

Fig. 4.11 (b) 2-D scanning Gaussian apodized Fresnel zone lens plate with $a = 2.023$ mm^{-2}, $and\, w = 3.33\, mm$.

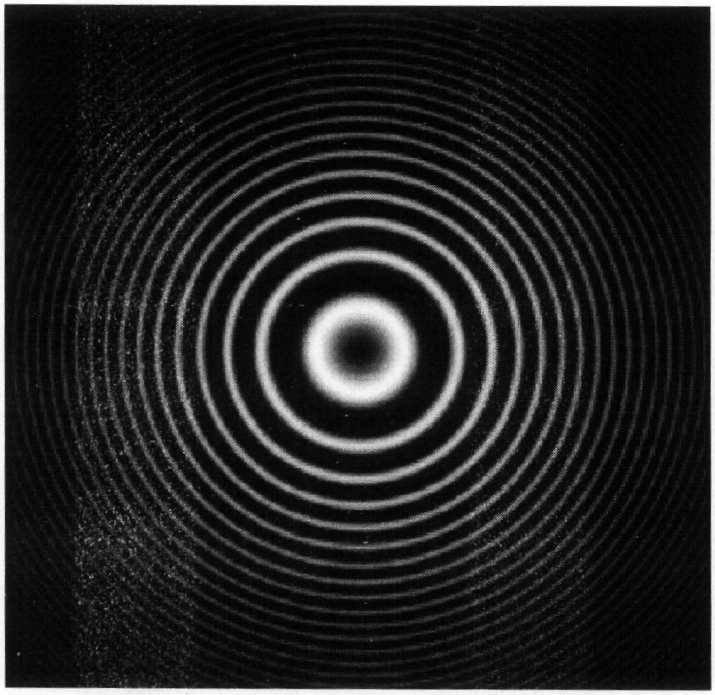

Fig. 4.11 (c) Same as (b) but with $a/3\,and\,3w$ (a larger beam with the same resolution).

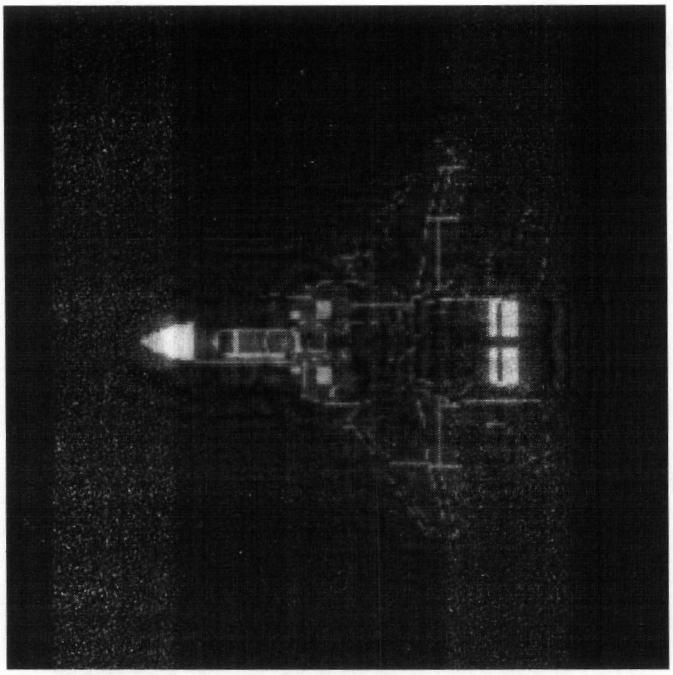

Fig. 4.12 (a) Near-field image reconstruction of Fig. 4.11(a) using scanning beam of Fig. 4.11(b)

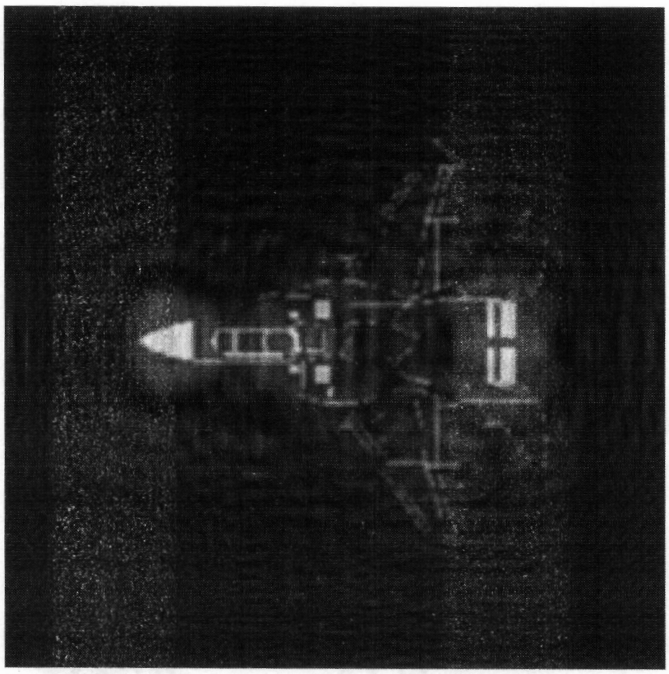

Fig. 4.12 (b) Near-field image reconstruction of Fig. 4.11(a) using scanning beam of Fig. 4.11(c).

CHAPTER 5: TWIN-IMAGE ELIMINATION IN OPTICAL SCANNING HOLOGRAPHY

In chapter 4, we discussed the origin of twin-image and twin-image noise on the use of Fresnel zone pattern for holographic recording. In this chapter, we introduce a novel multiplexing technique[10] to solve the twin image problem in optical scanning holography without the use of a spatial carrier as commonly used in conventional off-axis holography. The technique involves simultaneously acquiring a sine and cosine Fresnel zone-lens pattern coded images by optical scanning. A complex addition of the two coded images then will be performed and decoded to give a twin-image rejection reconstruction. Computer simulations and Experimental results will be presented to demonstrate the validity of the idea.

5.1 Introduction

In-line holography has been used as a simple means of high-resolution imaging. A bottlenect of In-line holography is an unwanted twin-image in the reconstruction plane. That is, the overlap of unfocused virtual image onto its focused real image in the

reconstructed field. This overlap gives a complex interference pattern in which details may be blurred or lost. In optical scanning holography, when the object is optically scanned, a photodetector collects the scattered light and delivers a heterodyne current as output. The current is then mixed down to become a demodulated signal. When the demodulated signal is synchronized with the x and y scans of the x-y optical scanning system and fed to a 2-D display, what is displayed in 2-D is a hologram or a Fresnel zone-lens pattern coded information of the object being scanned. To decode the information optically in real time, the holographic information could be transferred to a spatial light modulator (SLM) for coherent reconstruction [3]. Digital reconstruction is also possible by convolving the hologram with a free-space impulse response [4]. Whereas the work of optical scanning holography has been concentrated on on-axis techniques which inherently produce twin-image upon reconstruction (or decoding), we introduce a novel technique in which the twin-image can be eliminated in the context of optical scanning holography. We mention that twin-image elimination has been the subject of great interest. Interested readers may refer to some of the cited references [43-50]. In section 5.2, we introduce the concept of twin-image elimination and demonstrate computer simulation results. In section 5.3, we present the experimental results. In section 5.4, we make some concluding remarks.

5.2 Gaussian-Beam Theory of Optical Scanning Holography and Twin-Image Elimination

Conceptually, in optical scanning holography, an object is 2-D scanned by a time-dependent Fresnel zone-lens pattern (TDFZP) created by the interference of a plane wave

and a spherical wave of different temporal frequencies to generate a hologram of the object. Physically, we model the scanning plane wave and the spherical wave by two Gaussian beams of a broad and a narrow waist, respectively. The situation is shown in Fig. 5.1. The intensity pattern on the object, at a distance z away from the $x-y$ optical scanner, is given by

$$I(x,y;z) = |u(x,y;z) + v(x,y;z)|^2, \tag{5.1}$$

where

$$u(x,y;z) = \frac{1}{\pi\omega_u(0)\omega_u(z)} \exp[-(x^2+y^2)/\omega_u^2(z)]$$
$$\times \exp[-jk_o(x^2+y^2)/2R_u(z)]\exp(-j\phi_u)\exp(j\omega_0 t);$$

$$v(x,y;z) = \frac{1}{\pi\omega_v(0)\omega_v(z)} \exp[-(x^2+y^2)/\omega_v^2(z)]$$
$$\times \exp[-jk_o(x^2+y^2)/2R_v(z)]\exp(-j\phi_v)\exp[j(\omega_0+\Omega)t].$$

The notations in above are further defined as follows[13]:

$$\omega_u^2(z) = \frac{2z_u}{k_o}\left[1+\left(\frac{z}{z_u}\right)^2\right], \tag{5.2a}$$

$$R_u(z) = \frac{z^2+z_u^2}{z}, \tag{5.2b}$$

$$\phi_u(z) = -\tan^{-1}\left(\frac{z}{z_u}\right), \tag{5.2c}$$

and

$$z_u = \frac{k_o w_u^2}{2}, \tag{5.2d}$$

where k_o is the optical wave number of the two Gaussian beams, assuming that $\omega_0 \gg \Omega$ with Ω denoting the temporal frequency shift between the two beams. w_u is the waist of the broad Gaussian at $z = 0$, and finally the above equations are valid when replacing the subscript u by v for the narrow Gaussian. Note that the narrow Gaussian has a temporal frequency shift of Ω.

Eq.(5.1) can be expanded to give

$$\begin{aligned} I(x,y;z) &= |u(x,y;z)|^2 + |v(x,y;z)|^2 \\ &+ \frac{2}{\pi^2 \omega_u(0)\omega_u(z)\omega_v(0)\omega_v(z)} \\ &\times \exp\Big[-\frac{(x^2+y^2)}{\omega^2(z)}\Big] \cos\Big(\frac{k_o}{2R(z)}(x^2+y^2) + \phi + \Omega t\Big), \end{aligned} \tag{5.3}$$

where

$$\frac{1}{\omega^2(z)} = \frac{1}{\omega_u^2(z)} + \frac{1}{\omega_v^2(z)},$$

$$\frac{1}{R(z)} = \frac{1}{R_u(z)} - \frac{1}{R_v(z)},$$

and

$$\phi(z) = \phi_u(z) - \phi_v(z).$$

Note that the third term in (5.3) is a time-dependent Fresnel zone-lens plate (TDFZP). When the beam pattern $I(x,y;z)$ is used to scan over an object, a heterodyne scanned current $i_{scan}(x(t), y(t))$will be delivered at the output of the photodetector tuned at frequency Ω. After multiplying the heterodyne scanned signal with $\cos(\Omega t)$ and

lowpass filtering, we have a demodulated signal $i_d(x(t), y(t))$. When this demodulated signal is displayed on a 2-D monitor, we have a coded image (or hologram) of the object. The transmission function of the coded image, $t(x, y)$, is given by

$$t(x, y) = c + i_d(x, y). \tag{5.4}$$

In the above equation, the demodulated signal is given as

$$i_d(x, y) = f(x, y; z) \otimes \exp\left[- \frac{(x^2 + y^2)}{\omega^2(z)} \right] \cos\left(\frac{k_o}{2R(z)} (x^2 + y^2) + \phi(z) \right), \tag{5.5}$$

where $\otimes$ denotes a 2-D convolution operation. In writing (5.5), we have assumed that $f(x, y; z)$ is the 2-D object being scanned at a distance z away, and the z-dependent amplitude associated with the heterodyne term in (5.3) has been considered as constant for simplicity. Note that the undesirable space-variant terms in (5.3), i.e., $|u(x, y; z)|^2 + |v(x, y; z)|^2$, have been eliminated due to the heterodyne photodetection. Finally, c is a constant bias introduced so that the phase of $i_d(x, y)$ can be preserved when $i_d(x, y)$ is being recorded onto a square-law material such as films or spatial light modulators for possible coherent reconstruction. Note that, in (5.4), the 2-D object $f(x, y)$ has been coded by a cosine Fresnel zone-lens plate, and the Gaussian apodization of the Fresnel zone-lens plate is due to the nature of the two scanning Gaussian beams. Fig. 5.2a) shows an optically Fresnel zone-lens plate coded object "VT". The object, located about $z = 23$cm away from the optical scanner, is approximately 4 mm by 4 mm with line width of about 100μm, and is transmissive on an opaque background. The waists of the Gaussian beams are $w_u \approx 1$ cm and $w_v \approx 3.5$ μm with optical wavelength $\lambda_0 = 2\pi/k_0 = 0.6328\mu$m.

The coded image can be reconstructed optically by producing a transparency of the coded image, illuminating it with coherent light and observing the diffraction pattern at some distance away. Mathematically, this can be described as convolving the coded image with a filter response given by $h(x, y) = \exp(-ja(x^2 + y^2))$. By varying a, the coded image can be reconstructed at different depths [4]. Fig. 5.2b) shows a digital reconstruction of the optically coded image given by Fig. 5.2a). If the hologram is coherently reconstructed by a laser with wavelength λ_0, a real image and a virtual image will be formed simultaneously in the front and the back of the hologram, respectively at a distance given by $R(z)$; hence the problem of twin image. To understand the origin of the formation of the twin-image, we expand the cosine term in (5.5) as

$$\begin{aligned} &\cos\left(\tfrac{k_o}{2R(z)}(x^2 + y^2) + \phi(z)\right) \\ &= \tfrac{1}{2}[\exp(j\theta) + \exp(-j\theta)], \end{aligned} \tag{5.6}$$

where

$$\theta(x, y; z) = \frac{k_o}{2R(z)}\left(x^2 + y^2\right) + \phi(z).$$

The first exponential in (5.6) is responsible for the reconstruction of a real-image, whereas the second exponential produces the twin image which generates unwanted information on the real-image reconstruction plane. Fig. 5.3) shows a series of computer simulation which illustrate the twin image problem in the context of optical scanning holography. Note that the numerical values used for the simulations are identical to the physical experiment parameters with the exception that z is at a larger distance. In fact z = 230 cm has been used for the simulations. This choice of the distance is due to the fact

that at smaller distances, the computer available cannot handle the fast-varying changes inherent in the Fresnel zone-lens plate. Fig. 5.3a) shows the computer-generated "VT" image. Fig. 5.3b) displays the coded image computed by (5.4). Note the similarity between the simulated coded image and the optical hologram shown in Fig. 5.2a). Fig. 5.3c) shows the real-image reconstruction. The noise around the reconstruction is from the diffraction of the twin-image on the image plane. In Fig. (5.3d), we isolate and illustrate the twin-image noise formation on the real-image reconstruction plane. To generate Fig.(5.3d), we compute (5.4) with $\cos(\theta)$ replaced by $\exp(-j\theta)$. By comparing Figs. 5.3c) and 5.3d), we clearly distinguish the twin-image noise from the in-focus real image.

In order to eliminate the twin image, we need to suppress the term $\exp(-j\theta)$. Suppose that if we can generate a quadrature scanned demodulated signal $i_d^{\mathrm{Q}}(x,y)$ such that it is given by

$$\begin{aligned} i_d^{\mathrm{Q}}(x,y) &= f(x,y;z) \otimes \exp\left[-\frac{(x^2+y^2)}{\omega^2(z)}\right]\cos\left(\frac{k_o}{2R(z)}(x^2+y^2)+\phi(z)-\pi/2\right) \\ &= f(x,y;z) \otimes \exp\left[-\frac{(x^2+y^2)}{\omega^2(z)}\right]\sin\left(\frac{k_o}{2R(z)}(x^2+y^2)+\phi(z)\right), \end{aligned} \tag{5.7}$$

According to (5.4), the sine Fresnel zone-lens plate coded image is given by

$$t^{\mathrm{Q}}(x,y) = c + i_d^{\mathrm{Q}}(x,y), \tag{5.8}$$

Fig. (5.4) shows the sine-coded image of the "VT" image. By comparing this with the cosine-coded image shown in Fig. (5.3b), we see that in Fig. (5.4) that there is less brightness associated with hologram. Now, we can add $i_d(x,y)$ and $i_d^{\mathrm{Q}}(x,y)$ to form a complex scanned signal as

$$
\begin{aligned}
i_c(x,y) &= i_d(x,y) + j\, i_d^{Q}(x,y) \\
&= f(x,y;z) \otimes \exp\Big[-\tfrac{(x^2+y^2)}{\omega^2(z)} \Big] \exp\Big(j\tfrac{k_o}{2R(z)}(x^2+y^2) + j\phi(z) \Big)
\end{aligned}
\tag{5.9}
$$

Note that $i_c(x,y)$ is a phase-coded image (or phase hologram) of $f(x,y)$, which will only give rise to the real-image upon reconstruction. The question is how to create such a quadrature scanned signal given by (5.7). The idea of multiplexing is exploited. Recall that scanning the object by a TDFZP produces a heterodyne current. When the heterodyne current is subsequently multiplied by $\cos(\Omega t)$ and lowpass filtered, it gives rise to a cosine Fresnel zone-lens plate coded image given by (5.5). Now in addition to multiplying the heterodyne current with $\cos(\Omega t)$ to get (5.5), one could also multiplying the current by $\sin(\Omega t)$ simultaneously and lowpass filter to get (5.7), i.e.,

$$
i_d^{Q}(x,y) = f(x,y;z) \otimes \exp\Big[-\frac{(x^2+y^2)}{\omega^2(z)} \Big] \sin\Big(\frac{k_o}{2R(z)}(x^2+y^2) + \phi(z) \Big). \tag{5.10}
$$

We refer to this concept of simultaneous acquisition of the cosine- and sine-coded images as multiplexing. The proposed set-up is shown in Fig.(5.5). The signal $i_{scan}(x,y)$ is simultaneously multiplied by $\cos(\Omega t)$ and $\sin(\Omega t)$ to eventually obtain $i_d(x,y)$ and $i_d^{Q}(x,y)$, respectively. The complex addition of $i_d(x,y)$ and $i_d^{Q}(x,y)$ according to (5.9) is performed by the personal computer (PC). Fig. (5.6) shows the real-image reconstruction of the hologram computed by (5.9). Note that the twin-image noise has been completely eliminated as compared with that shown in Fig. (5.3c). We point out that the reconstructed image is not as sharp as the original image and this is due to lowpass filtering of the original image. Lowpass filtering arises because the scanning beam is of Gaussian apodization [see eq. (9)]. Fig. (5.7) shows a more complicated

object for simulation. Fig. 5.7a shows the original object and Fig. (5.7b) shows the cosine-coded image. In Fig. (5.7c), we show the reconstruction of Fig. (5.7b), and in Fig. (5.7d), we have the reconstruction in which twin-image noise has been completely suppressed by using the multiplexing technique.

5.3 Experimental Results

In this portion of the chapter we present results of an experiment that demonstrates the the optical scanned the cosine- and sine-coded images as multiplexing. We shall first describe the components and the hardware used in the holographic system and then present optical recording and reconstruction results of twin-image elimination. With reference to Fig. 5.5, the system description of the recording stage is well described in [4]. The 2-D object consists of transparency of the letters "V" and "T", located at distance of about 20 cm away from the scanning mirror. After 2-D scanning of the object, the heterodyne current $i(x, y)$ is splitted into two-way by using 50 ohms power splitter. SinΩt is also obtained by letting cosΩt go through the 50 ohms two-way-90° power splitter. The demodulated currennt i_d carring cosine-coded holographic information and i_d^Q carring sine-coded holographic information are sent to the Image Processing and Measuring System (IPMS). Fig. (5.8) shows the trace of phase difference between cosΩt and sinΩt in time base (Fig. 5.8a) and X-Y mode (Fig. 5.8b). Fig. (5.9) and Fig. (5.10) show optically scanned cosine- and sine-coded holographic image of "VT", respectively. Fig. (5.11) and (5.12) show the reconstruction of Fig. (5.9) and Fig. (5.10), respectively. In Fig. (5.13), we show the reconstruction of of the hologram computed by (5.9).

5.4 Concluding Remarks

We have addressed the twin-image problem in optical scanning holography and proposed a multiplexing scheme to eliminate the twin-image. The multiplexing scheme requires a simultaneous acquisition of the cosine and sine Fresnel zone-lens pattern coded images. The scheme does not require the use of a spatial carrier as commonly used in conventional off-axis holography which demands high spatial resolution required of the recording devices and materials. It is also important that simultaneously acquiring the two coded images is practical as well as important because it will not have problems about image registration when computing the final phase-coded image.

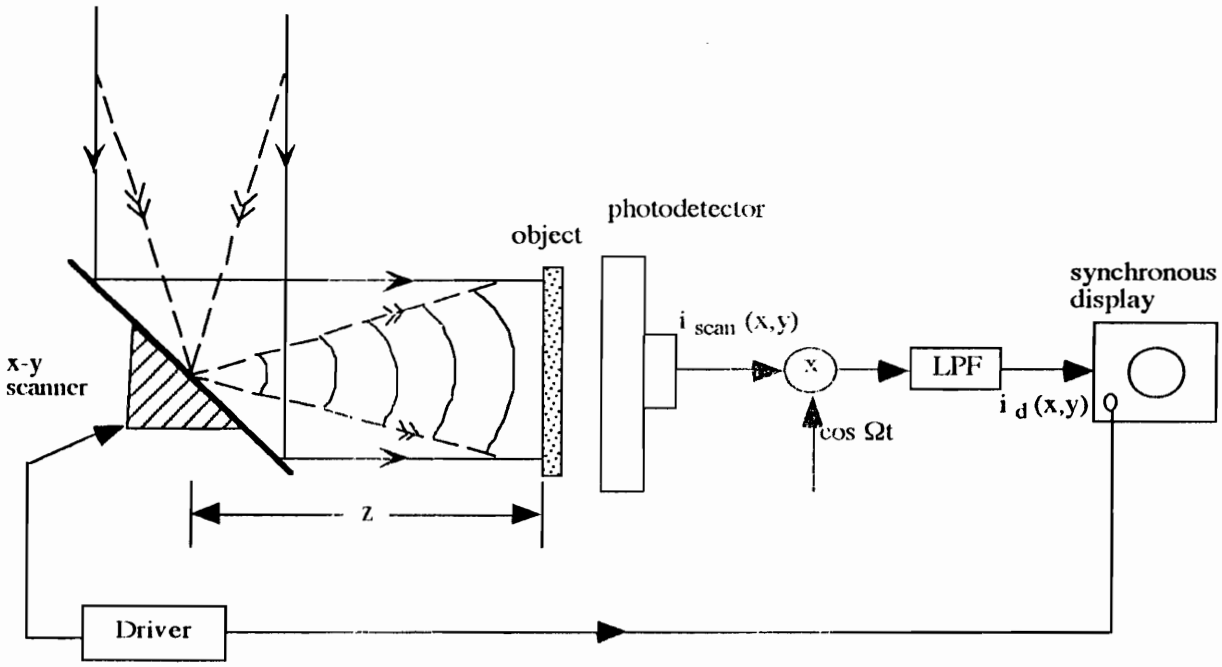

Fig. 5.1 Optical scanning holographic system

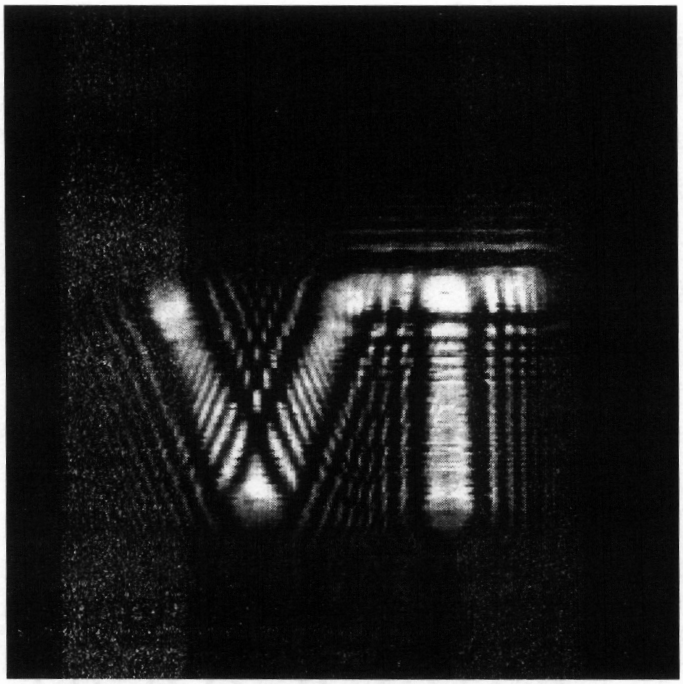

Fig. 5.2a Optically scanned hologram of the object "VT"

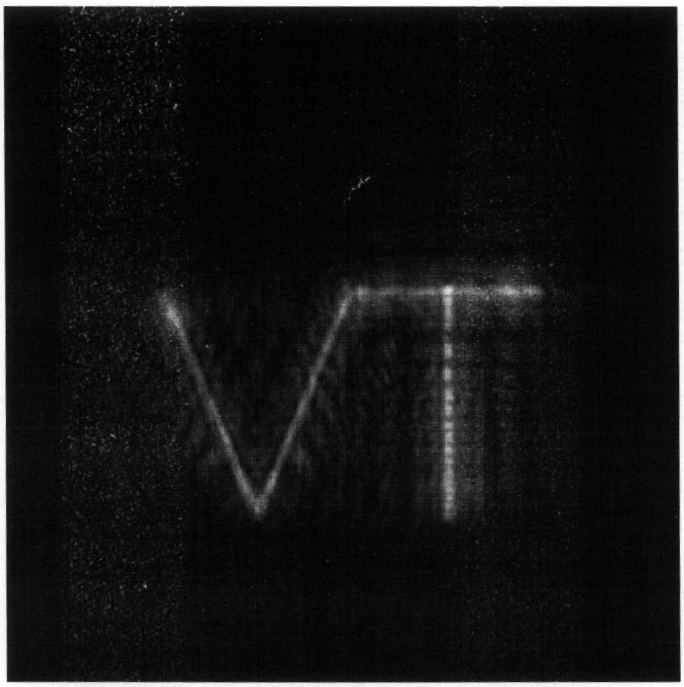

Fig. 5.2b. Digital reconstruction of the hologram shown in Fig. (5.2a)

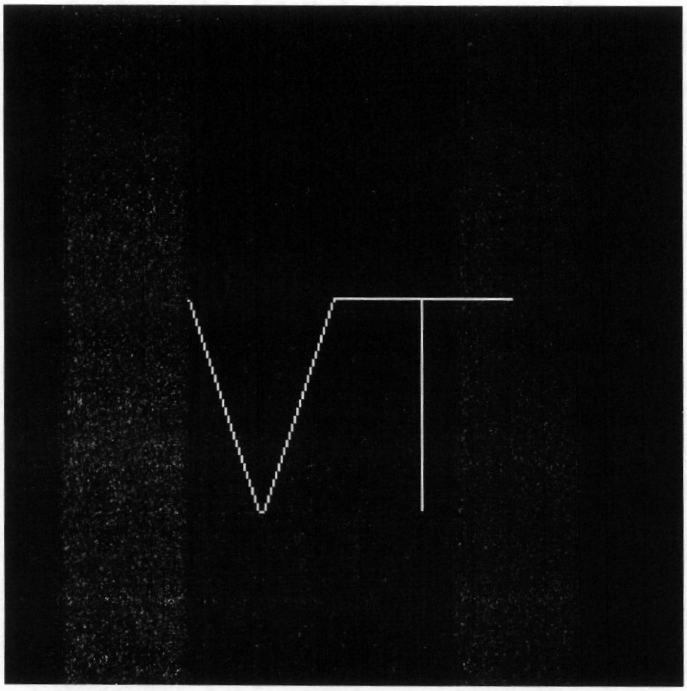

Fig. 5.3a. Computer-generated "VT" object

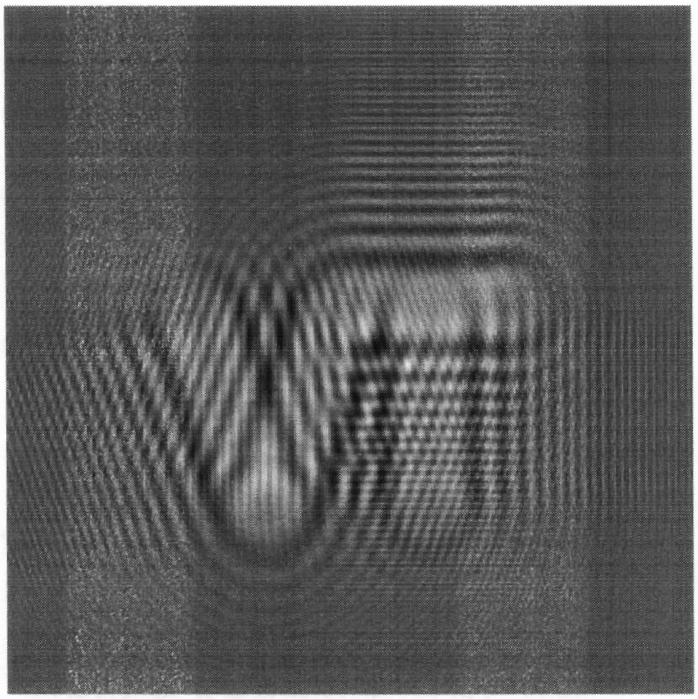

Fig. 5.3b. Cosine Fresnel zone-lens plate coded image of "VT" shown in Fig. (5.3a)

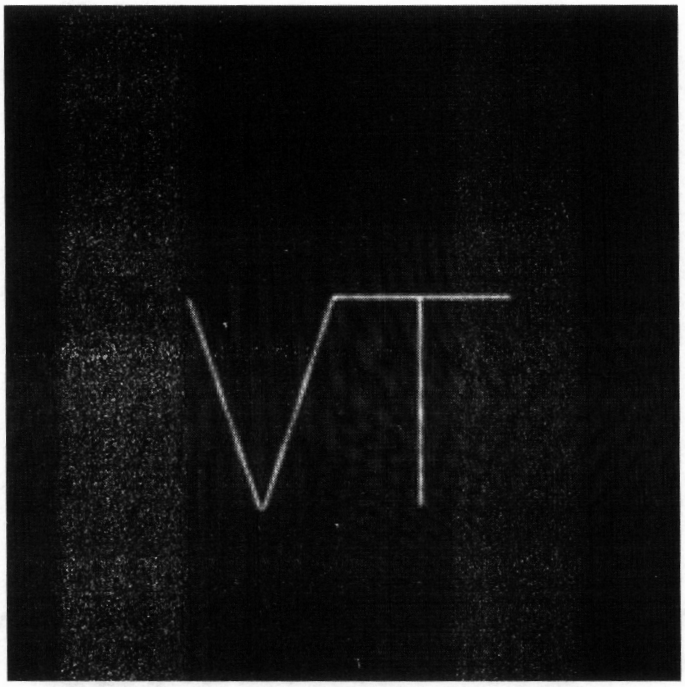

Fig. 5.3c. Digital reconstruction of "VT" shown in Fig. (5.3b)

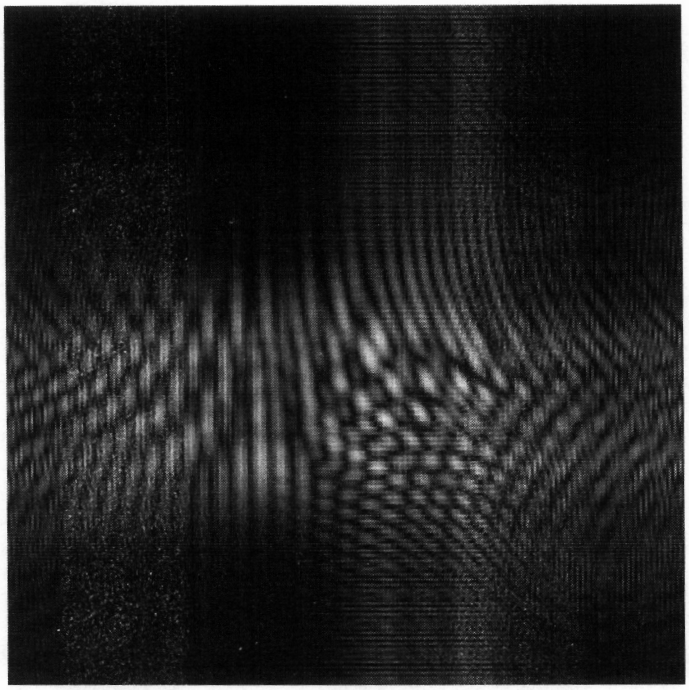

Fig. 5.3d. Twin-image noise on the real-image reconstruction plane

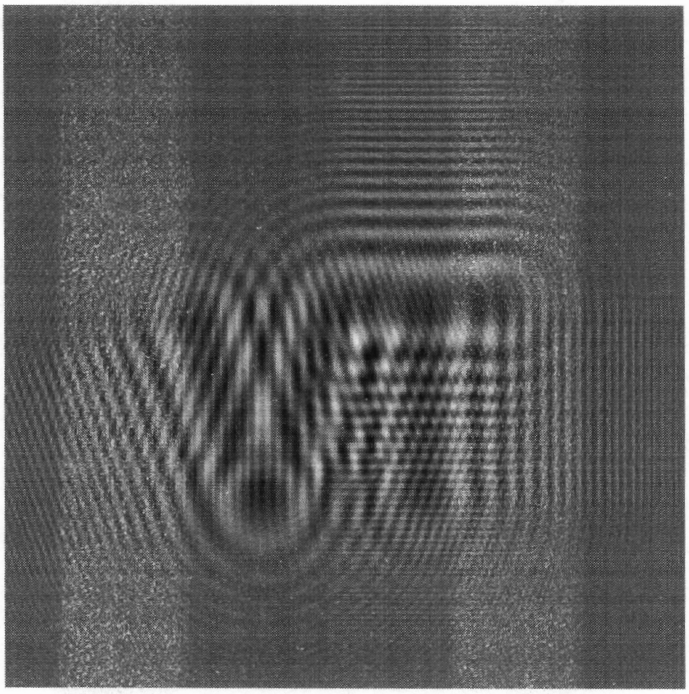

Fig. 5.4. Sine Fresnel zone-lens plate coded image of "VT" shown in Fig. (5.3a)

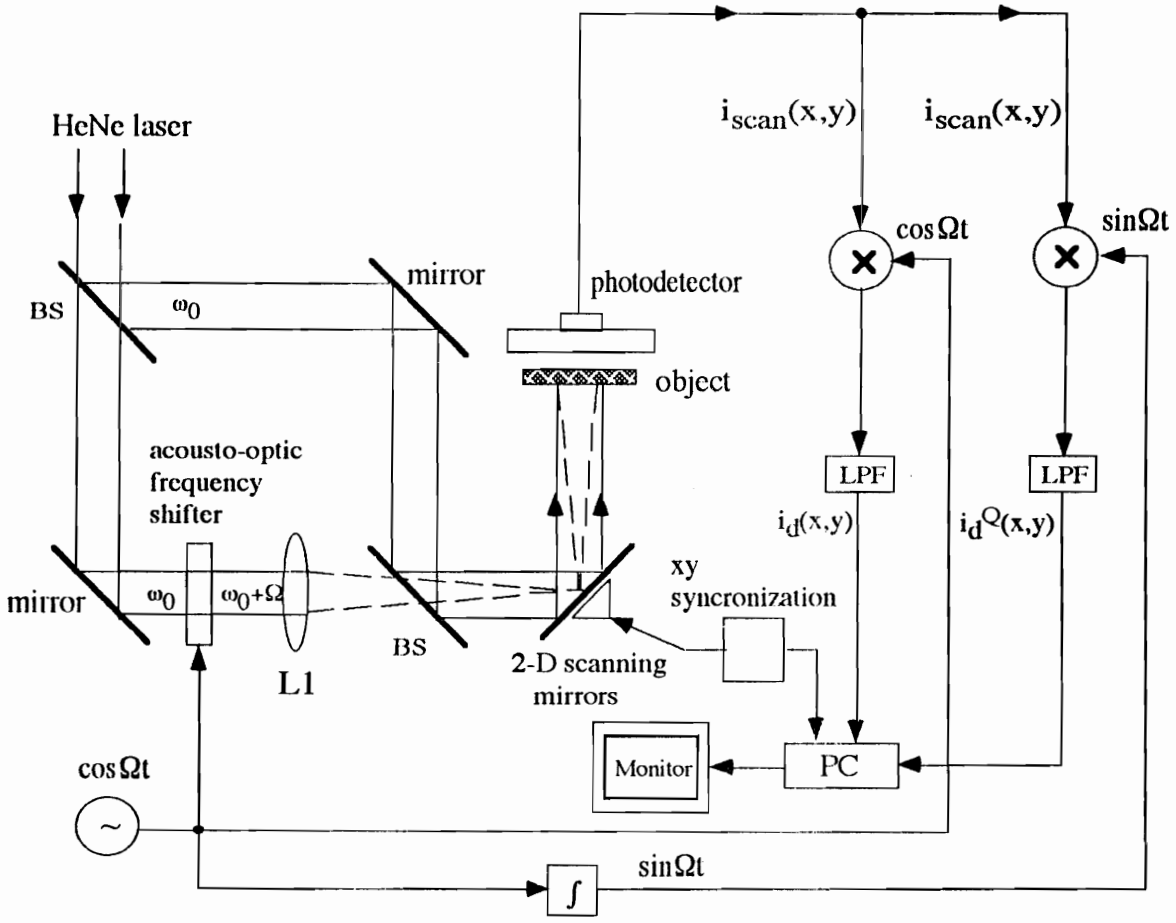

Fig. 5.5 Proposed multiple scheme for acquiring cosine and sine coded images simultaneously

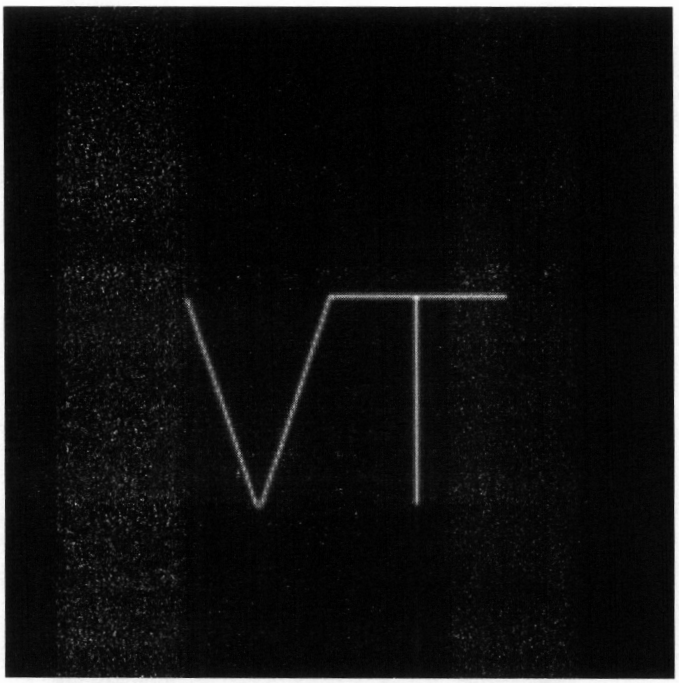

Fig. 5.6 Digital reconstruction of phase-coded hologram computed according to Eq.(5.9)

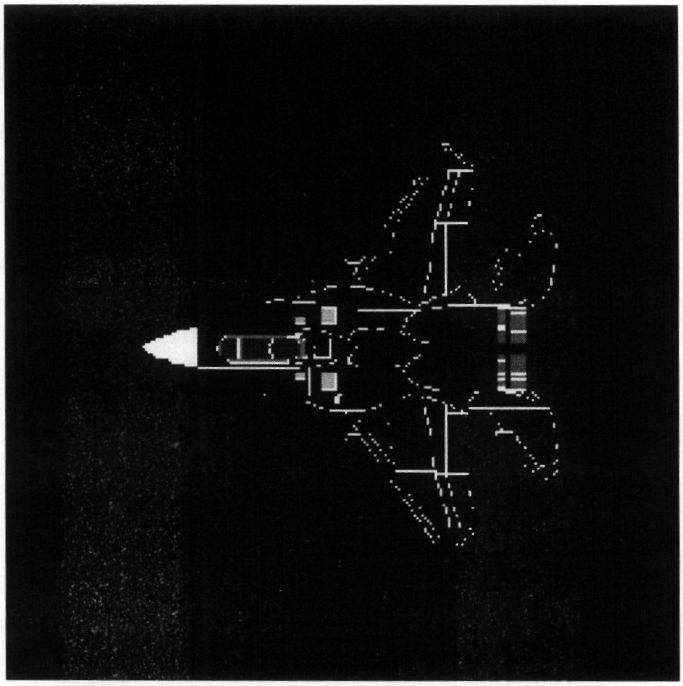

Fig. 5.7a Original object

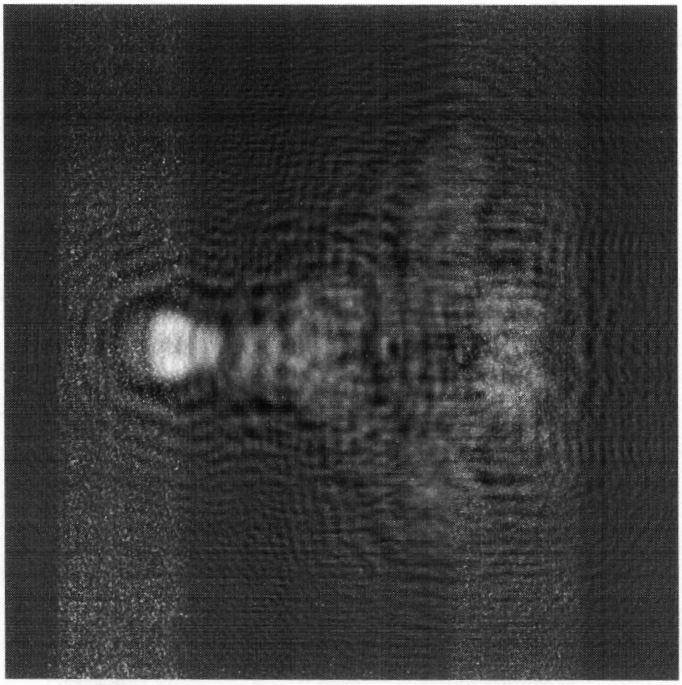

Fig. 5.7b Cosine Fresnel zone-lens plate coded image of Fig. (5.7a)

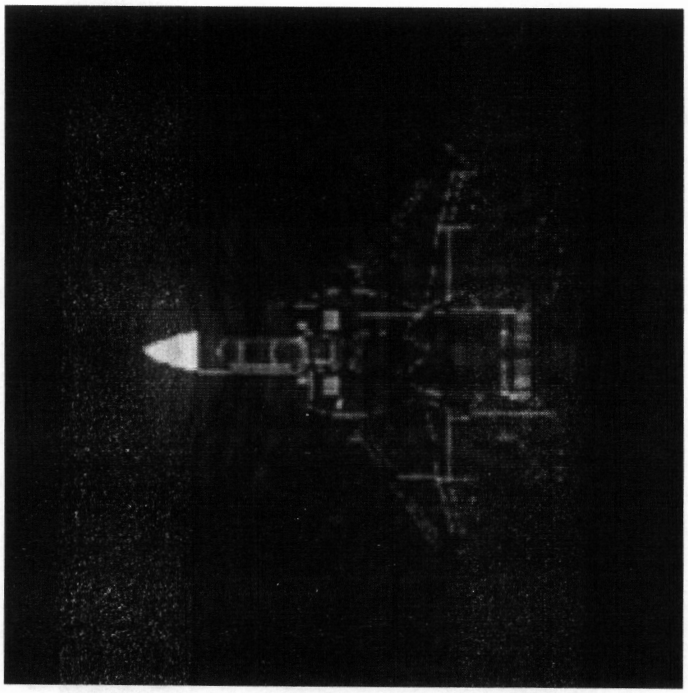

Fig. 5.7c Digital reconstruction of Fig. (5.7b)

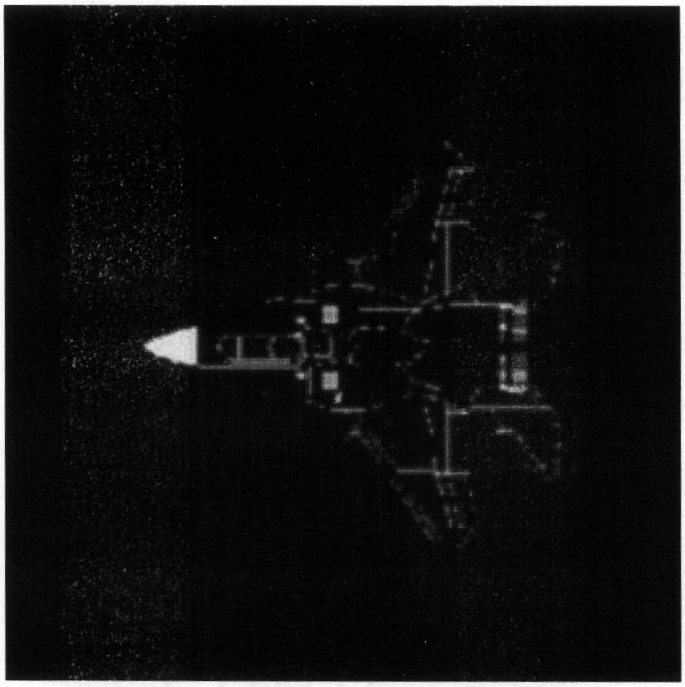

Fig. 5.7d Digital reconstruction of phase-coded hologram computed according to Eq. (5.9)

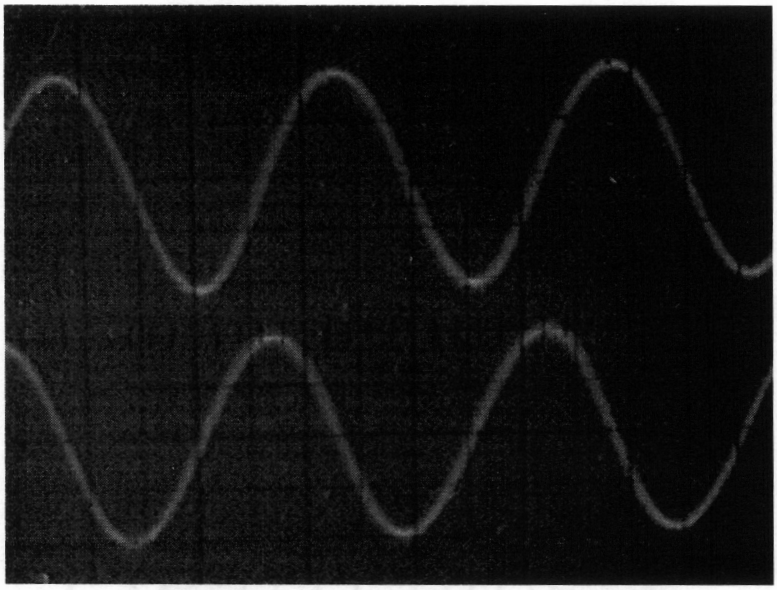

Fig. 5.8a Trace of phase difference in time base

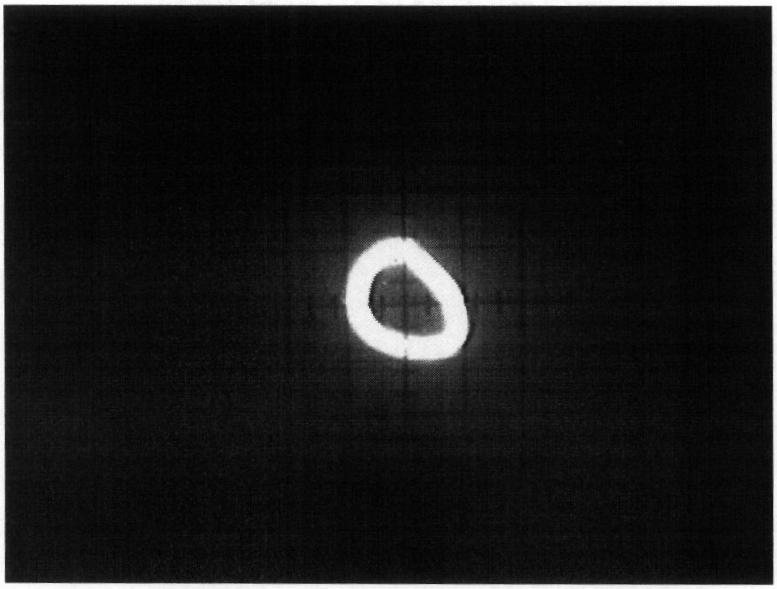

Fig. 5.8b Trace of phase difference in X-Y mode

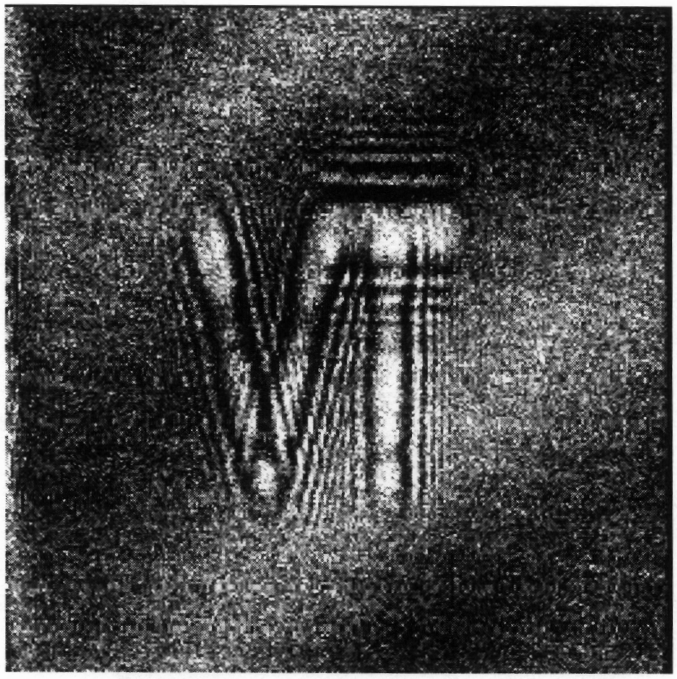

Fig. 5.9 Optically scanned cosine Fresnel zone-lens pattern coded hologram of "VT".

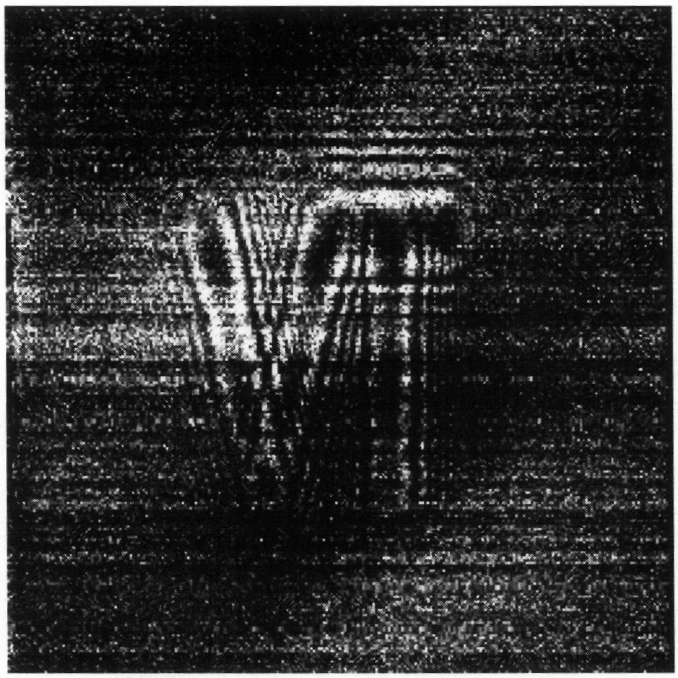

Fig. 5.10 Optically scanned sine Fresnel zone-lens pattern coded hologram of "VT".

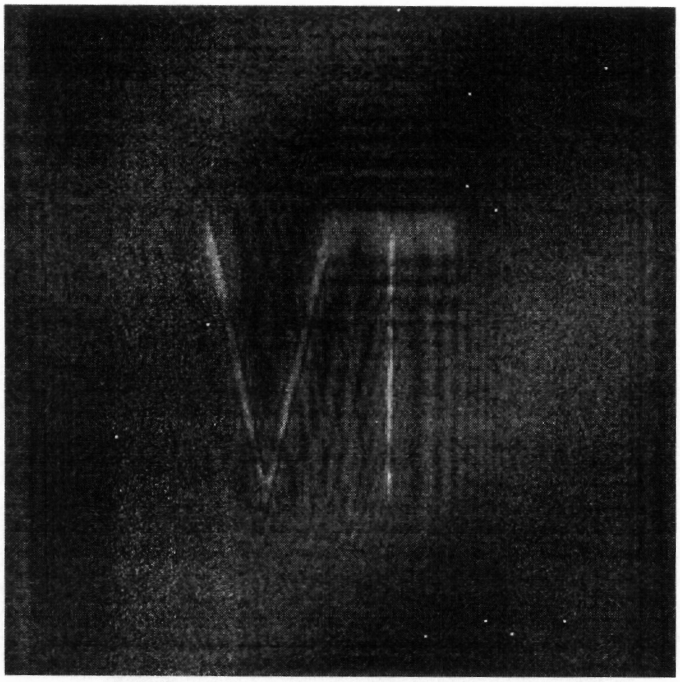

Fig. 5.11 Reconstruction of Fig. (5.9).

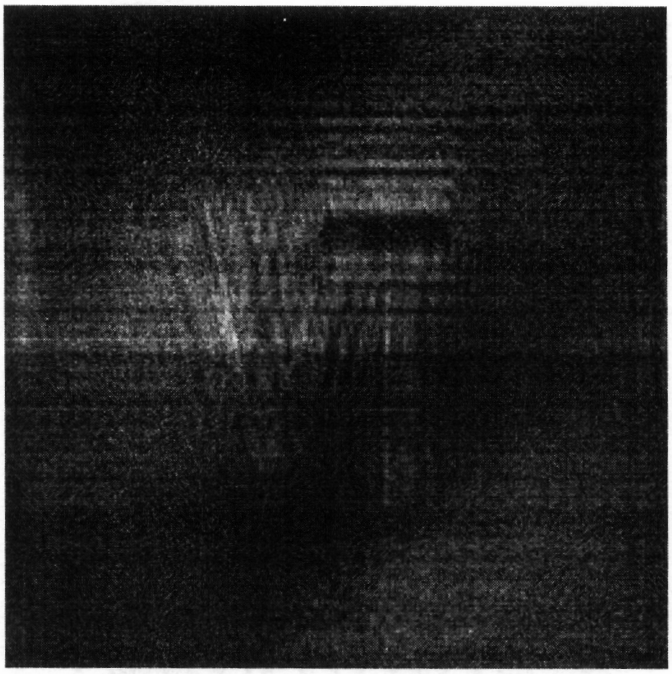

Fig. 5.12 Reconstruction of Fig. (5.10).

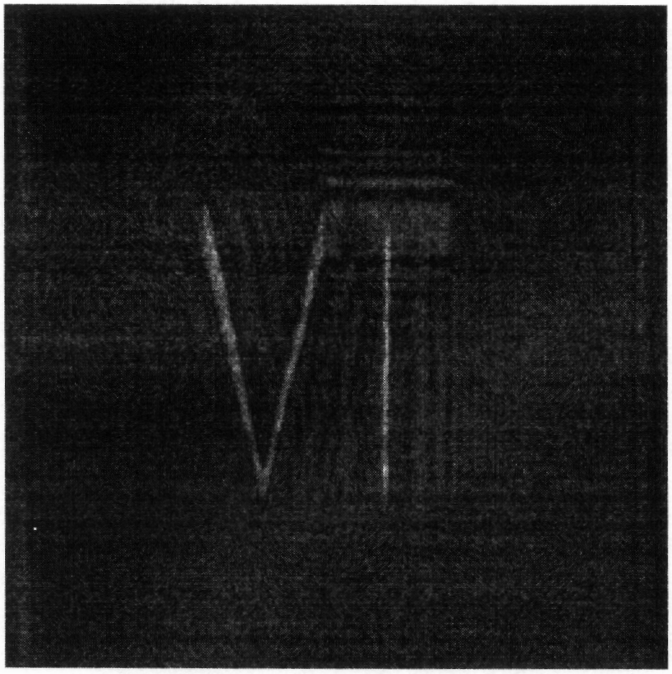

Fig. 5.13 Reconstruction of phase-coded hologram computed according to Eq. (5.9).

CHAPTER 6: CONCLUSION

6.1 Summary of the Research

In this dissertation we have examined an optical scanning system and have considered the subjects of scanning holography and heterodyne image processing by acousto-optic pupil synthesis. We have presented in detail the principle of optical scanning holography, with the analysis formulated on the basis of optical transfer function synthesis and Gaussian beam. In addition, the advantages which this method possesses over conventional incoherent holographic techniques have been presented. A technique for two-pupil synthesis has been discussed, emphasizing the similarities in the mathematical treatment with the conjunction of the incoherent imaging systems. OTF synthesis in the defocused case has also been discussed.

In addition, optical scanning holographic application to 3-D microscopy has been presented. Specifically, we have elucidated the concept by analyzing the recording and reconstruction of point objects. We have also derived holographic magnification in the context of OSH and shown how hologram scaling and wavelength scaling can be accomplished. The 3-D image, which recorded by optical scanning system, was both

numerically and optically reconstructed at different depths in order to demonstrate how a single plane can be brought into focus.

It has been shown that by scanning an object with a modulated Gaussian apodized Fresnel zone plate to acquire holographic information, the resolution achievable is directly proportional to the size of the beam and the number of zones within the beam. If the object is in the near field and as the object becomes more and more complicated, it is advantageous to use a smaller beam rather than a larger beam even though the two beams may lead to the same nominal resolution upon image reconstruction. We have also addressed the twin-image problems in optical scanning problems in optical scanning holography and proposed a multiplexing scheme to eliminate the twin-image.

6.2 Future Direction of the Research

To conclude the dissertation, we want to discuss a future direction of the research which is worth looking into. The optical scanning technique and its capability can be greatly enhanced if multiple beams are used to process or code the object. Fig. 6.1 illustrates the concept of multiple-beam scanning. The optical beam at frequency ω_0 represents a plane wave and the beam at frequency ω_0+Ω_1 generates a point source on the 2-D scanning mirrors. If the mask, $m_1(x, y)$, in general any programmable spatial light modulator equals one, we have the FZP generated on the 3-D object. If $m_1(x, y)$ is a Gaussian annular aperture, we have a structured beam scanning the object. We may add an array of beam-splitters and masks $m_n(x, y)$, so that many optical beams of different temporal frequency ω_n+Ω_n and of different spatial structures are combined and used to scan the 3-D object. The current $i(x, y)$ contains the multiple coded information of the

object. The different coded information at Ω_n can be extracted simultaneously using the detection scheme shown in Fig. 6.1 (b). This is a concept of frequency multiplexing and demultiplexing which is essential to the operation of radio and TV. $i_d(\Omega_n)$ represents the different demodulated signals corresponding to the different heterodyne frequencies Ω_n. These demodulated signals can be sent to a computer for further processing if needed or simply for digital reconstruction. Final results may be presented on a monitor. If real-time reconstruction is required, the computer may route the different signals to a spatial light modulator or modulators for coherent reconstruction. Some additional future research and development are summarized as follows:

1. Fine tuning of system to twin-image elimination using better equipment.
2. Realization of system in reflective mode.
   - 3-D optical remote sensing
   - 3-D robotic vision
3. Holographic image transmission through optical fiber.
4. Application to 3-D holographic microscopy.
   - Fluorescent response

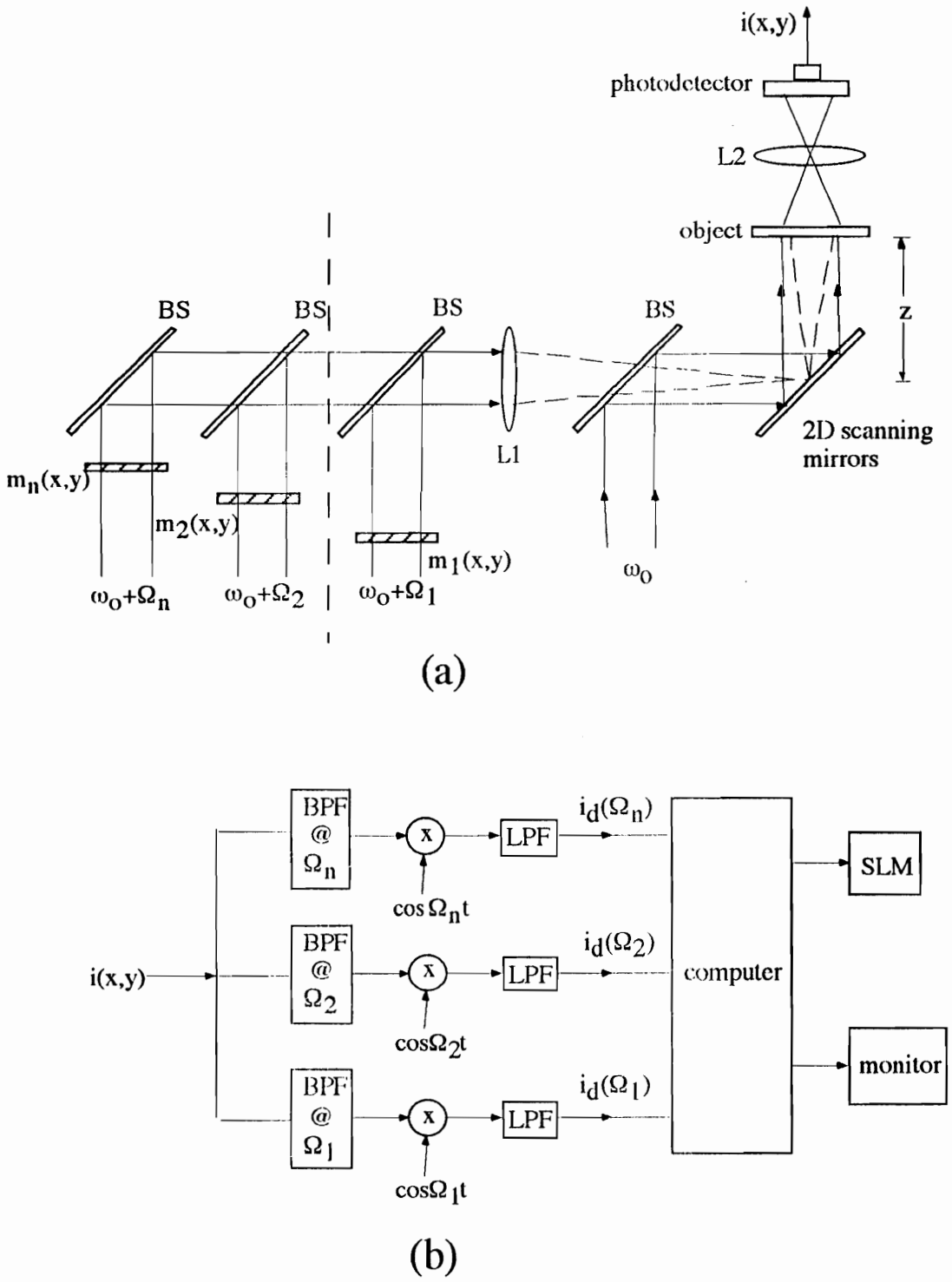

Fig. 6.1 Multiple-beam scanning holography. (a) Multiple-beam scanning and (b) information extraction scheme.

REFERENCES

[1] T.-C. Poon, "Scanning holography and two-dimensional image processing by acousto-optic two-pupil synthesis," *J. Opt. Soc. Am A* **4**, 521-527 (1985).

[2] B. D. Duncan and T.-C. Poon, "Gaussian beam analysis of optical scanning holography," *J. Opt. Soc. Am. A,* 9, 229-236 (1992).

[3] T.-C. Poon, B. W. Schilling, M. Wu, K. Shinoda, and Y. Suzuki, "Real-time two-dimensional holographic imaging using an electron-beam-addressed spatial light modulator," *Opt. Lett.*, **18**, 63-65 (1993).

[4] T.-C. Poon, K. B. Doh, B. W. Schilling, M. H. Wu, K. Shinoda, and Y. Suzuki, "Three-dimensional microscopy by optical scanning holography," *Opt. Eng.* **34**, 1338-1344 (1995).

[5] W. Lukosz, "Properties of linear low-pass filters for nonnegtive signals," *J. Opt. Soc. Am.* **52**, 827-829 (1962).

[6] A. W. Lohmann and W. T. Rhodes, "Two-pupil synthesis of optical transfer function," *Appl. Opt.* **17**, 1141-1150 (1978).

[7] D. Goerlitz and F. Lanzl, "Methods of zero-order non-coherent filtering," *Opt. Commun.* **20**, 68-72 (1977).

[8] T.-C. Poon and A. Korpel, "Optical Transfer Function of an Acousto-Optic Heterodyne Image Processor," *Optics Letters*, Vol. 4, pp. 317-319 (1984).

[9] B. W. Schilling and T.-C. Poon, "Real-time preprocessing of holographic information," *Opt. Eng.* **34**, 3174-3180 (1995).

[10] K. B. Doh, T.-C. Poon, M. H. Wu, K. Shinoda, and Y. Suzuki, " Twin-image elimination in optical scanning holography," *Optics & Laser Technology*, Vol. 28, No. 2, pp. 135-141 (1996).

[11] K. B. Doh, T.-C. Poon, and Guy Indebetouw, "Twin-image noise in optical scanning holography," *Opt. Eng.* **35**, no. 6, pp. 1550-1555 (1996).

[12] F.T.S. Yu and S. Jutamulia, *Optical Processing, Computing, and Neural Networks*, John Wiley & Sons, New York, 1992.

[13] J. W. Goodman, *Introduction to Fourier Optics*, McGraw-Hill, New York, 1968.

[14] A. W. Lohmann, "Incoherent optical processing of complex data," *Appl. Opt.* **16**, 261-263 (1977).
[15] W. Stoner, "Incoherent optical processing via spatially offset pupil masks," *Appl. Opt.* **17**, 2454-2466 (1978).
[16] T.-C. Poon, J. Park, and G. Indebetouw, "Optical realization of textural edge extraction," *Opt. Commun.* **65**, 1-6 (1988).
[17] T.-C. Poon, J. Park, and G. Indebetouw, "Real-time tunable incoherent spatial filtering: two-pupil processing technique," *Opt. Eng.* **29**, 1507-1510 (1990).
[18] D.A. Agard," Optical sectioning microscopy: cellular architecture in three dimensions," Ann. Rev. Biophys. Bioeng, 13, pp.191-219 (1984).
[19] T. Wilson, Ed., *Confocal microscopy,* Academic Press, London, 1990.
[20] D. Gabor," Microscopy by reconstructed wavefronts," Proc. Roy, Soc., A197, p.454 (1949).
[21] E. N. Leith, J. Upatnieks, and K. A. Haies, "Microscopy by wavefront reconstruction," *J. Opt. Soc. Am.* **55**, 981-986 (1965).
[22] B.J. Thompson, J. H. Ward, and W. R. Zinky, " Application of hologram techniques for particle size analysis," *Appl. Opt.* **6**(3), 519-526, 1967.
[23] W. K. Witherow, "A high resolution holographic particle sizing system," *Opt. Eng.* **18**, 249-255 (1979).
[24] Chandra S. Vikram, Ed., *Selected papers on holographic particle diagnostics*, SPIE Milestone Series, Vol. MS 21, 1990.
[25] J. B. De Velis and G. O. Reynolds, *Theory and Applications of Holography*, Addison-Wesley Publishing Co., Reading, Mass. 1967.
[26] M. E. Cox, " Microscopy" in Handbook of Optical Holography, H.J. Caulfied, Ed., Academic Press, Inc. 1979.
[27] A. Korpel, " Acousto-Optics," in Applied Solid State Science, Vol.3, R. Wolfe, Ed. New York: Academic, 1972.
[28] G. Indebetouw and T.-C. Poon, " Parallel synthesis of bipolar point spread functions in a scanning heterodyne optical system," Opt. Acta 33, 827 -834 , 1986.
[29] P.P. Banerjee and T.-C. Poon, *Principles of Applied Optics,* R. D. Irwin, Inc., Boston,1991.
[30] H. M. Smith, *Principles of Holography*, second edition, John Wiley & Sons, New York, 1975, Section 9.4.
[31] R.J. Collier, C.B. Burckhardt, and L. H. Lin, Optical Holography, Academic Press, New York, 1971, Chapter 3.
[32] R.W. Meir, "Magnification and hird-Order Aberrations in Holography," *J. Opt. Soc. Am.* **55**, 987-992, (1965)
[33] Image Processing and Measuring System (IPMS), Model DVS-3010/SS, Hamamatsu Photonics K.K. (Japan) and Hamamatsu Corp., Bridgewater, N.J.
[34] Hamamatsu Photonics K.K., Japan, and Hamamatsu Corp., Bridgewater, NJ, 1989, Product information sheet for EBSLM model X3636.
[35] C. J. Kuo and H. T. Chang, "Resolution studies for electronic holography," *Opt. Eng.* **34**, 1352-1357 (1995).

[36] J. Chovan, W. A. Penn, J. J. Tiemann, and W. E. Engeler, "Electronic holographic apparatus," U.S. patent No. 4,974,920 (1990).

[37] N. Hashmoto, S. Morokawa and K. Kitamura, "Real-time holography using the high-resolution LCTV-SLM," Proc. SPIE, Vol. 1461, pp. 291-302, 1991.

[38] R. L. Kirk, "Electronically generated holography," International patent No. WO 84/00070, Jan., 1984.

[39] L. Onural, G. Bozdagi, and A. Atalar, "New high-resolution display device for holographic three-dimensional video: principles and simulations," *Opt. Eng.* **33**, pp. 835-844, 1994.

[40] K. Shinoda, and Y. Suzuki, M. Wu and T.-C. Poon," Optical heterodyne scanning type holography device," U.S. Patent No. 5064257, Nov. 1991.

[41] S. A. Benton, "Experiments in holographic video," Proc. SPIE IS-08, pp. 247-267, 1991.

[42] T.-C. Poon, M. H. Wu, K. Shinoda, and Y. Suzuki, "Optical scanning holography," *Proc. IEEE,* to appear in May, 1996.

[43] Onural and P. D. Sccott," Digital Decoding of Holograms," *Opt. Eng.* **26**, pp.1124 - 1132, 1987.

[44] A. U. Baez, H. M. A. El-Sum, "X-ray microscopy and microradiography," Academic Press Inc., New York, 1957.

[45] D. Gabor, W. P. Goss, "Interference microscope with total wavefront reconstruction," *J. Opt. Soc. Am.* **56**, 849-858, (1966)

[46] J. B. DeVelis, G. B. Jr. Parrent, B. J. Thompson, "Image Reconstruction with Fraunhofer holograms," *J. Opt. Soc. Am.* **56**, 423-427 (1966).

[47] K.H.S. Marie, J. C. Bennett, A. P. Anderson, "Digital processing technique for suppressing the interfering outputs in the image from an inline hologram," *Electron. Lett.* **15**, 241-243 (1979).

[48] G. Koren, D. Joyeux, F. Polack, "Twin-image elimination in in-line holography of finite-support complex objects," *Opt. Lett.* **16**, 1979-1981 (1979).

[49] G. Liu, P. D. Scott, "Phase retrieval and twin-image elimination for in-line Fresnel holograms," *J. Opt. Soc. Am.* A **4**, 159-165 (1987).

[50] K. A. Nugent, "Twin-image elimination in Gabor holography," *Opt. Comm.* **78**, 293-299 (1990).

Vita

Kyu B. Doh was born on March 28, 1961 in Ye-cheon, Kyung-buk, Korea. After serving in Korean army for three years, he moved on to Virginia Polytechnic Institute and State University (Virginia Tech), where he received the BS, MS and PhD degrees in Electrical Engineering in 1989, 1992, and 1996, respectively. He joined the Optical Image Processing Laboratory in 1993, where he is a research assistant. His research interests include electro/fiber optics, optical image/signal processing, optical communication, optical scanning holography, computer-generated hologram, and microscopy. He is a member of SPIE, OSA and IEEE.